Downloaded from orbit.dtu.dk on: May 05, 2023

DTU Library

Advanced dry etching studies for micro- and nano-systems

Rasmussen, Kristian Hagsted

Publication date:
2014

Document Version
Publisher's PDF, also known as Version of record

Link back to DTU Orbit

Citation (APA):
Rasmussen, K. H. (2014). *Advanced dry etching studies for micro- and nano-systems*. DTU Nanotech.

General rights
Copyright and moral rights for the publications made accessible in the public portal are retained by the authors and/or other copyright owners and it is a condition of accessing publications that users recognise and abide by the legal requirements associated with these rights.

- Users may download and print one copy of any publication from the public portal for the purpose of private study or research.
- You may not further distribute the material or use it for any profit-making activity or commercial gain
- You may freely distribute the URL identifying the publication in the public portal

If you believe that this document breaches copyright please contact us providing details, and we will remove access to the work immediately and investigate your claim.

Technical University of Denmark

PhD Thesis

Advanced dry etching studies for micro- and nano-systems

Kristian Hagsted Rasmussen

Supervisors:
Ole Hansen
Stephan Sylvest Keller
Flemming Jensen
Anders Michael Jørgensen

DTU Nanotech
Department of Micro- and Nanotechnology

Abstract

Dry etching is a collective term used for controlled material removal by means of plasma generated ions. Dry etching includes several techniques, with reactive ion etching as one of the most used of its many derivatives. In this work inductively coupled plasma reactive ion etching has been applied for structuring of sapphire and many polymers. Metals and metal alloys have been structured by physical sputtering with argon ions in an ion beam etching system. The materials for which etch characteristics have been investigated are commonly used in device fabrication at DTU-Danchip.

Ion beam etching was first used for structuring of a magnetic device containing four different materials in nine layers. The materials, tantalum, tantalum oxide, iridium-manganese, and permalloy, can all be etched by reactive ion etching, however the thin layers and the need to etch all layers in one process makes ion beam etching an ideal choice. The physical nature of ion beam etching ensures etch rates of the different layers to only differ slightly, however, the etch rate is low. One problem with this technique can be redeposition of etched material at the sidewalls and at resist walls. This can introduce short circuits and even contaminate the surface with metal flakes after resist removal. Ion beam etching has also been used for etching of steel without any problems with redeposition. For steel the etch rate was low which reduced the selectivity to the photo resist.

Sapphire, a crystal of aluminum oxide, has a very low sputter rate limiting the applicability of ion beam etching. Structuring of sapphire is however interesting for fabrication of prepatterned substrates for gallium nitride epitaxial growth, among others. Such a substrate needs a certain structure height which can be obtained by introducing reactive ion beam etching in a boron trichloride plasma. The etch rates of sapphire in such a plasma can be up to a hundred times faster than rates in ion beam etching. The anisotropy of the etch can be controlled by changing the plasma conditions and fabrication of sloped sidewalls can be achieved.

Reactive ion etching of polymers can be used for several purposes, such as polymer removal, surface properties alternation, or polymer structuring. For material removal any polymer can be etched in an oxygen plasma, including all the polymers used in this project, which include, SU-8, TOPAS®, PLLA, PCL, and PMMA. However, just generating an oxygen plasma does not result in a controllable etch and may give rise to a poor surface for later use. It may be necessary to introduce other gases such as SF_6 to reduce surface roughness. Roughness can also be introduced by the mask in the form of redeposition of material on the surface. Since photo resist is a polymer the selectivity is inherently low and a hard mask below is a solution to increase selectivity. Nevertheless great controllability with many shared properties can be achieved for polymer etching in reactive ion etching.

Resumé

Tør ætsning dækker over flere metoder til fjernelse af materiale ved hjælp af plasma processer med ioner. Reaktiv ion ætsning er en meget brugt art af tør ætsning. I dette projekt er der blevet brugt induktivt koblet plasma reaktiv ion ætsning til at strukturere safir og flere forskellige polymere. Metaller og metal legeringer er blevet struktureret ved hjælp af fysisk erosion af overfladen med argon ioner i et ion stråle ætse system. Alle materialer, hvis opførelse ved æts er blevet undersøgt, er gængse i fremstillingen af forskellige enheder i DTU-Danchips renrum.

Ion stråle æts blev brugt til strukturering af magnetiske chips indeholdende fire forskellige materialer i sammenlagt ni lag. Selvom materialerne, tantal, tantal oxid, iridium-mangan og nikkel-jern, alle kan blive ætset ved hjælp af reaktiv ion ætsning, er ion stråle ætsning et bedre valg da de tynde lag skal ætses i en proces. Ætse raten for de forskellige lag vil være nogenlunde den samme da ion stråle æts er en fysiks proces, men ætse raten vil af samme grund også være lav. Der kan dog opstå nogle komplikation ved denne type æts, idet der kan være en tendens til at fjernet materiale sætter sig langs struktur og resist vægge. Disse materialedeponeringer kan være skyld i kortslutninger og ved resist fjernelse kan flager af metal kontaminere overfladen. Ud over æts af magnetiske materialer, er også stål blevet ætset med ion stråle ætsning. Her blev der ikke observeret problemer med redeponeringer, men ætse raten var lav hvilket resulterede i en laveselektivitet til photo resist.

Safir, som er krystallinsk aluminiums oxid, er kendt for at ætse langsomt i ion stråle ætsning, hvilket er begrænsende for anvendelsen af denne ætse metode. Struktureret safir har flere anvendelser, som for eksempel en struktureret overflade til dyrkning af epitaksal gallium nitrid. Sådanne strukturer skal have en vis højde som bedst opnås ved at bruge reaktiv ion ætsning i et bor klorid plasma. Ætse raten for safir er op til hundrede gange højere for reaktiv ion ætsning sammenlignet med ion stråle ætsning. Derudover kan formen på strukturene styres til en vis grad ved at ændre plasma ætse betingelserne.

For polymerer kan reaktiv ion ætsning bruges til flere formål, såsom resist fjernelse, ændring af overflade egenskaber for polymeren og polymer strukturering. Alle polymerer kan ætses i et oxygen plasma inklusiv de i dette projekt brugte som er, SU-8, TOPAS®, PLLA, PCL og PMMA. Det at udsætte en polymer for et oxygen plasma behøves ikke at give en kontrolleret fjernelse af materiale og kan ende med en overflade der er uegnet til det ønskede formål. Det kan være nødvendigt at tilsætte andre gasser såsom SF_6 til at fjerne biprodukter fra polymeren og sænke ruheden. Ruhed kan opstå som en følge af redeponering af det valgte maske materiale. Ved brug af foto resist som maske, hvilket er en polymer, er det ikke muligt at opnå en høj selektivitet, og derfor kan der bruges en hård maske. Det er dog muligt at ætse polymerer kontrolbart og forskellige polymerer har mange af de samme ætse afhængigheder i reaktiv ion ætsning.

Preface

The PhD thesis, 'Advanced dry etching studies for micro- and nano-systems' is submitted to fulfill the requirements for obtaining a PhD degree from the Technical University of Denmark (DTU). The research has been conducted at DTU Nanotech, Department of Micro- and Nanotechnology in the period from November 2010 until October 2013, by Kristian Hagsted Rasmussen. Ole Hansen from DTU Nanotech has been the main supervisor on the project. From DTU Nanotech Stephan Sylvest Keller has been a co-supervisor, just as Flemming Jensen and Anders Michael Jørgensen have been co-supervisors from DTU Danchip. The project has been funded by a grant to DTU Danchip from DTU in connection with the purchase of the IonFab 300Plus system.

During the three year course of this project I have enlisted the help of several people, which all deserve many thanks, just like DTU Danchip should be thanked for appointing me to this project. Most notable I would like to thank all my supervisors, which have contributed to this work in several ways. Through all three years I valued the supervision meetings twice a month, where we have discussed many problems concerning the project and a few with no relation to the work at all. Also the always open doors and the usually fast replies to any email I have send, have been of great value and ensured fast solutions to any problems encountered.

Most of the work has been conducted in the cleanroom facility driven and maintained by DTU Danchip, which should have thanks for their willingness to always answers to questions and requests. In particular process specialists Berit Herstrøm and Jonas Michael-Lindhard who are responsible for the IBE, ASE, and ICP-metal etcher, should be thanked for the help and suggestions regarding process development of the equipment. At the same time service coordinator Peter Windmann should be thanked for an always fast response time when I raised issues with the equipment.

The materials chosen for investigations of dry etching properties have all been chosen on a per request basis. In this respect I would like to thank Letizia Amato for our combined efforts in etching of SU-8 to suit her purposes. Johan Nagstrup should be thanked for introducing me to the world of biopolymers such as PCL and PLLA. TOPAS® which is used for injection molding was requested by several groups and Nikolay Ormstrup Christensen and Morten Bo Lindholm should be thanked for their help with sample preparation and defining of the etching goals with TOPAS®.

For the metals worked with in this project a thank to Frederik Westergaard Østerberg and Giovanni Rizzi for the delivery of magnetic samples for etching. Lasse Thamdrup from NIL Technology, Emil Søgaard, and Anas Fahad Al-Azawi were the people interested in steel etching, and did most of the work except etching. Finally Jakob Harming and Christine Thanner from EV Group in Austria should have many thanks for providing all sapphire samples used in development of a sapphire etch process.

In the end I would like to thank the employees at DTU Nanotech for a great working environment. Especially the guys and girl which have shared my lunch break with during the three years. My sister in law should be thanked for correcting some of my English. And last but not least my friends, family, and girlfriend should be thanked for bearing with my absence, especially through the writing process.

Kongens Lyngby, Denmark, April 3, 2014

Kristian Hagsted Rasmussen

Contents

Chapter 1

Introduction

Dry etching is a collective term for pattern transfer with a plasma source, either in the form of a physical, a chemical, or and combined process. There are several approaches for generation of a low temperature plasma by electric fields. Conrads and Schmidt have described the different types of plasmas relevant for this work [1], while Jackson gives an introduction to the theory of plasmas[2]. In this work the focus will be on the two etching setups called ion beam etching (IBE) and inductively coupled plasma reactive ion etching (ICP-RIE).

At DTU Nanotech there is a great interest in microsystems for many purposes, including bio-medical devices, energy harvesting, and sensor of many kinds. Fabrication of such systems are done by many of the same techniques used in microelectronic fabrication. However the diverse applications increases the need to expand the knowledge for processing of materials not commonly used in microelectronics. This project will cover dry etching of several materials used in the development of microsystems at DTU Nanotech.

1.1 Ion Beam Etching

Ion beam etching (IBE) is a physical etch method where material is removed from the surface of a substrate by sputtering. The process can to some extent be compared to powder blasting, where the blasting powder is exchanged with inert ions, and the pressure driven propulsion is exchanged with electric field acceleration. Hence ion beam etching is also known under the names Ion Beam Milling and Ion Beam Sputter Etching, however ion beam etching or milling is most commonly used. IBE is also available in a focused version for maskless machining of surfaces (FIBE). Here a focused ion beam (FIB) of some nm width is moved across the surface, writing the pattern defined on a computer. The two processes are not to be confused with each other as the equipment used for the two setups is completely different.

1.1.1 Development of IBE

Ion beam etching was developed in the early days of silicon technology. IBE depends on the extraction of ions from a plasma in the form of a glow discharge as described by Dugdale et al. [3]. A more specific discussion of IBE is given by Spencer and Schmidt [4] including a description of the equipment they used. Any ions accelerated towards a surface will to some degree be able to remove material from the surface. The use of noble gases ensures that no chemical reaction will take place at impact and thereby etching of any material should be possible. However use of chemical active ions can in some

cases improve the etch result. This kind of process is called either chemical assisted or reactive ion beam etching (CAIBE or RIBE). If the reactive gas is introduced at the target surface the process is call CAIBE, while introduction of the reactive gas into the plasma makes it a RIBE process

The system available at DTU-Danchip is equipped with argon as the primary etch gas, with the possibility of adding oxygen, chlorine, and trifluoromethane to the plasma for reactive IBE (RIBE). Other noble gases such as neon, krypton, and xenon are also used for IBE etching. Neon is best applied for etching of light materials, while krypton and xenon with their higher masses, are more suitable for removal of heavy elements. Etch rates with ion sputtering naturally depend on the sputter yield, which again is dependent on the sputter ion and the material to be sputtered. However also the energy of the ion and the incident angle have a large influence on the sputter yield.

Laegreid and Wehner did an elaborate test of many metallic elements with respect to the sputter yield [5]. The sputter yield for the elements were found for both an argon and a neon ion beam. In addition to the two sputter gases, different ion energies were tested. The sputter yield is not directly convertible to etch rate but gives an indication of the differences between different materials. For this reason it is possible to give an estimate of the etch rate of a material if the etch rate is known for another one.

The use of sputter yield to estimate etch rate can be seen in the work of Glöersen [6]. The etch rate of several materials is listed in the paper, not only metals, but also metal oxides, alloys and even some photo resists. It is clear that etch rates are moderate with values around $40\,\mathrm{nm\,min^{-1}}$. The low etch rate make it unfeasible to use IBE for deep etching in materials which can form volatile compounds as happens in reactive ion etching (RIE) discussed later.

In some cases the use of IBE is warranted, such as for structures containing several different layers of materials. Even if the materials can be etched by RIE, IBE etching has some advantages. If the materials in the stack are etched by different plasma chemistries RIE processing is made difficult. Or if one of the materials etches with low anisotropy, unwanted gaps between layers may arise at the edges.

However materials such as gold, cobalt, copper, and nickel do not form volatile etch products in halogen plasmas and must hence be etched by IBE [7]. The etching of single metals is rather simple if not trivial since most parameter settings are shared between materials. In the same sense metal alloys can be etched, however Betz have shown that one element in the alloy may be etched preferentially [8]. It is more difficult to etch multilayer structures as etch rates change through layers and IBE effects such as material redeposition may introduce problems for the final device. One problem generated by redeposition is electrical short circuits between different layers in an etch stack.

1.1.2 Magnetic materials

In recent days IBE has primarily been explored in connection with fabrication of different magnetic devices. The increase in data density on hard disk drives have lead to the use of a patterned magnetic disk for storage. The pattern on these disks can be made by IBE, as shown by Naito et al. [9]. The magnetic layers used by them are based on cobalt, chromium and platinum making IBE the obvious choice for etching.

Even more recently a lot of interest in alternative random access memory (RAM)

types to the ones used in computers today have been shown. One of these technologies that in principle should be able to compete both with flash memory and DRAM is based on magnetic tunneling junctions (MTJ). Several groups have published work on the optimization of IBE for fabrication of MTJ on different magnetic layers [10, 11, 12]. The MTJ described in literature are in general based on permalloy (NiFe) and some other magnetic materials such as IrMn or CoFe.

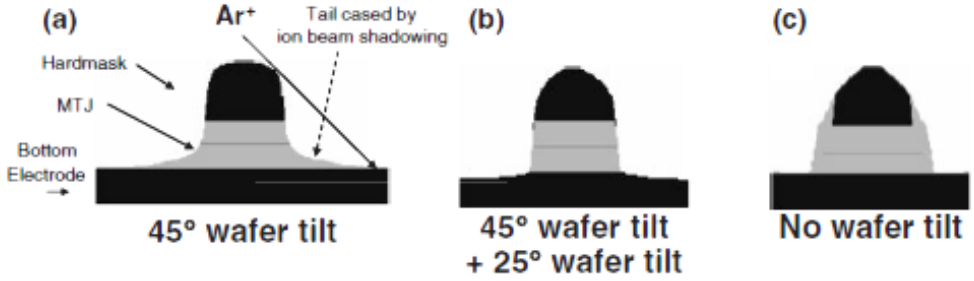

Figure 1.1: Sugiura et al. reduced tailing by etching at two angles. Image is borrowed from [12].

Takahashi et al. [11] and Sugiura et al. [12] have worked on reducing redeposition fabrication of better devices. They agree that high incident angles of the beam are the best way to limit the redeposition. This will however introduce tails at structure edges, which Sugiura et al. have successfully limited the effect by a small over etch at a lower incident angle fig. 1.1. The redeposition can be avoided if an RIE etch is used instead, even though such an etch is much more complicated.

Both Ra et al. [13] and Kinoshita et al. [14] have investigated ICP-RIE for MTJ fabrication. Both groups have reported etches primarily based on argon which will still be a sputter process just as IBE. However they have reported that the inclusion of small amounts of chlorine in the plasma results in better sidewall definitions. This indicates that the added chlorine makes some volatile metal compounds that will reduce the redeposition. However the small amount of chlorine in the etches does suggest that a RIBE process might also improve the sidewall definition.

As a side note it should be mentioned that focused ion beam etching (FIBE) should etch all materials in the same fashion as IBE. However the serial nature of the etch limits its usability to prototyping and sample preparation for characterization. Kato et al. has for instance shown that FIBE with gallium ions can be used to structure permalloy and IrMn [15].

1.2 Reactive ion etching

Reactive ion etching (RIE) is a plasma etching technique that combines chemical etching by radicals and ions, with physical bombardment. The technique was developed in connection with fabrication of integrated circuits, and just as nowadays when semiconductor producers present new technology it was demonstrated on memory chips [16]. Bondur published a more formal presentation of reactive ion etching in 1976 [17]. The same year Somekh compared different dry etch techniques such as IBE and RIE [18].

As so many other techniques in micro technology RIE was developed for use in silicon technology. Etching of silicon is a well described process with several different approaches, such as cryogenic etching or the patented Bosch process for deep etches [19, 20, 21]. RIE etching of many materials rely on halogens for generation of volatile etch products and the well documented silicon etching is no exception. For silicon etching the use of fluorine is common and the reaction kinetics are to some extend known. For SF_6 Iio et al. have listed a few of the plasma reactions [22], while Kokkoris et al. have made a model of the plasma processes for use in computer simulation [23].

In this project an enhanced derivative of RIE has been used for processing, namely two inductively coupled plasma (ICP) reactive ion etching systems. In comparison to conventional RIE, ICP-RIE enables better control of sputter energy, since ion acceleration towards the target is controlled by a separate electric circuit than the one creating the plasma. Boswell and Porteous described the used of an ICP setup in 1987 [24], while Perry and the same Boswell described its applications [25].

The separation of the plasma generation electric circuit and the acceleration circuit, enables better control of etch rate and profile. ICP-RIE is not limited to silicon etching, as many materials are etched by such systems nowadays. Metals, semiconductors, and dielectrics can for many elements be etched by ICP-RIE on the condition that volatile etch products will be formed in the process. All these materials are in general etched by halogens, where fluorine, chlorine, and bromide are the most commonly used. However iodine is also used in special cases such as etching of indium containing layers [26]. Indium is widely used for photonics where sapphire substrates are often used for fabrication of light emitting diodes for future lightning application.

1.2.1 Sapphire

In the modern world a large amount of the energy is consumed by lightning, both in homes, companies, and outside. The light sources used do in general not have an extremely high efficiency. However with the fabrication of the blue light emitting diode (LED) and laser diode (LD) in the 1990th this is soon going to change. As of the first of September 2012 the European union made it illegal to sell incandescent bulbs which was first introduced to the market by Thomas Edison over 130 years earlier. This leaves the market for lightning to fluorescent lamps, halogen lamps, and LEDs.

LEDs have a large potential since the efficiency is high compare to other light sources. However, at the moment the acquisition price is quite high compare to competing light bulbs. This again should be seen in relation to the life time and the power consumption which actually make LED light bulbs competitive with other light bulbs. LED light is soon to be found in most lightning applications, such as home lightning, street lights, and even car headlights [27].

For fabrication of white LEDs, the demonstration of the blue LED by Nichia Corporation was a missing piece [28]. Blue LEDs are made in gallium nitride, aluminum gallium nitride, or indium gallium nitride which are normally grown on a sapphire substrate. However, sapphire, which is crystalline aluminum oxide, and gallium nitride have a lattice mismatch of around 0.5 Å or 10 %. This lattice mismatch will introduce crystal defects that will lower the efficiency of the fabricated diodes.

To decrease the lattice mismatch several groups have investigated the epitaxial growth of gallium nitride on patterned sapphire substrates see fig. 1.2, [29, 30, 31, 32, 33]. The

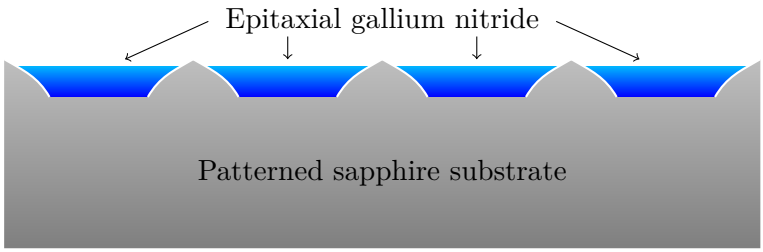

Figure 1.2: A patterned sapphire substrate allows for lattice relaxation at the cone edges, since gallium nitrate only growths from a crystal plane.

pattern made on the substrates should in general be some form of cone, with no crystal planes exposed. Gallium nitride only grows from a crystal plane and on a patterned substrate the growth will then not initiate on the whole surface. In the process of epitaxial growth the device layer will slowly cover the cones but without being fixed to the underlying sapphire crystal. This will result in a relaxation of the crystal lattice and limit the amount of defects present in the device layer.

As mentioned in the literature a patterned sapphire substrate does not only minimize the amount of lattice defects, but it will also enable more light to escape from the diodes. The light generated in a diode will only escape the diode, if the incident angle to the surface does not result in internal reflection. In a normal diode the two surfaces of a diode are parallel and if light is reflected from one surface, it will have the same incident angle for the second try and hence not escape. On a patterned surface one surface of the diode will not be flat and will hence allow light to escape at other angles. A photon will hence change its incident angle on the surface for each time it is reflected back and forth and at some point it will escape the diode and hence increase the light output.

Patterning of sapphire is not trivial as sapphire is one of the most difficult materials to etch in a controlled fashion. Sapphire is known to have a very low sputter yield and great resistance to typical plasma etch chemistries. This is one of the reasons that aluminum oxide is used as masking material for deep reactive ion etching of silicon, with selectivities up to 70000:1 possible. Thus enabling via hole etching in silicon with only some nanometers of masking material [34].

However it is not impossible to etch sapphire and a wide selection of ICP chemistries and more exotic approaches have been used for the purpose. For example Dongzhu et al. [35], showed that surface damage by ion implantation in the areas of sapphire that should be removed, enables selective etching in a HCl-HF solution and in IBE. Etch rates of amorphous sapphire was between 1.5 to 2.5 times higher than for crystalline sapphire. Also gases not available in the etching systems at DTU-Danchip have been used. Kang et al. [36] has successfully used a C_2F_6 - NF_3 plasma for etching with etch rates up to $150\,\mathrm{nm\,min^{-1}}$. For masking they used chromium and were able to get a high selectivity of 8:1.

However most etching of sapphire is done in chloride based inductively coupled plasmas. Several groups have achieved etch rates between $350\,\mathrm{nm\,min^{-1}}$ and $380\,\mathrm{nm\,min^{-1}}$ in a BCl_3 - Cl_2 plasma, [37, 38, 39, 40]. The groups agree that the best etch rates are achieved with a gas ratio of 80 % BCl_3. The plasma chemistry of the BCl_3 - Cl_2 plasma is described by Meeks et al. [41] in their paper on the simulation of the plasma reactions

taking place.

Higher etch rates of sapphire have been achieved by adding HBr to the plasma, [42, 43]. Not only does the use of HBr enable higher etch rates but also a higher anisotropy has been achieved by the use of HBr. Jeong et al. compare the anisotropy of several etch chemistries based on a BCl_3 plasma [39]. In their experiments the lowest anisotropy is found by adding Cl_2 to the plasma, while a plasma containing only BCl_3 or with HCl as an added gas results in higher anisotropy. However HBr as additive gas enables the highest anisotropy.

All BCl_3 plasmas showed a selectivity to photo resist around 1 underlining the difficulties in etching sapphire. The higher etch rates achieved with BCl_3 compared to Cl_2 are generally accepted to be due to borons ability to generate volatile $BOCl_x$ compounds. This is not only used in aluminum oxide etching but also in etching of other materials such as ZrO, ZnO, HfO, and other dielectrics [44, 45, 46]. The chloride is then responsible for generation of metal chlorides and hence enables the removal of the metal part of the material.

1.2.2 Polymer etching

If the halogens in ICP-RIE are exchanged by oxygen the systems are able to etch polymers with a higher degree of control than the typical ashing processes used for resist removal and wafer cleaning. Etching of many polymers are to some degree similar independent on the polymers. However if the polymer matrix contains elements that are not etched by oxygen, such as metals or silicon, a halogen must be used in connection with oxygen for polymer etching [47]. The polymers for which etching is best described in the literature are polystyrene (PS), Poly(methyl methacrylate) (PMMA), and polydimethylsiloxane (PDMS).

PMMA is a common material in micro system fabrication and can be used both as an e-beam and imprint resist. The patterned surfaces in PMMA can also be used for device purposes in microfluidics, or with surface modifications to change the surface properties. Tsougeni et al. have used an oxygen and C_4F_8 plasma to tune the surface for hydrophilic or hydrophobic behavior [48]. In the process they etched the surface generating a rough surface that also changed the hydrophilic nature of the surface. For a more dedicated etch process Zhang et al. etched PMMA in an oxygen plasma with either argon or CHF_3 added to the plasma [49]. They showed that if the amount of oxygen in the plasma became small the etching process would change from ion-enhanced to a physical defined etch. At the extreme with no oxygen in the plasma but only halofluorocarbons the etch rate was linearly proportional to the bias voltage [50], which indicates a physical etch.

Halofluorocarbon etching was also investigated for PS and showed the same dependencies. PS can however easily be etched in an oxygen plasma as shown by Jung and Ross [51]. In their work they have selectively removed PS for a PS-PDMS diblock copolymer. This is possible since PDMS contains a high level of silicon, which is not etched by oxygen. Leaving them with a surface with only the PDMS part of the polymer left after etch. This can be used for self assembly masking with the PDMS layer used as mask.

PDMS can easily be etched in RIE, simply by adding a gas to the plasma that will remove silicon. Both Garra et al. [52] and Hwang et al. [53] have reported the use of CF_4 and oxygen for PDMS etching. The gas ratio should at least be 2 to 1 of CF_4 compared to oxygen to achieve reasonable etch rates. The use of CF_4 will however change the

surface properties, as changes in contact angle have been reported for this etch. Just like PDMS oxygen and CF_4 have been used to etch polyimide and again the bias power showed a high influence on the etch rate [54].

All indications for polymer etching are towards the use of oxygen as the primary etch gas and then adding a fluoride containing gas if the result is not satisfying. In addition to the use of oxygen the bias voltage seem to have a large influence. However in the systems available for this work it were not possible to measure the bias voltage. However the bias power is controllable and linked to the energy transfered to the surface in the etch. Several polymers have been investigates in this project some of them is mentioned above while others are shortly introduced below.

1.2.3 SU-8

SU-8 is an epoxy based, photo sensitive polymer developed by IBM in the late 1980s [55]. SU-8 photo resist is derived from EPON™ resin [56], with in average eight epoxy groups and eight aromatic benzene groups per monomer as indicated by the name. The viscous polymer contains between 5 % and 10 % photo-initiator enabling cross linking by standard I-line lithography. The photo-initiator used for the SU-8 resin is based on triarylsulfonium-hexafluoroantimonium, adding fluorine, sulfur, and antimony to the carbon, hydrogen, and oxygen from the polymer as elements in the SU-8 resin.

SU-8 in microtechnology was early on applied for use in LIGA[1] [57] where the polymer is used to make a structured mold. The easy structuring of SU-8 combined with resistance to a wide variety of chemicals makes SU-8 interesting for masking of etch processes in more exotic materials. The chemical resistance of SU-8, however, complicates the removal of the resist, with plasma removal as one of the only reasonably reliable option.

More recently SU-8 has been used as a device layer rather than a sacrificial layer. Fabrication of devices in SU-8 can in general be accomplished by photo-lithography, with devices spanning a large field of applications. Lab on a chip (LOC) systems with microfluidic channels made in SU-8 [58, 59], have advantages such as biological compatibility and easy fabrication. Devices for optical applications such as polymer waveguides [60] and optical transducers [61] have been shown. Furthermore, the mechanical properties of SU-8 make it an obvious choice for cantilevers for sensor systems [62].

Plasma treatment of all of these devices can be used for several purposes. Probably the most used case of plasma treatment of SU-8, in addition to removal, is functionalizing or activating a surface. Functionalizing the surface can for example be used to tune the hydrophobicity of a surface or change the surface termination to alter the bonding capabilities. For some applications further patterning of the SU-8 after the initial photolithography in the form of etching might be interesting. If for example groves needs to be fabricated in the whole width of a line, etching of a single layer SU-8 is preferable to subsequent patterning of two layers of SU-8 with the risk of misalignment, where the the structures on top of the first line is not dead center. An isotropic etch can be used to increase the aspect ratio or decrease the line width of lithography defined structures.

In the scarce literature on SU-8 etching available, all authors seems to agree on the need for fluorine in the plasma chemistry. However, nobody has offered a satisfying

[1] Lithographie, Galvanoformung, Abformung

explanation for the need of fluorine. The first and also most thoroughly discussed subject in SU-8 etching is the obvious and important subject of complete removal of SU-8 after its use as masking material.

Dentinger et al. [63] made a study on different methods for SU-8 removal, including removal using solvents, chemical removal in different plasma etching configurations, and other more exotic methods. For our study the chemical removal in any type of plasma setting is interesting. Both results from Reactive Ion Etching (RIE), as well as Downstream Chemical Etching (DCE) can help to clarify the different mechanism involved in the process. Etch rates of $1\,\mu m\,min^{-1}$ to $4\,\mu m\,min^{-1}$ can be obtained in RIE using a mixture of CF_4/O_2 in approximately equal proportions [63].

In DCE, Dentinger et al. observed that only two to four percent of CF_4 is needed to obtain etch rates as high as $10\,\mu m\,min^{-1}$. However, to obtain such high rates the temperature must be elevated to 275 °C. Such high temperatures will introduce thermal stress in the polymer, increasing the risk of cracking and peeling. It will also cause compatibility issues with some materials in practical applications. While high SU-8 removal rates are obtainable, the surface of the wafer is heavily contaminated with antimony after complete SU-8 removal. The surface antimony is by Dentinger et al. ascribed to residues left from the photo initiator.

The influence of fluorine on etching of cured SU-8 is also discussed by Hong et al. [64] and Mischke et al. [65]. Hong et al. used CF_4 just as Dentinger et al. did, while Mischke et al. added SF_6 as fluorine source for the plasma. Hong et al. limit the discussion to etch rate and anisotropy without discussing antimony. However Mischke et al. [65] used Energy-dispersive X-ray spectroscopy (EDX) on etched SU-8 surfaces to identify antimony and fluorine in addition to the expected carbon and oxygen. Mischke et al. however conclude that fluorine is only introduced by the etch chemistry, despite the fact that the photo initiator in SU-8 is triarylsulfonium hexafluorantimonium which includes the SbF_6^+ ion.

De Volder et al. [66] used plasma etching to produce nanowires in SU-8. Their process is basically an oxygen plasma etch where they also see an accumulation of antimony at the surface; the antimony is believed to act as local masking agent and starting point of the nanowires. X-ray photoelectron spectroscopy (XPS) analysis of the surface shows up to $19\,\%_{atom}$ antimony surface concentration in their experiments. Similar to Mischke et al.'s experiments no external source for antimony was present, and the antimony must hence all originate from the SU-8 photo-initiator.

The presence of antimony in plasma treated surfaces is a problem for biological applications since antimony is toxic. This does not only apply to samples structured by plasma etching, but also surfaces cleaned or primed in an oxygen plasma will have increased concentrations of antimony in the surface after a shallow etch. Small amounts of antimony may not be critical since the toxicity is weaker than e.g. that of arsenic [67, 68]. However, since etching generates thin hairlike structures it can be assumed that the antimony present in the surface is on nanometer scale, for which Bregoli et al. [69] has evaluated the toxicity and found it poisonous. It is important to minimize the antimony concentration to achieve relevant results for biological experiments performed on SU-8 chips.

1.2.4 TOPAS®

Another polymer of interest is TOPAS® which is a commercial name for cyclic olefin copolymer. Cyclic olefin copolymers (COC) consist of a polyethylene backbone with norbornane incorporated along the chain, as shown in fig. 1.3.

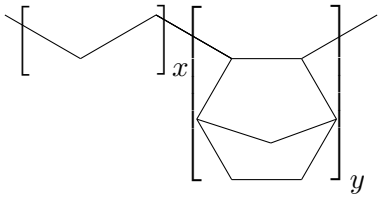

Figure 1.3: Cyclic olefin polymer (COC) structure is a polyethylane backbone with norbornane periodically placed on the chain. TOPAS® is a commercial name for COC and the different grades are due to different numbers of x and y.

TOPAS® has many advantages compared to other bio-compatible polymers [70]. Like in most polymers it is possible to fabricate sub-micron structures in TOPAS®. It is inert to most common solvents used in microfluidics while maintaining a high glass transition temperature (T_g). If microfluidics is taken one step further, to an integrated diagnostic device, TOPAS® excels in its high light transmittance, enabling integration of optical fibers on chip. Markos et al. has shown that TOPAS® can be used for optical purposes in the form of a bragg grating [71]. TOPAS® is made in several grades, with different T_g, light transmittance, and other properties. Some TOPAS® grades have high light transmittance at short wavelengths around 200 nm, enabling the use of UV light for sample diagnostic. UV light has been used on bulk samples for diagnostics of breast cancer among other applications [72].

TOPAS® is often used for injection molding of small samples. However for prototyping TOPAS® can also be used as an imprint resist [73]. It is possible to achieve good structure definition and small structures in TOPAS®. There may be several reasons to etch TOPAS® after such structuring, including residual layer removal, additional patterning, and surface chemistry modification. Hwang et al. have used oxygen plasmas to change surface properties such as the contact angle [74].

The main focus of this thesis is on dry etching for which only limited literature with regard to COC are available. Some of the first experiments with COC polymers in plasma etching systems were done with the purpose to find a deep UV photo resist. For this usage Wallow et al. investigated the etch resistance of two candidates for 193 nm resist, where one is cyclic olefin based [75]. In the case of COC used for masking the etch resistance should be high, and the plasma composition would be geared towards halogenated etching components.

At DTU-Nanotech Wang et al. have investigated oxygen etching of TOPAS® in a conventional RIE system [76]. They showed a reasonable etch rate between 0.5 µm min^{-1} and 1 µm min^{-1} but with some degree of under etching of the mask. In this thesis I will discuss TOPAS® etching in an ICP-RIE system with better control of the ion bombardment of the surface. This should in theory result in better control of the etch speed and under etching.

At DTU-Nanotech there has also been some interest in patterning of bio-compatible polymers such as poly-L-lactide (PLLA) and polycaprolactone (PCL). These polymers

can be used for devices in life science such as drug delivery [77]. However no knowledge of patterning or residual layer removal of these polymers with dry etching is available, and experiments have been based on the knowledge of how other polymers behave in plasma conditions.

In addition they have relative low glass transition temperatures, making it difficult to mask the materials, without risking to melt them. Also there interaction with the solvents used for photo resist may have unwanted effects on the polymers and hence a hard mask underneath the photo resist has been adapted and some experiments with shadow masking have also been carried out.

Chapter 2

Theory

Some basic theory of the most used techniques in the project will be outlined in this chapter. This will of course include an introduction to some of the important parameters for the two etching techniques IBE and ICP-RIE. Since design of experiments (DoE) has been applied for many of the experiments a short introduction to the method is obviously warranted. Last but not least two of the more advanced characterization methods are discussed. A short introduction to X-ray photoelectron spectroscopy with a discussion of some relevant constraints needed for good mole fraction estimates ares given. Also the sheet resistance measurement will be discussed as the setup is custom build and hence all data treatment is programmed by me.

2.1 Ion beam etching

Ion beam etching (IBE) is characterized by spatial separation of plasma and etch target. The plasma has been generated in several different ways over time, from a DC plasma in a Kaufman source to the RF generated plasma in the ICP source available [1] on the Ionfab 300Plus system from Oxford Instruments used here and sketched in fig. 2.1.

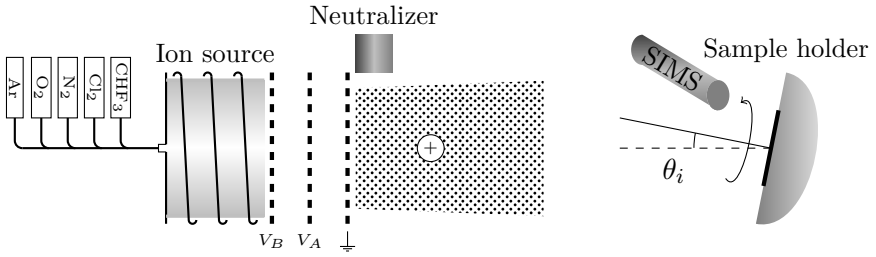

Figure 2.1: An ion beam etching system consist of a ion source where ions are generated from a gas by an electric field. The ions are extracted from the source through a set of grids, after which the beam is neutralized. The energetic ions will be used to sputter material of a sample, and the end point can be monitored by SIMS.

The plasma is generated by feeding gas into a plasma chamber made of ceramics with a coil wound around. The neutralizer is started before the actual plasma, and some emitted electrons from the neutralizer enters the plasma chamber. These electrons helps to generate the plasma by collision with other particles when power is applied to the coil. The RF power applied to the coil sets electrons vibrating in the gas and induce generation of more electrons and ions. An advantage of an ICP setup is that the power used to generate an electric field to maintain the plasma, also induces a magnetic field

that to some extend confines the plasma. ICP sources are known to have almost no contamination from the chamber walls in the beam due to plasma confinement.

In the IonFab 300Plus ions are extracted by a three grid setup. The grid in contact with the plasma is called screen grid and is positively biased to the beam voltage. When ions enter the screen grid they are accelerated towards the next grid by applying a negative voltage to that grid. The negatively biased grid is called the accelerator grid and should be aligned to the screen grid to allow the beamlets to leave through the holes in the grid. The final grid is called the decelerator grid and this should also be well aligned to avoid sputtering. The decelerator grid is grounded so that ions leave the ion gun with an energy defined by the voltage applied to the screen grid. The use of an accelerator-decelerator setup enables better control of beam divergence and the control on accelerator voltage can be used to tune this [78].

The beam that leaves the ion gun is positively charged and must be neutralized. There are several reasons to neutralizing the beam, such as beam divergence and target charging. The positive ions repel each other, however by injecting electrons into the beam the net charge is minimized, reducing the beam divergence. Electrons further ensure recombination at the target, and hence limit the charging of non conductive materials.

When ions reach the surface of the etch target they sputter material from the surface. The sputter yield is a complex quantity that measures the average amount of atoms removed per incoming ion, and depends on many parameters. The kinetic energy of incoming ions should have a linear effect on the sputter yield, while the incident angle has a more complicated dependency. The sputter yield is largest if the sputter ions have the same mass as the materials to be sputtered, to ensure optimum energy transfer between the materials.

When an ion impact the surface of the target it can either transfer its energy or it can be reflected of the surface. The wanted process is for the ion to sputter material, however if the incident angle is too high the ion simply bounces of the surface. This often happens at structural edges and the amount of ions impacting the bottom of a structure are increased as a result. The increased bombardment at the bottom of a structure results in a local increased etch rate, a phenomenon called trenching, fig. 2.2. Trenching is seen at low incident angles where ions impact the photo resist and structure wall at glancing angles.

At higher incident angles the opposite phenomenon of an area that is not etched as much as the rest of the target is seen. This phenomenon has several names, such as tailing or hilling and is also shown in fig. 2.2. An incident angle at which trenching and tailing are counter acting each other can be found. However at such angles other unwanted effects are often present.

One typical and unwanted effect present when neither trenching nor tailing are present is material redeposition at structure and photo resist edges. The redeposition generates high thin layers of material at the edge of the photo resist which may or may not break after resist removal. In either case these "hare ears" are problematic for further processing. Redeposition at the side wall is sketch in fig. 2.2. Redeposition of mask material at the etch surface can also happen. This, however, rarely has an effect on the etch result as the redeposited material is just removed by the next incoming ions.

It is seldom that under-etching is seen in IBE due to the physical nature and hence the

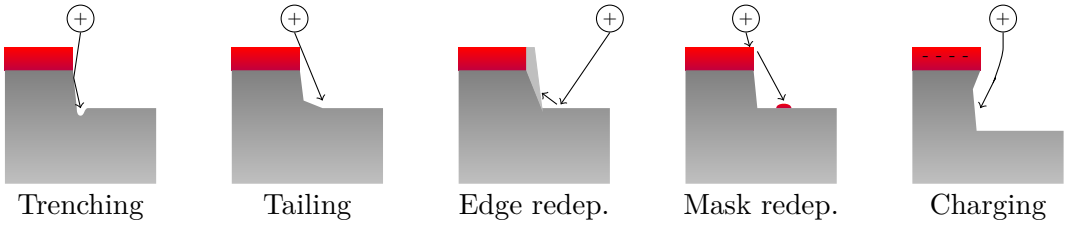

Figure 2.2: IBE effects that may distort pattern transfer. Trenching and tailing are two defects that mostly depends on the sputter angle, while etch redeposition is a common problem at low incident angles. Mask redeposition is not a big problem in IBE, while charging is only a problem for insulating materials.

line of sight etching character. However, if charging of some of the substrate such as the mask occurs, this charge might locally distort the ion path and result in under etching. These charging effects are not as common as trenching, tailing, and redeposition. A sketch of a charge influenced etch is seen in fig. 2.2.

2.2 Inductively coupled plasma reactive ion etching

The reactive ion etching (RIE) systems used in this project were both of the inductively coupled plasma (ICP) type [1]. This is referring to the technique used for plasma generation which is the same as for the IBE system. In a conventional RIE system the plasma is generated between two parallel plates over which an RF potential is applied. The sample is usually placed on the lower plate, and hence the same potential that generates the plasma is also used for ion acceleration. However, in an ICP system the potential generating the plasma and the potential which accelerates the ions towards the surface can be controlled individually, see fig. 2.3.

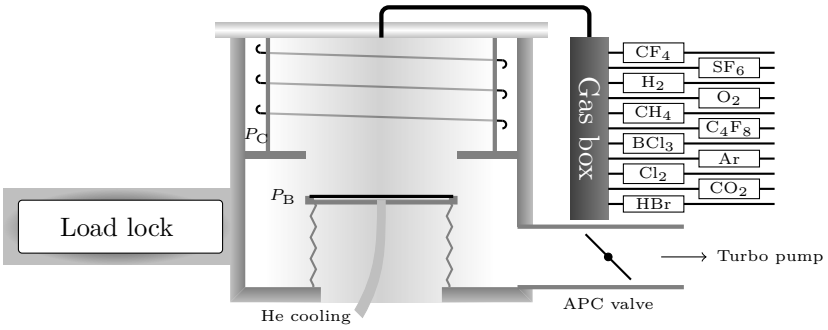

Figure 2.3: Sketch of an ICP etch system which both the ASE and ICP-metal etcher are. The plasma is generated in the top and a separate bias power is applied to enhance etching. The APC valve can either be fixed during etch or it can by controlled to keep a fixed pressure. The gases shown are not all available on both systems.

Just as for the IBE plasma source the plasma is generated by feeding one or more gases into the plasma chamber and applying power to the surrounding coil. The energy in the coil is coupled into the charged particles of the gas, which in turn by collisions with

neutral particles generates more charged particles. The generation of charged particles and the removal of ions and electrons will quickly reach an equilibrium. Particles with excited electron states emit light if relaxing, and the plasma glows, hence the name glow discharge. The color of the emitted light depends on the electron energy levels for the species and is hence a signature of the different particles available in the plasma.

The lighter electrons are accelerated to a higher speed and leaves the plasma body faster, giving raise to a positively charged plasma. The positive charge repels ions towards the chamber walls and etch substrate. However the ICP coil generates a magnetic field that helps to keep a dense plasma. To accelerate the ions towards the substrate a secondary RF power supply adds a negative potential to the substrate holder. In this setup the main acceleration of ions towards the substrate is decoupled from the plasma circuit and it is easier to tune the plasma settings.

Even though ion bombardment of the surface is important, a RIE etch including ICP-RIE is dependent on the gas composition to achieve high etch rates. For chemical etching halogens are commonly used due to their generation of high vapor pressure etch products or in some cases just high sputter yield products. High vapor pressure enables etch products to leave the surface more easily, and hence expose the underlying layer for etching. The chemical species used for etching is not molecules of the feed gas itself, but radicals and ions generated by the plasma. The ions and radicals are generated by five main process in the plasma:

Exitation:	$BCl_3 + e^- \rightarrow BCl_3^* + e^-$,
Dissociation:	$BCl_3 + e^- \rightarrow BCl_2 + Cl + e^-$,
Ionization:	$BCl_3 + e^- \rightarrow BCl_3^+ + 2e^-$,
Dissociative ionization:	$BCl_3 + e^- \rightarrow BCl_2^+ + Cl + 2e^-$,
Dissociative attachment:	$BCl_3 + e^- \rightarrow BCl_2 + Cl^-$.

Attachment processes without dissociation are not possible in low pressure plasma due to energy and momentum conservation. Other processes such as two differently charged ions exchanging an electron to generate two neutral particles can also occur. The process listed for BCl_3 above is only the first step to generate reactive species. The products of those reactions will undergo some of the same processes until the molecules are reduced to single atom ions and radicals.

The process is further complicated by the introduction of other gases to optimize the plasma composition. For the BCl_3 plasma, adding chlorine gas raises the level of chloride ions in the plasma, balancing the boron to chloride concentration which may be important to not to have too much of one specie.

At the wafer surface, reactions between the incoming particles and the surface takes place. The etchant is adsorbed on the surface, and one of three things may happen. The etchant may react with the surface layer and the product of the reaction leaves the surface. However this is based on the assumption that the etch product is volatile. If the etch product is solid another ion has to impact the surface transferring the energy needed to remove it from the surface. However, the surface reaction may not happen spontaneously and an active site in the form of an energized surface state needs to be available for the etchant to react with. These states may be generated by ion impact on the surface, transferring energy or breaking bonds between surface atoms.

The directional etch and fast etch rate obtained in RIE are due to these effects and known as ion-enhanced etching. Ion-enhanced etching may result in etch rates that are many times higher than the sum of the individual chemical and physical etch rates. This synergy between the two etch regimes enables fast etching with chemicals which is almost directional or anisotropic. However if under-etching is to be completely avoided a sidewall passivation with a molecule that is not etched in the particular etch chemistry can be used. The directional ions will then remove the passivation layer on surfaces exposed to the beam, but not surfaces that are parallel with the beam. The use of passivation is the principle behind the Bosch process, where a two step process with passivation and etch steps ensures anisotropy [19, 20, 21]. For etching of some materials adding a specie to the plasma that will react with the surface but only be removed by sputtering can be used for passivation.

One problem with the directionality that can be obtained in RIE systems is local masking due to mask redeposition. The ion impact on the masking material may sputter material from the mask to unmasked areas, see fig. 2.2. If the etch is completely directional or even a slight over passivation is taking place high thin structures may be introduced to the surface. This surface roughening is known as black silicon, however it can of course also be a problem on many other materials [79].

2.3 Design of Experiments

In this Ph.D. project experiments were in general carried out with the help of design of experiments (DoE). Plasma etching is a complicated process, with many parameters which have an influence on the result. Many of these parameters interacts to further complicate characterization of an etch response. To explain these interactions and find a path of improvement design of experiments and response surface methodology are used. Not only does design of experiments allow for explanation of interactions between parameters, it can also reduce the number of experiments needed to generate models of the significant factors for an etch outcome. Many parameters influence the etch outcome of a plasma etch, and only those parameters that from screening experiments are deemed important or interesting for the etch outcome are included in the experimental design. The exclusion of controllable parameters was done to keep the number of experiments reasonable. This chapter is based on the text book "Design and Analysis of Experiments" by Douglas C. Montgomery, [80].

A three factor factorial design can be visualized as sketch in fig. 2.4. The left part of fig. 2.4 shows the 8 measurements for the different parameters at their high or low values and a center point value. The right part shows the face centered points which experiments could be augmented with to obtain a better understanding of second order effects. The figure shows the 2^3 factorial design, however in most experiments a 2^4 factorial setup was used. This however is only a question of setting one such cube to the lower value of the fourth parameter and one the higher value. In addition all center points should be taken at the center points of all parameters and not at the high and low value of the fourth parameter.

The typical DoE in this thesis was a factorial design with three or four parameters and two or three center points. Many times the standard factorial design was not able to explain the results with the included center points. This is due to second order

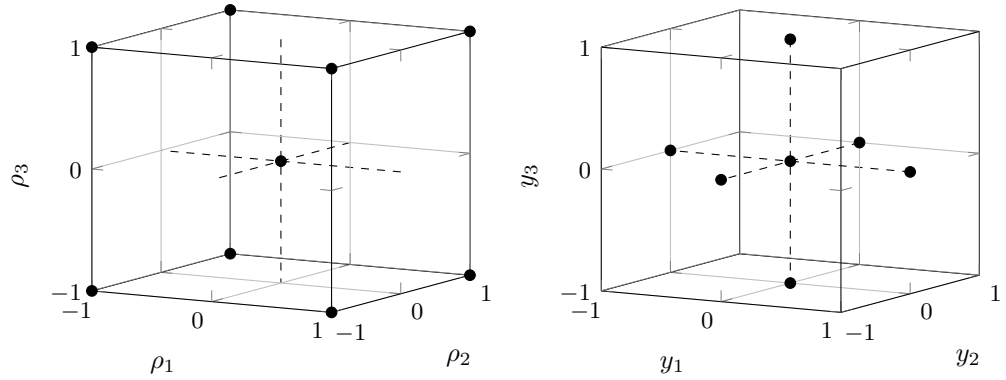

Figure 2.4: Three factor factorial DoE design with the 8 corner points and center point shown. To the right the augmented model is shown where 6 face centered point are included. Augmentation of a three factor experiment has not been used. Expansion into four parameters is simple from this point.

effects which are checked for by the center points but not explained by these. To explain curvature found in the initial experiments, face centered points were added to the design. The face center point experiments were supplemented by a couple of extra center points to ensure that the data obtained did not vary from the first set of data.

Experimental designs are generated in the software package SAS JMP, and data treatment after completion of experiments are also done by the software package. The software will calculate the response surface for a wanted response, such as etch rate, and the DoE coefficient and the corresponding level of significance (P-value) will be given. A DoE coefficient is chosen to be significant on a 5 % level of significance. Hence DoE coefficients with a P values above 0.05 will be excluded from a model. This is done one coefficient at the time, so the response surface is first calculated for all interactions included. Then if one or more DoE coefficients have P values above 0.05, the coefficient with the highest P value is removed from the model and a new response surface is calculated. This is repeated until no DoE coefficient have a P value above 0.05. However, if a parameter is included in a significant interaction, the DoE coefficient for the parameter will not be removed from the model even if it is insignificant.

Table 2.1: The table outlines an example of the reduction of a response surface design based on the level of significance. The sample response, etch rate (r), is list with regards to three parameters 1, 2, and 3.

Term	P(r)	P(r)	P(r)	P(r)
Parameter 1	$< 10^{-4}$	$< 10^{-4}$	$< 10^{-4}$	$< 10^{-4}$
Parameter 2	0.156	0.153	0.154	-
Parameter 3	0.049	0.051	0.051	0.051[a]
Interaction 1x2	0.23	-	-	-
Interaction 1x3	0.02	0.019	0.017	0.017
Interaction 2x3	0.12	0.123	-	-

[a] Included since interactions are significant.

The approach is outline in table 2.1, for design with 3 factors. In the first calculation three DoE coefficients have P values above the chosen significant level. The interaction for which the DoE coefficient is highest is removed and a new response surface is calculated. In the new response surface a DoE coefficient which in the first calculation was significant, no have a P value above the significance level. However, two coefficients have higher P values, the parameter with the largest P value is included in the interaction which have the next highest P value. Since it is included in an interaction, the interaction with the next highest P value is removed instead.

In the response surface calculated after this, two DoE coefficients are insignificant. The one with the highest P value can be removed as no interactions depends on the parameter. In the last response surface on DoE coefficient is insignificant, however this cannot be removed since an interaction including the parameter is significant. The design cannot be reduced more at this point and a plot of the response surface can be generated from the DoE coefficient listed in table 2.2.

Table 2.2: The table outlines an example of how DoE coefficient can change when insignificant parameters or interactions are removed from the design. The sample response, etch rate (r), is list with regards to three parameters 1, 2, and 3.

$\beta_{i(jk)}$	r ($\mu m\,min^{-1}$)	r ($\mu m\,min^{-1}$)	r ($\mu m\,min^{-1}$)	r ($\mu m\,min^{-1}$)
β_r	10.1	10.1	10.2	10.2
β_{r1}	5.2	5.7	5.7	5.7
β_{r2}	3.5	3.0	2.9	-
β_{r3}	1.7	1.7	1.9	1.9[a]
β_{r12}	-1.4	-	-	-
β_{r13}	-2.2	-3.1	-3.2	-3.2
β_{r23}	0.6	0.7	-	-

[a] Intercept was negligible, but included in model.

When setting up a factorial design the parameters are encoded to span from -1 to 1, ensuring that the center point is at origin. A coded value relates to the real parameters by

$$x_j = y_j \frac{x_j^{max} - x_j^{min}}{2} + \frac{x_j^{max} + x_j^{min}}{2}, \tag{2.1}$$

where x denotes the real parameters and y the coded value. The values measured, also called the response, are not given in coded values. When the coded design is used to model the expectation value of a set of parameters, these parameters must be transformed to coded values before used. Hence a model derived from DoE can be written as

$$r_i = \beta_i + \sum_j \beta_{ij} y_j + \sum_{j,k} \beta_{ijk} y_j y_k, \tag{2.2}$$

where r and β are the response and the found DoE coefficient respectively, and $_i$ denotes the measured parameter, while $_j$ and $_k$ denotes the controlled parameters. Transforming

this simple equation back to real parameters gives rather long expressions for each DoE coefficient. First eq. (2.1) is rearranged to isolate y_i,

$$y_j = \frac{2x_j - \left(x_j^{max} + x_j^{min}\right)}{x_j^{max} - x_j^{min}}. \tag{2.3}$$

By inserting this in eq. (2.2) the response as a function of the real parameters can be calculated. The response equation can be rearranged to

$$\begin{aligned} r_i = \beta_i &+ \sum_j \beta_{ij} \frac{2x_j - \left(x_j^{max} + x_j^{min}\right)}{\left(x_j^{max} - x_j^{min}\right)} \\ &+ \sum_{j,k} \beta_{ijk} \frac{4x_j x_k + \left(x_j^{max} + x_j^{min}\right)\left(x_k^{max} + x_k^{min}\right)}{\left(x_j^{max} - x_j^{min}\right)\left(x_k^{max} - x_k^{min}\right)} \\ &- 2\sum_{j,k} \beta_{ijk} \frac{\left(x_k^{max} + x_k^{min}\right)x_j + \left(x_j^{max} + x_j^{min}\right)x_k}{\left(x_j^{max} - x_j^{min}\right)\left(x_k^{max} - x_k^{min}\right)}. \end{aligned} \tag{2.4}$$

From eq. (2.4) the real coefficients can be written, by sorting for same x_j. It should be noted that for $j = k$ both contributions from the last part of eq. (2.4) must be included. The regression coefficients for the real parameter space is then;

$$\begin{aligned} \alpha_i =& \beta_i - \sum_j \beta_{ij} \frac{\left(x_j^{max} + x_j^{min}\right)}{\left(x_j^{max} - x_j^{min}\right)} \\ &+ \sum_{j,k} \beta_{ijk} \frac{\left(x_j^{max} + x_j^{min}\right)\left(x_k^{max} + x_k^{min}\right)}{\left(x_j^{max} - x_j^{min}\right)\left(x_k^{max} - x_k^{min}\right)}, \end{aligned} \tag{2.5}$$

$$\begin{aligned} \alpha_{ij} =& 2\beta_{ij} \frac{1}{\left(x_j^{max} - x_j^{min}\right)} - 4\beta_{ijj} \frac{\left(x_j^{max} + x_j^{min}\right)}{\left(x_j^{max} - x_j^{min}\right)^2} \\ &- 2\sum_{k \neq j} \beta_{ijk} \frac{\left(x_k^{max} + x_k^{min}\right)}{\left(x_j^{max} - x_j^{min}\right)\left(x_k^{max} - x_k^{min}\right)}, \end{aligned} \tag{2.6}$$

$$\alpha_{ijk} = 4\beta_{ijk} \frac{1}{\left(x_j^{max} - x_j^{min}\right)\left(x_k^{max} - x_k^{min}\right)}. \tag{2.7}$$

Looking at the regression coefficients in the real space does not tell much, since a small regression coefficient may belong to a parameter which is expected to have a large numerical change, and vice versa. This will hide the effect of a parameter in real space but make it obvious in coded space.

When contour plots are shown later in this thesis, the plots are generated from the coded regression coefficients and axis are designated in the real space. By doing this the risk of errors due to conversion between parameter spaces are minimized. In general the contour plots for a given DoE experimental run are kept with the same parameters along the axes. So if for example the etch rate has parameter β_1 along the inner x axis, the selectivity calculated from the same experiment will also have β_1 along the inner x axis. There might be exceptions from this principle, however this will then be stated in the text and in the figure caption for the corresponding figure.

In the section of each etch experiment the parameters used for the specific etch DoE is listed, with high and low values. Also the response parameters are listed and thoroughly treated in each section.

2.4 X-ray photoelectron spectroscopy

X-ray photoelectron spectroscopy (XPS) is a technique where X-rays are used for electron binding energy measurements. A surface is radiated by X-rays with a fixed energy ejecting electrons from the surface atoms. The energy ($E_{kinetic}$) of the ejected electrons is

$$E_{kinetic} = E_{photon} - E_{binding} - \phi. \tag{2.8}$$

Where the photon energy is defined by the radiation source, which for the instrument used is an AlKα monochromatic source with output light energy of 1486.88 eV. The binding energy ($E_{binding}$) is the energy needed to eject the electron from its electron shell, and is unique for each element in the periodic table. Last ϕ is an instrument work function adjusting for energy loss in the electron detection process.

XPS enables determination of the material composition in a surface layer as the ejected electrons will be from the first few nanometers of the surface. In addition to the composition of the surface material, a high resolution scan of a certain energy spectrum can reveal information of the chemical shift of single elements. The chemical shift gives information about the different types of bonds in a material. This can for example be used to distinguish alkane, alkene, and alkyne bonds and the ratio between these type of bonds for carbon.

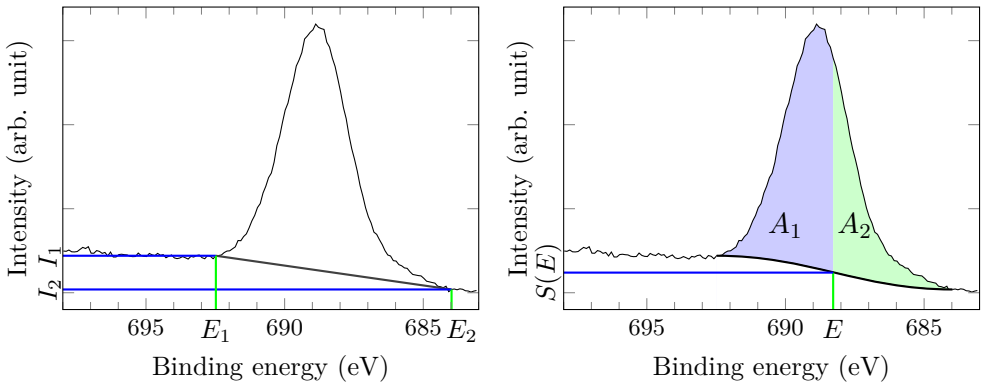

Figure 2.5: The sketch shows the different values involved in calculating the Shirley background for an XPS spectrum. The iterations starts with a linear background shown to the left and the background is accepted when no change between two calculations is found. The Shirley background looks approximately like to the right.

Finding atomic ratios of atoms and bonds is done by peak fitting Gaussian Lorentzian functions and calculating the areas of the functions which is related to the atomic concentration. Before peaks are fitted the background noise on the data must be estimated and subtracted. There are many different models for backgrounds all estimated

to the data. In this thesis a Shirley background [81] is chosen and used both for fitting in the software Avantage from Thermo Scientific and in scripts written in MATLAB. The Shirley background is calculated as a best fit to the data and is hence an iterative process.

The Shirley background at each binding energy $S(E)$ is defined as

$$S(E) = I_2 + (I_1 - I_2)\frac{A_2(E)}{(A_1(E) + A_2(E))}, \tag{2.9}$$

where I_1 and I_2 are spectrum intensities just around the peak for which the background is calculated. A_1 and A_2 are the areas spanned by the spectrum and the background at higher and lower energies than the point for which the background is calculated, see fig. 2.5. Since A_1 and A_2 in this fashion depend on the background, the background is calculated by starting with a linear background and iterating until new and old is the same. If two peaks are present in the same spectrum but with a clear separation a background for each peak is found.

When the background is calculated and subtracted from the data, peak fitting to the Gaussian Lorentzian function with a 70:30 ratio between Gaussian and Lorentzian functions can be done.

$$GL(x) = A\exp\left(-4\ln 2\left[1 - \frac{30}{100}\right]\left[\frac{x-E}{F}\right]^2\right)\left(\frac{1}{1 + 4\frac{30}{100}\left[\frac{x-E}{F}\right]^2}\right), \tag{2.10}$$

A is an amplitude since the data is not normalized, E is the peak center energy and F is the FWHM value. When fitting this function to data sets with more than one peak for an element, e.g. if the C1s peak is split in 4 chemically shifted contributions, each peak is fitted by itself. However all C1s peaks in a specific dataset should have the same FWHM and the fits are hence correlated. Also the distance between the peaks can be fixed if the different expected chemical components are known, which will constrain the binding energies. With these two constraints all peaks are fitted at the same time to ensure the best fit to the data.

In the special case of antimony the two peaks for $Sb3d_{5/2}$ and $Sb3d_{3/2}$ are close together and the $Sb3d_{5/2}$ peak is overlapping the O1s peaks. This complicates the peak fitting, however the distance and ratio between the free and well defined $Sb3d_{3/2}$ peak and the $Sb3d_{5/2}$ peak is known. This can be used to fix the $Sb3d_{5/2}$ peak before calculating the oxygen peaks and hence separate the two contributions.

Since most polymers are insulating and even though a flood gun is used to prevent charging, a small drift in the energies will be seen. The shift varies from sample to sample and will also widen the peaks. If this was not the case the energies and FWHM should be the same on all samples but small variations will occur in actual data. For fitting all data sets together a MATLAB script has been used, however the small drift in FWHM and energy values between samples resulted in poor fits. The data used in the thesis is primarily calculated by Avantage and checked with MATLAB.

2.5 Sheet resistance

For conducting structures, characterization of the sheet resistance can be used to measure line width and line spacing of devices by carefully designing a measurement structure.

Buehler and Hershey [82] describe a design for a split cross bridge, with eight measurement pads for this purpose. The structure contains a Greek cross for sheet resistance measurement, a cross bridge resistor for line width measurement, and split cross bridge for measuring the spacing between two lines. The structure is shown in fig. 2.6, three split cross bridges with different spacing were on the mask.

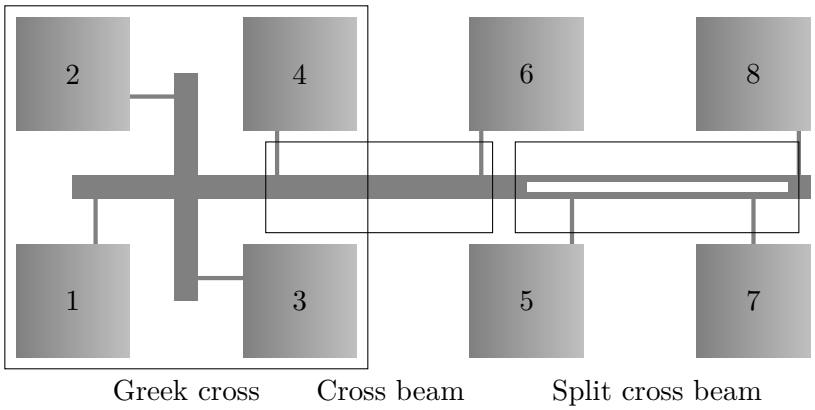

Figure 2.6: Sheet resistance can be measured on a Greek cross. With a known sheet resistance the beam width can be measure on the cross bridge. The split cross bridge allows for measurement of line spacing.

Measurement of the sheet resistance is done in two configurations on the Greek cross, where the current is forced either from opposite pads or from pads which are adjacent. The voltage is then measured on the two other pads, and the average of the two measurements is taken. This results in the sheet resistance calculated by the simplified van der Pauw relation as

$$R_s = \frac{\pi}{2\ln 2}\left(\frac{V_{12}}{I_{34}} + \frac{V_{13}}{I_{24}}\right), \tag{2.11}$$

numbers refers to fig. 2.6. When the sheet resistance is measured it becomes a simple matter to calculate the beam width and spacing. This is simply done by measuring the resistance of the beams and use the known length.

$$W_{\text{beam}} = R_s L_{\text{beam}} \frac{I_{13}}{V_{46}} \tag{2.12}$$

$$W_{\text{split beam}} = R_s L_{\text{split beam}} \frac{I_{13}}{V_{57}} \tag{2.13}$$

$$W_{\text{split}} = W_{\text{beam}} - 2W_{\text{split beam}} \tag{2.14}$$

In addition some structures for contact resistance and mask alignment have been designed as described by Walton [83]. These structures are arranged around a larger structure design to measure misalignment. The four smaller structures are for measurement of sheet resistance, contact resistance, and x and y misalignment of two layers. However the need for two layers in this project has been limited and the structures have not been used.

Chapter 3

Equipment and methods

In this project a wide range of equipment has been used for sample preparation, etching, and characterization. This chapter will introduce some of the most important pieces of equipment and should be considered in connection to chapter 2. The specific settings used on the different equipment will not be given here, as they vary quite a lot depending on the experiments that were performed.

3.1 Test mask

As part of the optimization of etching parameters a mask design with different kinds of test structures for measuring the process outcome were made. For most applications in this project a surface inspection of the etch result was the best way to check the etch characteristics. However,also some electrical test structures for testing of metal layers were included.

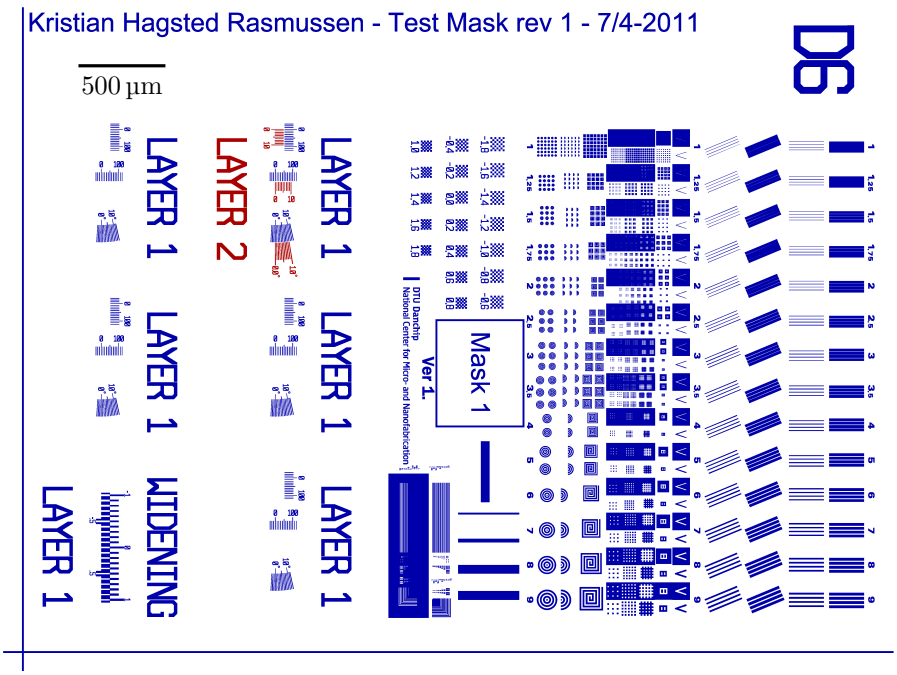

Figure 3.1: Lithography test structures for pattern transfer from resist to mask and onto substrate. The left part of the chip is a DTU Danchip text structure, while the right part is structures for measuring of misalignment.

To inspect the lithography process and the etch outcome with regards to feature size, a test structure developed by DTU-Danchip was implemented in the mask design, see fig. 3.1. The DTU-Danchip test structure is a large set of all kind of shapes varying in size from just below 1 µm and to 5 µm in small steps to enable the detection of the smallest feature size that is feasible with a process. The test structures include everything from straight lines to circles, pillars, holes, and other structures. The purpose of these structures is to check the quality of the pattern transfer from the mask to the resist and into the etched material.

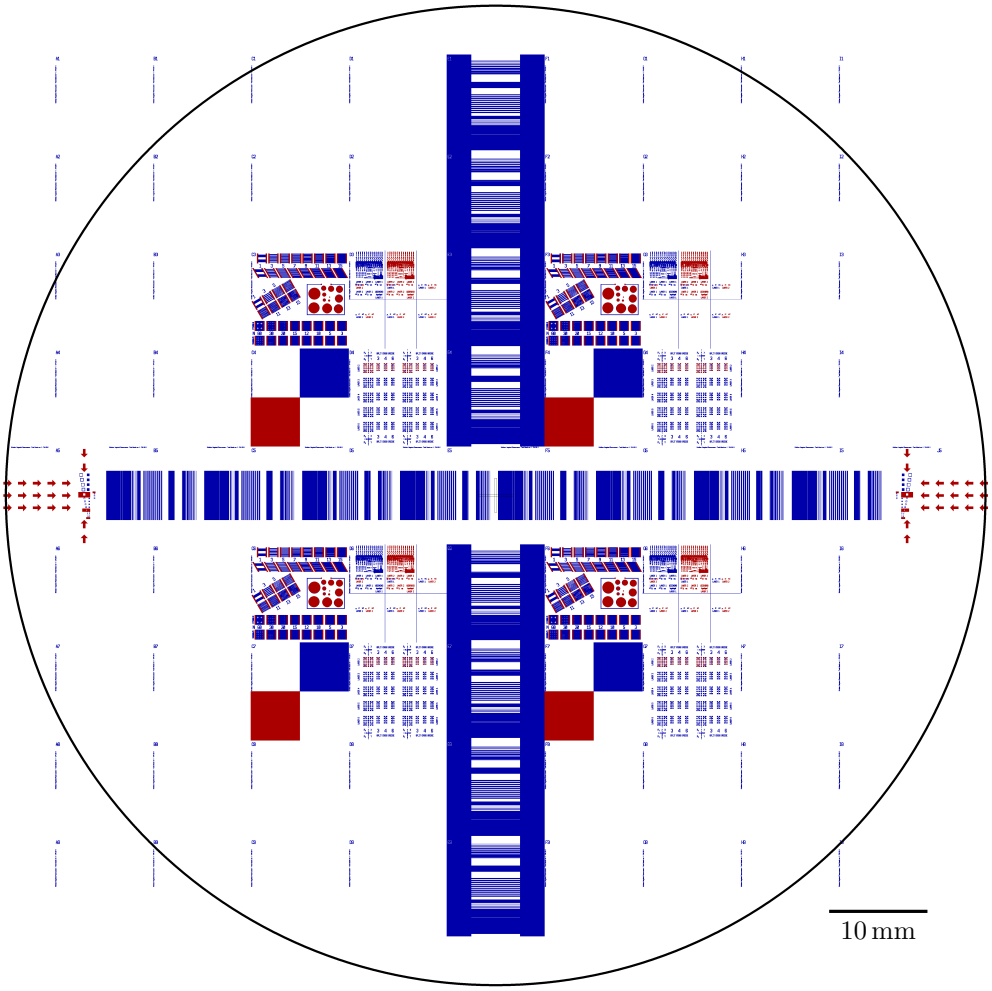

Figure 3.2: Mask 1 in red and 2 in purple as they are seen from the CAD program. The big cross structure in the center is used for most measurements of height and structure transferring. The lines in the cross are 5 mm wide to enable easy cleaving of the wafer through the lines, enabling visualization of the cross section.

Together with the DTU-Danchip structures, as set of structures to test alignment of several masking steps were placed in the mask design, also seen in fig. 3.1. The alignment tests includes structures both for measuring pattern shift and rotation compared to the first layer. In this part of the pattern there is also included at test for pattern widening in the processing. These structures were incorporated to increase the versatility of the

mask set for use when more layers are needed.

In addition to the lithography test structures, structures for inspecting the cross section of the etched wafers and easy measuring of etch depth were on the test mask. These structures are placed in a cross over the wafer as seen in fig. 3.2. The cross consist of lines with varying widths, and among others enable testing of micro loading effects. Each line is 5 mm long and if the mask and wafer are aligned reasonably well they will be parallel or more important perpendicular to a crystal direction. The alignment to the crystal direction is important as cleaving through the lines makes it possible to observe the etch profile.

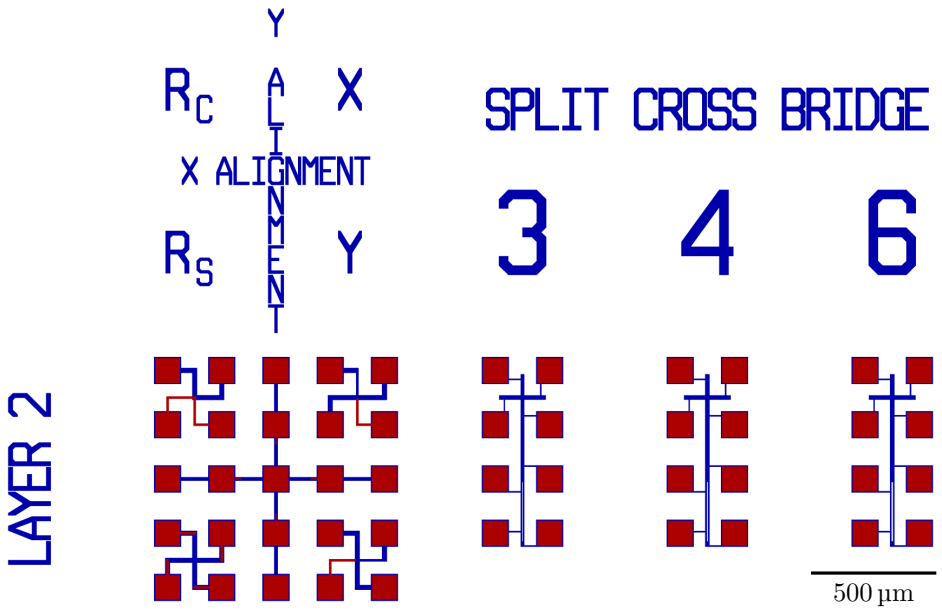

Figure 3.3: Electrical test structures for measurement of sheet resistance, misalignment, and line width reduction. The measurement structures are variations of the Greek cross, cross beam, and split cross beam structures.

Besides the structures for visual inspection, a set of structures for electrical testing is on the test mask, see fig. 3.3. These structures include structures for testing of the sheet resistance and electrical measurement of width reduction during etching and are mainly useful for metal layers and other conducting materials.

3.2 Photo resist and polymer preparation

Both photo resists and polymers are in most cases spin coated on substrates. However only for photo resist, standard recipes on automated equipment are available, while polymers are often spun manually one wafer at a time.

3.2.1 Photo lithography

Photo lithography was used for pattern transfer in most cases where the material to be etched was neither itself a photo resist nor incompatible with the solvent or developer used for lithography. The resists used were of the novolac type. In most cases, AZ5214e was used which is a positive photo resist which also can be used for image reversal. This resist enables layers from approximately 1 µm to 5 µm in thickness to be spun on wafers. When in need of thicker resist layers the AZ4562 resist was used. This is also a positive photo resist but it is not capable of image reversal. The thicker AZ4562 resist enables layers with thickness of 5 µm and above.

The use of different resist thicknesses was necessary as both IBE and ICP-RIE of polymers have a relative bad selectivity to photo resist of around 1:1. The low selectivity in IBE is a problem for all materials since it is a pure physical etch were the sputter yield is the determining factor. For polymer etching selectivity is dependent on the differences between the composition of the photo resist and the polymer to be etched.

Photo resist was applied to wafers by spin coating in a Maximus 804 resist spinner from ATM group. The resist coating recipes used were all standard recipes developed by DTU-Danchip with no modifications unless otherwise stated for the explicit experiment. The resist coated wafers were always left in a nitrogen flow box for at least 30 min to allow removal of non evaporated solvent before pattern exposure.

The exposure was accomplished by a SÜSS Mask Aligner MA6, with a constant intensity of $7\,\mathrm{mJ\,cm^{-2}}$. The exposure time was increased with resist thickness to ensure full exposure, with exposure time of 7 s for 1.5 µm resist and 20 s for 10 µm resist. Exposed resist was developed in accordance with its thickness, in some cases a little more time was spent on development if it was obvious that it was not completed after the initial time. The developer used for both AZ-resist is the NaOH based AZ351 mixed 1:5 with DI-water and heated to 22 °C before use.

If wafers had an aluminum layer as a hard mask just beneath photo resist, this layer was also etched by the developer. The aluminum removal by the developer can be used for fast fabrication of hard mask structures. However, the etching of the aluminum in developer results in decreased edge definition and rounded corners of the masking layer. These reductions in pattern quality can limit the ability to achieve all the wanted data from an etching experiment. This problem can be circumvented by using another hard mask material, but the choice is limited due to compatibility issues with the etching equipment.

3.2.2 Polymers

Polymer coating was done on four different systems, depending of the polymer in question and the upgrade to newer and more stable equipment. SU-8 coating was done on a manual RC8 Spin Coater from SÜSS dedicated to SU-8 and normal photo resist, with a syringe dispense system for the SU-8 attached. Other polymer coatings were applied first on an OPTIcoat SB20+ from ATM group, but this equipment has been unreliable, and an old manual system which is now decommissioned was used instead. However recently a new manual spinner (WS-650) from Laurell Technologies Corporation has been installed in the clean room, which has shown to be more reliable. Changing between the three systems has not been problematic as the important parameter for layer thickness is spin

speed. Specific spin and bake setting for a polymer will be given in the relevant section.

3.3 Metallization

Metal coatings were used both as the materials to be etched and for hard masks. For hard masks aluminum was preferred as this material is compatible with all etching equipment. All metallization was done in physical vapor deposition (PVD) mode, either by sputter deposition or electron beam (e-beam) evaporation.

3.3.1 Electron beam evaporation

E-beam evaporation is a line of sight deposition method with the possibility to control the deposition rate in a wide range. The line of sight deposition makes the process well suited for lift-off processes and where a low step coverage is preferred. For the projects described in this thesis the step coverage is of no significance as the materials are deposited on flat surfaces. The only exception is for a few cases of gold deposition to make contact pads with lift-off. Aluminum was used the most due to the compatibility with other equipment. Other metals were deposited for a number of small test etches with IBE of the metals in question.

Two pieces of equipment were used for e-beam evaporation depending of the number of wafers that needed to be handled. For single or only a couple of substrates the Alcatel SCM 600 system, capable of handling a single wafer at the time, was used. If more wafers needed to be coated a Wordentec QLC 800 system, capable of handling up to six wafers at a time, was preferred. The Wordentec was only chosen when many wafers needed a coating since the pumping time of the system is almost an hour.

Aluminum used for hard masks was deposited as a layer of 50 nm at a deposition rate of $10\,\text{Å}\,\text{s}^{-1}$ giving a total deposition time of approximately 50 s. The rate in both systems is not a fixed magnitude but a value at which the process parameters try to stabilize. For other materials such as gold, chromium, platinum, and titanium the rate was also $10\,\text{Å}\,\text{s}^{-1}$, but if thicker layers were needed the rate could be increased for some of the materials. All metals but gold were deposited directly on top of the substrate, whereas gold was deposited with a titanium barrier layer in between gold and silicon. This is needed because gold has a poor adhesion to silicon dioxide.

3.3.2 Sputter deposition

For some materials e-beam evaporation is not an option and instead sputter deposition can be used. In sputter deposition the material to be deposited is not evaporated by electrons, but sputtered from the surface of the target by bombardment with argon ions. Sputter deposition was mainly used for magnetic materials such as IrMn and permalloy, however for better edge definition with hard masks, sputtered silicon was used in some cases. Just as for e-beam evaporation two pieces of equipment were used for sputter deposition. For silicon sputtering the deposition part of the IonFab 300plus was used. This is the same machine as used for IBE but a different gun is used for sputtering. For all other materials that were sputter deposited a CMS series system from K. J. Lesker company was used.

Silicon sputter deposition in the IonFab 300plus is done from a relatively large target which should give a high uniformity of the deposited layer. The recipe used for silicon depositing in the IonFab 300plus was a standard recipe. In the system from K. J. Lesker group it is possible to deposit an incredibly long list of materials. The amount of materials that can be deposited in the system, does however limit wafer compatibility with other equipment, due to cross contamination with metals. For further etching the IBE part of the IonFab 300plus is used and most materials are allowed in this system, the exceptions are the highly toxic metals. Iridium manganese, permalloy, and tantalum are not toxic and have no compatibility limitations with the IonFab 300plus. One advantage of the K. J. Lesker group system is the possibility of depositing up to 6 different materials without the need to remove the sample. This ability is crucial for the fabrication of magnetic multi layer stacks, were it is important that the layers inside the stack are not oxidized.

If instead an oxidized layer is wanted, either a target of the right composition can be used or oxygen can be added to the sputter gas to oxidize the deposited layer in the deposition process. The choice between these two types of processing should be made dependent on which process gives the best layer and processing conditions. For the tantalum oxide used in this project, oxygen was added to the chamber to obtain reactive sputter deposition, as tantalum oxide targets have shown a tendency to crack.

For alloy deposition two different methods are also available, either co-sputtering from two targets at the same time or sputtering from an alloy target. With co-sputtering it is possible to control the composition of the deposited layer with a small uncertainty. If only one mixing of a material is needed, co-sputtering might be to time consuming. It can be necessary since just as for tantalum oxide targets, alloy targets can be to difficult to handle. However, both IrMn and permalloy targets are easy to work with so no co-sputtering has been used in this project.

As with other sputter processes the sputter parameters are quite similar from process to process, the small variations are due to differences in sputtering a single material compared to an alloy. The use of reactive sputtering changes the conditions somewhat more, as the sputter gas is now composed of both an inert and a reactive gas. The use of a reactive sputter gas changes the surface of the sputter target. In the case of oxygen it generates an oxide layer on the target which is non-conductive. This oxide layer is removed by continuing the sputtering after closing the shutter with the oxygen flow turned of. This ensures that the plasma in the gun can ignite for the next process run.

3.4 IonFab 300Plus

The IBE equipment available at DTU-Danchip is an IonFab 300Plus system delivered by Oxford Instrument Plasma Technology [84]. The system is a combined etching and deposition system equipped with separated ion sources for deposition and etching. The system is made for 200 mm wafers with steel carriers for etching or depositing on substrates of smaller dimensions. The system is equipped with secondary ion mass spectroscopy (SIMS) from Hiden Analytical Ltd. The SIMS is mainly used for endpoint detection even though it also can be used for destructive sample analysis.

3.4.1 Ion source

As the equipment has mainly been used for Ion Beam Etching (IBE) in this project, only the etch source will be discussed. The ion source for the etch part of the system is a 35 cm RF source with a three grid setup and a plasma filament for beam neutralization. The gas is introduced into a quartz tube surrounded by the RF-coil where the plasma is generated. The three grid setup used for the ion source consist of a screen grid, an accelerator grid, and a decelerator grid see fig. 3.4. The use of three grids and hence two separate acceleration steps enables the generation of a more columnar beam. When the ion beam leaves the last grid the neutralizer filament emits electrons into the beam to ensure charge neutrality, less spreading of the beam, and no charging of the etch target.

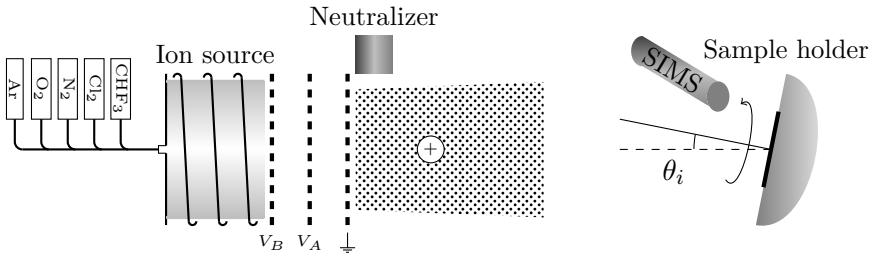

Figure 3.4: An ion beam etching system consist of an ion source where ions are generated from a gas by an electric field. The ions are extracted from the source through a set of grids, after which the beam is neutralized. The energetic ions will be used to sputter material of a sample, and the end point can be monitored by SIMS.

First the neutralizer is started to deliver electrons for beam plasma ignition. The plasma is started by introducing one or several gases into the discharge chamber. Five gases are available for the etching source; argon, oxygen, nitrogen, chlorine, and trifluoromethane. Chlorine and trifluoromethane are banned from the system when SIMS is not sealed off, to avoid damage to its delicate electronics. Hence when those two gases are wanted, the SIMS is sealed off by a special cap.

The accelerated ion beam is directed towards the sample holder which can be tilted to change the incident angle. On the equipment the angle of the substrate is given so zero is perpendicular to the beam, and this angle will be denoted incident angle θ_i. The sample is rotated during etching to ensure an even etch from all angles, around 100 rotations per etch should ensure this. All parameters are defined on the control computer, and each recipe is built from several steps.

Editing IBE recipes is a little more advanced than for most equipment. A recipe consists of a number of steps which can change different settings on the equipment. There are three types of settings that are important for normal processing which cannot be changed in the same recipe step.. The plasma settings are controlling the sputter beam and are used for the main etch step which can also be time limited. The platen settings control platen position, sample rotation and shutter positions. The last important setting is sample cooling, controlling the temperature of the sample holder and the helium backside cooling gas flow.

A normal recipe contains six steps or more, starting with a step closing all shutters and positioning the sample for the right incident angle. Then a step for turning on the

sample cooling, both the sample holder cooling and the backside helium flow. This is followed by a step starting the neutralizer and igniting a plasma without extracting ions. This step includes a short time for plasma stabilization. When the plasma is deemed stable a 2 min beam warm up is done, where the beam is turned on with the shutter still closed. This is done to have the grids reach a steady state temperature.

When the grids are warm, the plasma and beam are ready for etching and a step for shutter opening follows. When the shutter is opened the process timer is started by plasma step with. If SIMS is used it must be started manually just before the shutter opening. If SIMS is not used some sample cooling can be done post sample etching.

The tricky part with this recipe system is, that to ensure fast skips between steps, it is important to change values in all steps where they appear. This means that if changes to the plasma and beam settings are done, they must be applied in both the beam start step and in the process step. More important still is the change of sample position, because changing the incident angle takes some time and influences the etch rate. However if all steps are correctly changed a good recipe flow is ensured.

3.4.2 Secondary Ion Mass Spectrometry

The IonFab 300Plus is equipped with a Secondary Ion Mass spectrometer (SIMS) for endpoint detection when etching with inert gases. The SIMS is manufactured by Hiden Analytical. The SIMS usage is limited to inert gases to avoid damaging the detector or other parts of the SIMS by reactions with the etching gases CHF_3 or Cl_2 or any reactive species generated from these gases. To prevent these gases to enter the SIMS, a cap is fitted instead of the normal SIMS aperture which seals the SIMS from the gases in the chamber. As this cap must be fitted manually in the chamber, the system effectively has three configuration modes: deposition, etching with argon and oxygen, or etching with any gas available.

SIMS analysis is a measurement of the ions that leaves the surface of the substrate during etching. The ions are accelerated through a magnetic field, where a torque proportional to the ion mass will alter the direction of each ion. The change of direction is used to separate ions of different mass and determine which mass is be detected.

The ability to differentiate between layers, is limited by contamination from the chamber. The stainless steel used for chamber and sample holder, contains metals that might be of interest when etching for example magnetic materials. The steel contains metals such as Fe, Ni, Mn, and Cr, but also small amounts of silicon are present in the steel, resulting in a background level of significant size. The background can for samples with only small amounts of a material, make it difficult to observe the breakthrough of a layer. For deep etches the signal becomes to some degree elongated. The elongation is caused by several effects in the etching, where one of the most significant is non-uniformity of the etch, however, also the exposed sidewalls and resputtering of redeposition material contribute to the signal. The elongation of the shift from one material to another in the SIMS data is hence a good indicator of the uniformity of the etch.

3.5 Advanced Silicon Etcher

The advanced silicon etcher (ASE) used for polymer etching is a converted system made for silicon etching by Surface Technology Systems, a STS MESC Multiplex ICP system of type HC250M. The system is equipped with two RF power supplies as sketch in fig. 3.5. The main power supply (coil power) ignites and maintains the plasma with a power output of up to 3000 W. A second power supply (bias power) controls the energy of the ion flux to the etched substrate with a variable power of up to 300 W.

The system has a pressure range from 0.1 mTorr to 95 mTorr, however this is strongly dependent on the gas flow. The pressure is effectively controlled by the gas flow and a throttle valve controlling the opening to the chamber turbo pump. During etching two modes for the pressure are available, either the system can be in automatic pressure control (APC) or not. If APC is active the pressure is kept constant throughout the process by changing the valve opening. In manual mode the pressure is measured before plasma ignition and the valve is kept at a fixed opening. The use of manual mode is crucial for the Bosch process as the change of gas composition every few seconds otherwise may result in plasma quenching. However, for all processes in this thesis APC mode has been used since gas switching has not been used.

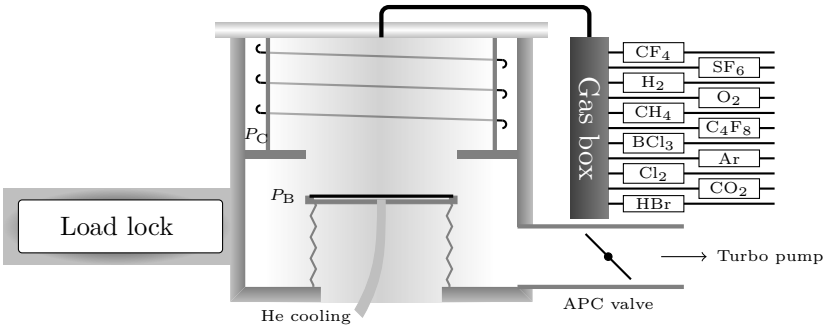

Figure 3.5: Sketch of an ICP etch system which both the ASE and ICP-metal etcher are. The plasma is generated in the top and a separate bias power is applied to enhance etching. The APC valve can either be fixed during etch or it can by controlled to keep a fixed pressure. The gases shown are not all available on both systems.

The system has several gas connections, where the silicon etching past is obvious. A typical Bosch process uses an etch step with SF_6 and O_2, and a deposition step with a polymerizing agent such as C_4F_8. These three gases and also CO_2 and Ar are available on the system. The carbon dioxide has been specifically added for the purpose of polymer etching. The different gases have different maximum flows rates, with SF_6 flow rates of 600 sccm possible, while oxygen and carbon dioxide flow rates are limited to maximum 100 sccm.

The gas is introduced in the top of a ceramic process chamber which is surrounded by the coil for plasma generation. The sample which is loaded through a load-lock is placed at the bottom of the coil and is electrostatically clamped to the sample holder. The sample is cooled by helium on the backside and the sample holder temperature can be fixed between −20 °C and 70 °C. A RF circuit applies the bias power to the sample holder, separating the sputter energy from the plasma generation. For a more detailed

description of the ICP etchers from STS see [85].

3.6 ICP-metal etcher

The ICP-metal etcher is manufactured by the same company as the ASE, however the company has changed its name between the delivery of the two systems, hence the system is from SPTS. The system is also similar to the ASE in design, see fig. 3.5

The system is similar to the ASE in design, however it is equipped with another range of gases and there are some other minor differences. The ICP-metal etcher is equipped with a larger selection of halogen gases in addition to the gases available on the ASE, but CO_2 is not available on this tool. The additional gases on the system are used to enable etching of metals that otherwise do not generate volatile etch products. The extra gases available are; CF_4, H_2, CH_4 BCl_3, Cl_2, and HBr and all except H_2 and CH_4 have mass flow controllers allowing flow rates up to 100 sccm.

The pressure range for the system is 0.1 mTorr to 100 mTorr, with the same possibility to use APC or a fixed throttle valve opening. The coil power can be up to 1500 W and bias power up to 600 W. The chuck temperature is managed through the control program and can be varied between $-20\,^{\circ}C$ and $90\,^{\circ}C$, with backside helium cooling on the wafer.

The system is equipped with an optical emission spectrometer (OES) which can be used for end point detections. It can measure on 1024 channels simultaneously and hence it is possible to obtain a reasonably high resolution data set of the emitted light from the plasma. From the emitted wavelengths different plasma species can be identified, such as chloride or aluminum chloride species. A change in the signal strength will mark a change in plasma conditions. However, since the plasma chamber is made of alumina a change in aluminum species signal is hard to detect as discussed in the results.

3.7 Characterization

For characterization of etched samples different tools have been used. For a quick glance of the structures, one of several optical microscopes available in the cleanroom has been used. For the images of surface structures used in this thesis two scanning electron microscopes have been utilized. For surface profiling two different approaches have been taken: if only a height measurement was needed a stylus profiler was used, while atomic force microscopy was used for roughness and 3D surface profiling.

To characterize the surface composition of materials X-ray photoelectron spectroscopy (XPS) enabled a quantitative measurement. For conductive materials a system for measurement of the sheet resistance-structures defined by the mask outlined in section 3.1 will also be discussed. As all the used methods are well described in literature, only a summary of the possibilities with the systems will be given.

3.7.1 Scanning electron microscopy

Two scanning electron microscopes have been used for the images in this thesis. For polymers a FEI Nova 600 NanoSEM in low vacuum mode has been used. In low vacuum mode the chamber pressure was increased to between 0.5 mbar and 0.8 mbar depending on the amount of charging. To further reduce sample charging spot size and electron

energy were also varied to some degree. Finally the detector voltage was lowered only if no other means reduced the charging. For polymers a long working distance between 5 mm and 15 mm gave the best images.

For conducting materials a Zeiss Supra 40 VP was used in high vacuum mode. Many of the images taken of conductive wafers were cross sectional images, where the wafers were cleaved along the crystal direction, by the help of a diamond pen. These wafers were mounted in a special holder so the cleaved edge of the wafer was perpendicular to the electron beam. With a working distance of only 1 mm excellent cross sectional images could be obtained by the InLens detector. A beam voltage of 5 kV was used and as the materials characterized in this system were conductive no charging wes seen.

3.7.2 Stylus profiler

For simple height measurement a Veeco Dektak 8 stylus profiler was used. The height of structures made by the mask in section 3.1 was measured over a set of 100 µm wide lines. The measurement was leveled in the software and the height was measured as the difference between two averages for the high and low level respectively. If the first measurement was curved a new measurement at the same place was taken. If this measurement was curved, a new place for measurement was found.

3.7.3 Atomic force microscopy

Surface profiles were obtained by a Bruker AXS Dimension 3100 platform Atomic Force Microscope, also called NanoMan AFM. AFM has been used for both measurements of surface roughness and surface profiles for some etches such as the ones on sapphire. Roughness measurements were done in a 10 µm × 10 µm large area with a standard tip. The surface characteristics were then calculated by the freeware program Gwyddion [86]. Surface profiles were in general measured using a standard tip, however some experiments were done with a high aspect ratio tip to achieve high definition side wall images. All AFM images in this thesis were generated with Gwyddion and all profiles were exported from the program.

3.7.4 X-ray photoelectron spectroscopy

X-ray photoelectron spectroscopy (XPS) is a method where an X-ray beam is used for analysis of a surface material composition. The analysis was carried out in a Thermo K-Alpha XPS instrument with a monochromatic Al-Kα-source and charge compensation. The equipment can only load small samples, hence the wafers that needed to be analyzed were cleaved into smaller samples with a diamond pen. For an XPS measurement the area of measurement only needs to be 400 µm × 400 µm and up to 20 samples were loaded at the same time. This allowed for overnight samples testing of a whole etch batch in one run.

The atomic concentrations of surface elements were extracted using the software package Avantage provided by Thermo or MATLAB, see section 2.4. In the Avantage software it is possible to fix or link values between different peaks. Polymer samples are non conductive hence during analysis a flood gun was used to avoid charging of samples. For

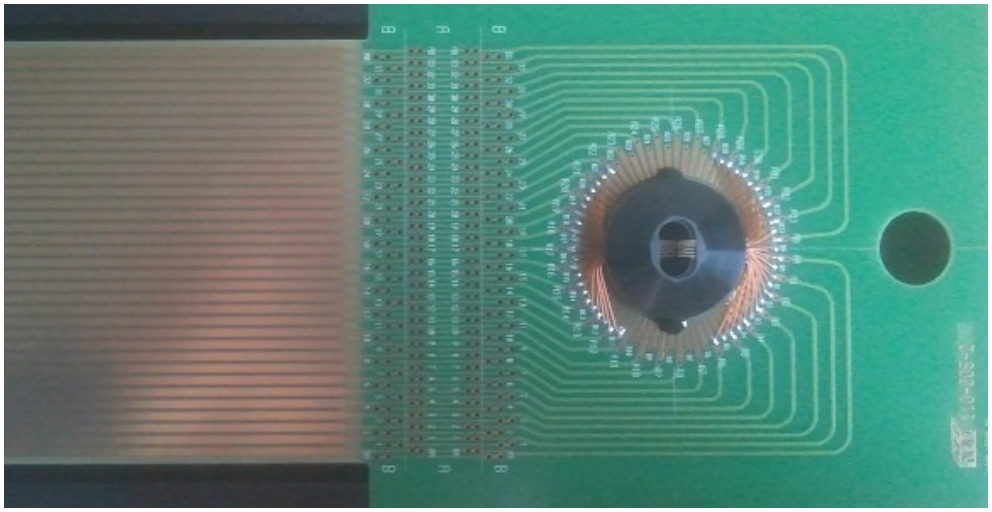

Figure 3.6: The probe card was made to fit the measurement pattern on the mask. In total 49 probes are will contact the wafer for measurement.

every sample a survey of the whole spectrum together with higher resolution spectra of elements that were of interest was done.

3.7.5 Sheet resistance

The sheet resistance was measured with an Agilent 34970A data acquisition unit, paired with a 16-Channel High-Speed Multiplexer card (34902A). For contacting the wafers a probe card with connections for all relevant measurement pads was aligned to the test pattern, see fig. 3.6. The probe card has 49 pins to connect to a complete test setup as shown in fig. 3.3. The probe card was mounted on a probe station with an insulating chuck for measurements. At the probe station fine alignment was possible by millimeter screws and the wafer could be raised to meet the probe pins.

When the probes were connected with the probe pads a slight scratching with the pins ensured a good contact to the pads. Measurements by the Agilent unit were controlled from a computer with the LabView software package. To ensure stable measurements several runs of a test were done in fast succession and the average of these measurements wes calculated. It became obvious that up to the first five measurements were incorrect, which was ascribed to a thin insulating layer that needed to be shorted by high current before actually measuring.

All electrical measurements were four point measurements on dedicated structures eliminating the need for a fixed distance between the probes.

Chapter 4

Metal and dielectric etching

For dry etching of metal and dielectrics two processes are in general used, either IBE or RIE in some form. Ion beam etching is in general used for etching of hard to etch materials, multiple thin layers, or alloys with no developed chemical etch process. For some metals, dielectrics, or alloys a chemical etch in form of a RIE process is possible and will in general have higher etch rates than the IBE process. In this project investigation on etching of a magnetic multi layer, steel, and some single metal layers have been conducted. The single metal layers were mostly etched at one setting and used for tests of the electrical test patterns included in the mask designs.

Reactive ion etching in the form of ICP-RIE was carried out on sapphire, which is known to be extremely slow to pattern by plasma etches. This becomes clear in the sense that selectivities are poor and etch rates are quite low. The etch rates, however, exceed rates obtained by IBE, as a physical etch is even more time consuming.

4.1 Magnetic stack etching

Ion beam etching is used widely in the industry to pattern stacked materials. For instance the use of magnetic layers in thin films often requires a stack of several different magnetic materials to obtain the wanted properties. At DTU-Nanotech a Hall-sensor has been fabricated by means of lift-off in a magnetic stack containing the magnetic materials iridium manganese and permalloy, [87]. These two magnetic alloys were encapsulated in tantalum, and if multiple layers were needed a thick tantalum oxide or silicon oxide was used to separate them.

Lift-off however yielded poor results with regards to many aspects of the fabricated chips, especially when two stacks of magnetic layers separated by an oxide were used. To increase the quality of the fabricated chips the use of ion beam etching was investigated instead of lift-off for structuring the layers. The use of a physical etch process is much easier than a chemically based etch since the different layers could need different chemicals.

4.1.1 Experimental

Magnetic thin-films can consist of many different alloys, which are chosen with respect to their use or in some cases their availability. At DTU-Nanotech a permalloy and iridium manganese stack sandwiched between two layers of tantalum patterned by lift-off. However, lift-off has shown some poor results for the multilayer stacks with a high number of short circuits between the layers. This problem should be eliminated by ion beam etching. For etching experiments the metal layers were deposited in the same fashion as

for lift-off, just on a blank silicon substrate. The deposition was done in a PVD-sputter system from KJ Lesker group with the possibility to control the magnetization of the deposited layers, see section 3.3.2. The metals were deposited in two steps, by first depositing the four layers in the bottom stack together with the insulating tantalum oxide layer, followed by the deposition of the four layers in the top sandwich. In between the two deposition steps the position of the permanent magnet in the chamber was rotated 180° to align the top and bottom magnetic sandwiches anti-parallel to each other. The direction of the magnetic field was also aligned to the flat of the wafer to ensure that structures made later, would have a correct magnetization.

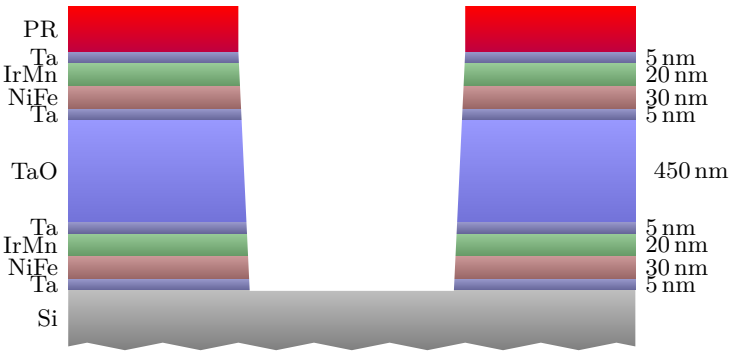

Figure 4.1: The magnetic stack of materials contains two stacks of Ta-NiFe-IrMn-Ta separated by a thick TaO layer.

The final magnetic stack is sketched in fig. 4.1 and is deposited as follows. First a layer of 5 nm tantalum was deposited by sputtering for 35 s with an argon plasma at 180 W and a bias of 3 V. This layer was followed by 30 nm of permalloy (NiFe) sputtered by a 157 W argon plasma with the same sputter bias of 3 V for 290 s. The third layer of IrMn is 20 nm thick and was deposited with the same plasma settings as for permalloy but only for 187 s. To complete the sandwich a layer similar to the first tantalum layer was deposited on top of the IrMn.

Separation of the two sandwiches of magnetic layers was achieved by a tantalum oxide layer of approximately 500 nm. This layer was deposited by reactive sputtering of the same tantalum target as used in the sandwich layers, but with oxygen added to the plasma for generation of the oxide. The amount of oxygen added to the plasma was fixed at 45 % of the argon flow, with the oxygen introduced after plasma ignition. The plasma was generated by only 80 W of power, but an increased sputter bias of 20 V. The use of reactive sputtering is a slower process than normal sputtering and hence the process time for the tantalum oxide was 5000 s. Reactive sputter deposition of tantalum oxide can sometimes result in plasma quenching and problems of re-ignition of the plasma. This is due to growth of an electric insulating oxide layer on the sputter target.

To ensure that the plasma will ignite for the next tantalum layer in the top stack, the reactive sputtering step of tantalum oxide is concluded by a short step where the oxygen flow is turned off after the substrate shutter is closed but with the plasma still on. This cleaning step in general removes the problems with ignition of the plasma in the next step. However, this is of no help if the plasma is quenched during the deposition, where some turning the plasma power off and on again in general can restart the plasma. This

however, did not guarantee that the plasma would not quench again, and hence resulted in slight variations of the thickness of the insulating layer. Plasma quenching during deposition was only seen on sputter guns, where the power supply was shared between several guns. Guns with a dedicated power supply had not problems with quenching. After the insulating tantalum oxide layer was deposited on the wafers the permanent magnet in the system was rotated 180° and the same sandwich of Ta - NiFe - IrMn - Ta was deposited.

The metalized wafers were coated with 1.5 µm photoresist of the AZ5214E type. The test mask outlined in section section 3.1 was used during a 7 s exposure followed by 70 s development with agitation in the standard NaOH based developer AZ351. The developed, rinsed, and spin-dried wafers were not treated further before etching experiments were conducted.

The optimization of the etch was done by help of DoE, with four variables, see table 4.1. The beam current (I_B) and voltage (V_B) controlling the density and energy of the sputter beam. The accelerator voltage (V_A), used to control the beam collimation translating into uniformity, and the incident angle (θ_i) which is important both for sputter yield and anisotropy. The beam current was varied between 400 mA and 500 mA. The current density was not measured, but can be estimated since the beam is extracted through a 35 cm grid. The beam voltage, responsible for the kinetic energy of the ions, was varied between 400 V and 600 V. The accelerator voltage was also varied between 400 V and 600 V. The incident angle of the beam was varied between 5° and 15°. To check for curvature and reproducibility three center point measurements were used. The resulting 19 experiments were done in random order by changing a recipe with all standard parameters between each experiment. The gas flow for the plasma and the neutralizer was kept at 10 sccm and 5 sccm respectively.

Table 4.1: The parameters used for magnetic stack etching and their corresponding coded values. All other parameters were kept constant.

		min	center	max
Coded value		-1	0	1
Beam current (mA)	I_B	400	450	500
Beam voltage (V)	V_B	400	500	600
Accelerator voltage (V)	V_A	400	500	600
Incident angle (°)	θ_i	5	10	15

The complete experiment was conducted over two days, with each etch conducted on a new wafer numbered from 1 to 19. For each etch a sample wafer was fixed to the carrier for 100 mm wafers with fixation pins in six places and the carrier was loaded into the IonFab 300plus system. The parameters for the specific DoE run were changed in the recipe and the process was started. When the beam warm-up step was reached, SIMS measurements were initiated to follow the etch progress through the layers. The SIMS data were monitored throughout the process and when the signal for the last tantalum layer disappeared the etching process was manually terminated on the etch controller. The sample holder was unloaded and left to cool to room temperature on a metal table before the wafer was removed and a new sample was loaded. The temperature of the sample and sample holder were not unreasonable high as the sample holder could be

removed from the load-lock by hand.

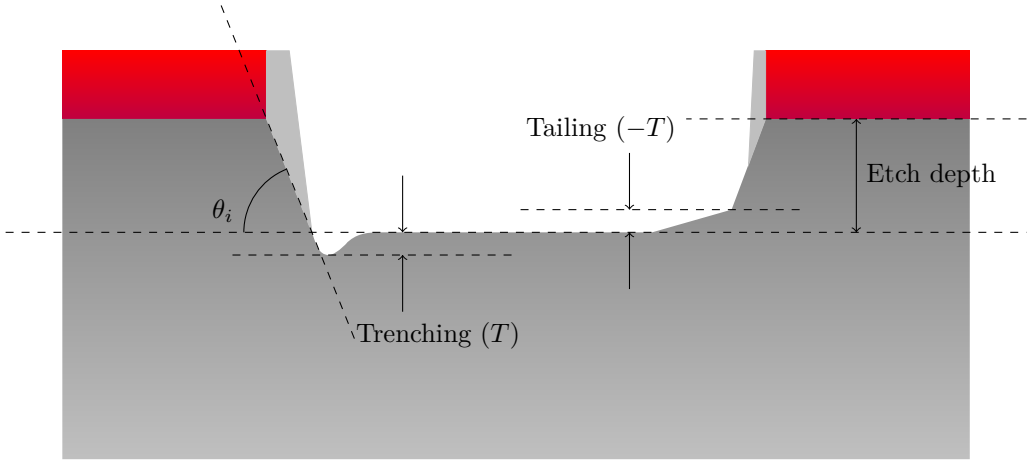

Figure 4.2: The corner angle is measured as the angle between the surface and the edge without redeposition. Trenching (tailing) is measured as the height difference between the normal etched surface and the height at the foot of the structure. The height is measured from the normal etched surface to the interface between photo resist and metal.

To get a full overview of the etched structures the wafers were cleaved along the lines in the center of the mask design. The profile of the cleaved wafers were examined by SEM and from the images the layer thickness, corner angle, and trenching was determined, see fig. 4.2. The photo resist was intentionally left on the wafers when taking the SEM images to keep the redeposited material at the resist edge visible. The remaining photo resist was stripped in acetone after the SEM visualizing and if some burning of the resist had occurred the wafer in question was left in acetone over night. Neither plasma ashing nor other more aggressive strippers were used, as these tend to be oxidizing and would then oxidize the top tantalum layer in a matter of seconds. However a thin layer of oxide will be present on the tantalum when exposed to air, but this layer is expected to protect the layers underneath, which cannot be guaranteed if an oxidizing resist removal method is used.

The sheet resistance and resistance between the top and bottom layers were measured on the designated test structures. The sheet resistance measurements were done with the probe card described in section 3.7.5. The probe station with manual probes was used for testing of short circuits between the layers.

4.1.2 Results and discussion

In the preparation of the sample wafers some problems with the sputter deposition system were experienced. Namely the sputter deposition of the tantalum oxide layer was not consistent on all wafers, since the plasma was quenched by the oxidation for some of the runs. This resulted in different tantalum oxide thicknesses on all wafers, however, a sufficiently thick tantalum oxide of more than 400 nm was deposited in between the two magnetic stacks on all wafers.

SIMS monitoring

During sample etching the composition of the sputtered materials was surveyed by means of SIMS. Two SIMS spectra are shown in fig. 4.3 which, even though they look quite similar, give valuable information about the process and samples. From a SIMS spectrum it is possible to determine which layer is currently being etched and to stop at a certain layer. Reading a spectrum from left to right, the initiation of the etch which is the same as opening the sample shutter is seen as a spike in signal for almost every material. When this spike disappears all signals except tantalum decrease to a low value indicating that a tantalum layer is at the top. This tantalum signal is only visible for a short time, since the tantalum layer is only 5 nm thick, before being replaced by a high signal of both manganese and iridium.

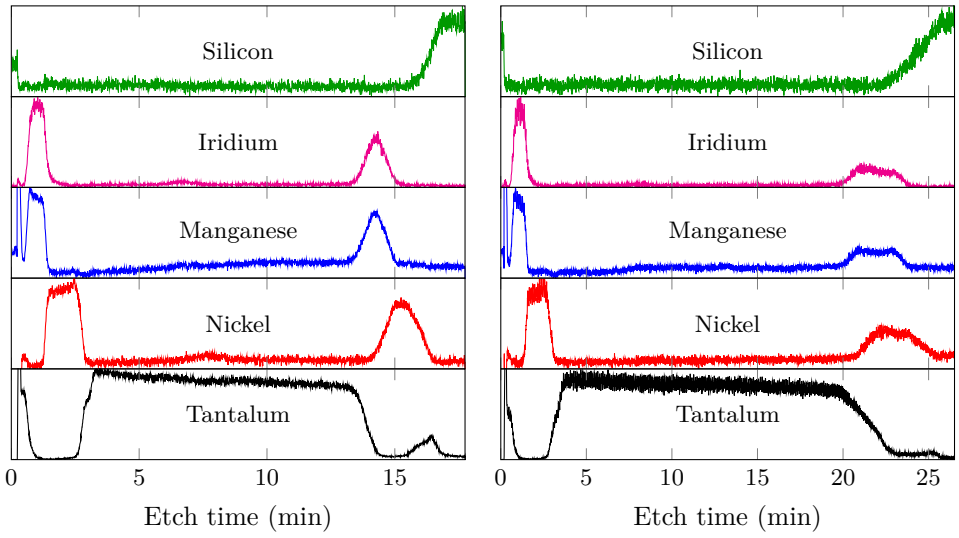

Figure 4.3: During etch the SIMS signals were monitored. When the sample shutter was opened a peak in all signals was seen, followed by a high level of tantalum, as the first tantalum layer was etched. After this the tantalum signal decreased to almost zero, while an increase in manganese and iridium were observed. When these signals decreased the nickel signal increased indicating etching of permalloy (NiFe). Iron was not monitored since the background level from steel made it indistinguishable. Following the permalloy tantalum raised again with a small step indicating the changing from tantalum to tantalum oxide. This step was not visible when the tantalum oxide was etched through. On most samples during the etch of the last stack of magnetic materials it was hard to see a separation between the different layers, which is probably due to nonuniformity of the etch. The left graph deciphers an erroneous etch where the substrate was not rotated. During the etch showed in the right graph the substrate was rotated correctly.

The time used to etch through the IrMn layer is less than the time used to etch through the underlying layer of permalloy. This is in agreement with the fact that the IrMn layer is only two thirds of the thickness of the permalloy layer. The permalloy layer is only visualized in the SIMS measurement as nickel, since the steel sample holder has three

times the area exposed to the plasma compared to the sample and hence contributes with so much sputtered iron, that changes in iron signal are hard to distinguish.

When the nickel signals starts to decline the tantalum signal raises again. During the signal increase it is possible to observe a small step in the signal before it reach a steady level. The small step marks the interface between tantalum and the thick tantalum oxide insulator. Even though tantalum oxide does not seem to etch faster than the other materials the signal is higher than for pure tantalum. This might be caused by generation of more tantalum ions compared to non charged sputtered tantalum which results in more tantalum ions detected for the oxide etch.

When the etch is through the tantalum oxide, the signals from the different materials become more stretched out, and the transition between the signals is not as clear as in the beginning of the etch. This is due to several factors, including a non uniform etch of the wafer. By non uniform etch is meant a difference in etch rate between the center and the edge of the wafer. This difference is due to an uncollimated beam with different current densities depending on the distance from the beam core.

Even though the stretched signal makes it difficult to distinguish between the last layers in the stack, all layers were easily observable except the last tantalum layer, which in many cases did not result in a clear peak but merely a continuation of a low signal. The absence of a peak did however not limit the useability of SIMS for endpoint detection, since the tantalum signal decreased to almost zero some time after the nickel signal disappeared. This final decrease of the tantalum was interpreted as the endpoint and the small signal left was ascribed to etching of the sidewalls.

If the graphs in fig. 4.3 are compared it is evident that the noise on the right figure is more pronounced. If a sine curve is fitted to the noise oscillations it becomes evident that the period on the noise is closely linked to the rotation speed of the sample. A period of 3 s is found, which is in agreement with a rotation speed of 10 rpm, when it is taken into account that the resist pattern is symmetric in one axis. The function used to fit a sine function is,

$$I = y_0 + y_1 \cdot t + A \cdot \sin\left(\frac{2\pi}{\lambda} \cdot t + \rho\right) \tag{4.1}$$

where y_0, y_1, and A are the y-offset, a correction for declining signal, and the amplitude of the signal change respectively, while λ and ρ are the period and sine offset respectively. The fit is only done where the average signal is constant, making the long tantalum oxide etch time ideal for fitting this periodicity. A sine curve fit to a part of the data from the right part of fig. 4.3 is showed in fig. 4.4. There is a good agreement in the period, however the amplitude is not correct on the figure. It is obvious that every second top is higher than its neighbors which might be due to more than one symmetry effect. If two symmetry effect are present it might be linked to a full wafer rotation and a half wafer rotation. To describe two symmetry effects a second sine part must be added to eq. (4.1) with twice the period (λ) of the first.

$$I = y_0 + y_1 \cdot t + A_1 \cdot \sin\left(\frac{2\pi}{\lambda} \cdot t + \rho_1\right) + A_2 \cdot \sin\left(\frac{\pi}{\lambda} \cdot t + \rho_2\right) \tag{4.2}$$

the A and ρ parameters are the same as above, but for each of the sine functions.

As seen in fig. 4.4 two sine waves in superposition are better able to capture the periodic variation of the SIMS signal. The fits are however not perfect due to fluctuations in the

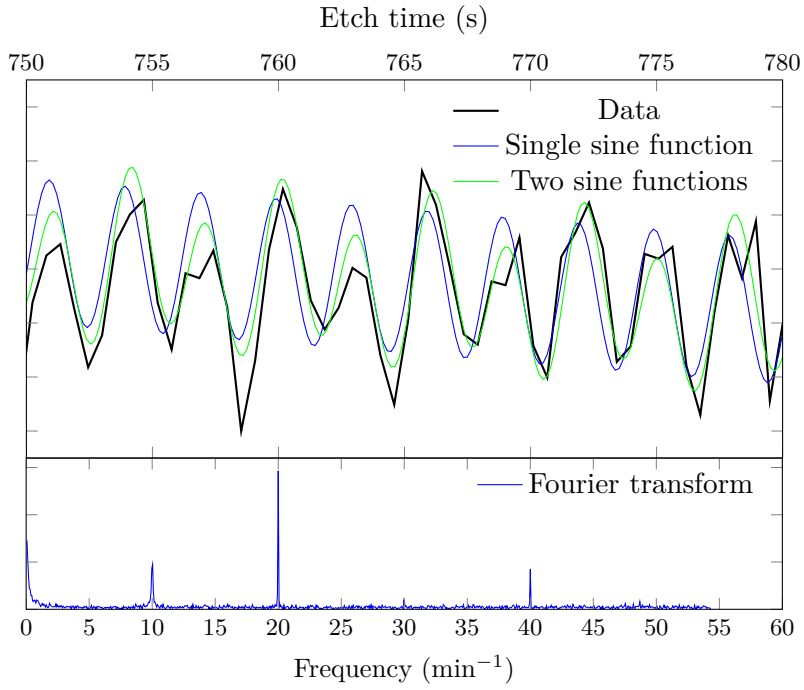

Figure 4.4: A zoom in on the SIMS signal reveals a periodic pattern in the noise signal. If a sine function is fitted to this pattern a period of half the sample rotation time is found with a small error. This can be explained by the change in material shadowed by the resist due to mask design.

SIMS signal not generated by the rotation of the wafer. From a Fourier transform it is obvious that effects for a whole, a half, and a quarter rotation of the wafer are present, see fig. 4.4. These fluctuations are ascribed to standard noise on the signal, and is seen even when the wafer are not rotated during etching. As expected the period of the wave did not change and the amplitude of the longer wave corresponding to a full rotation, was between one fourth to one fifth of the shorter wave.

On the left graph in fig. 4.3 the noise level is low, and it is not possible to obtain a good fit to a flat part of the tantalum spectrum. This is explained by an error on the equipment during etch, as the wafer was not rotated in the chamber. This resulted in an etch from one side only which is also evident in the SEM pictures. Since there is no change of beam incident angle the effect will be constant and hence the noise has no periodic component.

Pattern transfer quality

The pattern transfer quality was measured based on several criteria, namely the corner angle, the amount of redeposition, and the height of trenching. All of the above measures are found from SEM pictures, on which it was clear which wafers were not rotated correctly during the etch. The experiments where rotation did not work as intended were redone and the new results were used instead. It is not possible to give a correct measure of corner angle and trenching from the wafers which were not rotated.

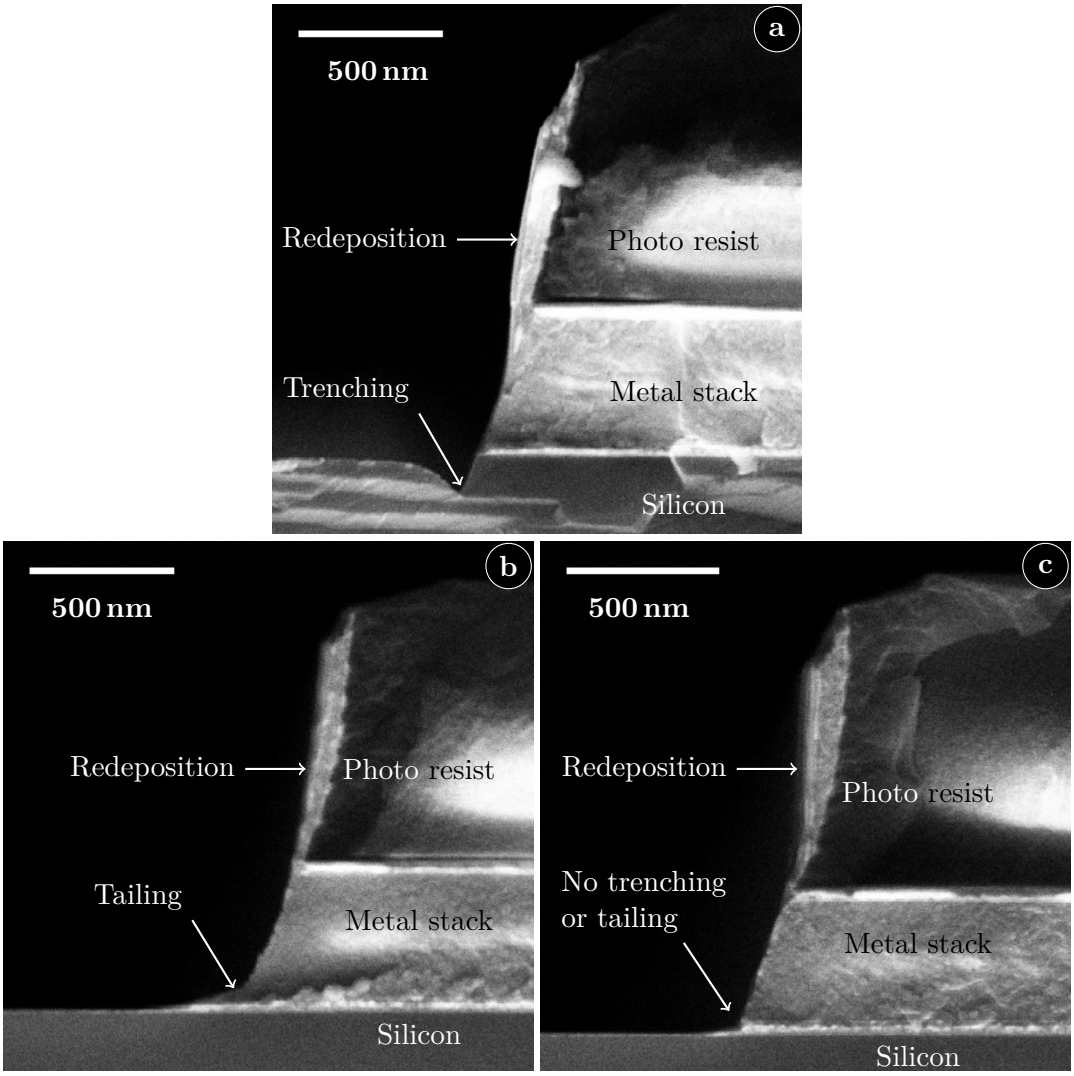

Figure 4.5: Trenching (a), tailing (b), and an etch with sharp corner definitions (c) outline the different result from the DoE experiments. Trenching has a tendency to expand shorter into the normal etch area than tailing.

Defects generated by IBE are in most cases located at the edge of the structures. In fig. 4.5 the three typical corner outcomes are shown. In fig. 4.5a trenching at the edges of the structures is seen. This often happens at low incident angles, close to perpendicular, due to ions being reflected at glancing angles at the resist walls. At higher incident angles a tendency to hilling is observed at the structural edges, seen in fig. 4.5b. In between the two cases it is possible to obtain a sharp corner, as seen in fig. 4.5c. Unfortunately this is not only dependent on the incident angle.

The corner angle measured as shown in fig. 4.2 did not show significant variations, and the small variations could not be linked to the parameter space. The corner angle is measured as the angle between the bottom of the etched trench and the sidewall without redeposition. The mean corner angle for all samples was 110.4° with a standard

deviation of 2.8°. The small deviation from the mean value was not systematic with regards to the parameters that were controlled in the etch.

Table 4.2: The DoE for the magnetic layer etching showed the following dependencies for etch rate (r) and trenching (T), on the variables beam current (I_B), beam voltage (V_B), accelerator voltage (V_A), and incident angle (θ_i). Both for etch rate and trenching some parameters were insignificant but interactions including them were not.

$\beta_{i(jk)}$	r ($\mathrm{nm\,min^{-1}}$)	P(r)	T (nm)	P(T)
β_i	18.12	$< 10^{-4}$	25.6	0.03
$\beta_{i(I_\mathrm{B})}$	0.88	0.1	-10.3[a]	0.37
$\beta_{i(V_\mathrm{B})}$	3.31	$< 10^{-4}$	-27.6	0.03
$\beta_{i(V_\mathrm{A})}$	0.24[a]	0.6	-15.7[a]	0.18
$\beta_{i(\theta_\mathrm{i})}$	-	-	59.2	$2 \cdot 10^{-4}$
$\beta_{i(I_\mathrm{B})(V_\mathrm{A})}$	-	-	-24.1	0.05
$\beta_{i(I_\mathrm{B})(V_\mathrm{B})}$	1.18	0.03	-	-
$\beta_{i(I_\mathrm{B})(\theta_\mathrm{i})}$	-	-	-29.2	0.02
$\beta_{i(V_\mathrm{B})(V_\mathrm{A})}$	-1.26	0.03	-	-
R^2		0.82		0.80

[a] DoE coefficient was negligible (P> 0.05) but include due to interactions.

The trenching and hilling as seen clearly in fig. 4.5 were measured as the height difference between the normal etch bottom and the lowest or highest point at the edge. From this measurement a clear correlation between the etching parameters and the amount of trenching were seen. In table 4.2 the values from the DoE fit are listed. From these it is clear that the incident angle has a large effect on the amount of trenching. The three other parameters in contrast have smaller contributions. The beam current and the accelerator voltage are not significant as such, but must be included in the model as their interaction is significant.

In fig. 4.6 the large effect of the beam incident angle is clearly visible. To achieve low or no trenching the beam incident angle must be around 10°, depending on the other parameters. The interaction between beam incident angle and beam current is obvious on fig. 4.6 resulting in a change in direction for increased trenching. The interaction between beam current and accelerator voltage is also easily observable.

It should be noted that the model only explains the trenching with an coefficient of determination of 80 %. This can be seen because the highest measured value for trenching is 189 nm while the model at max predicts 160 nm. Despite the limited precision of the model, it is still possible to determine the parameter space for no trenching or tailing.

In fig. 4.5 a layer of redeposited material is visible. From what has been tried in these experiments, a matching of the resist height to the etching time needed is the best way to reduce redeposition on the resist walls. If the redeposition is not limited the often high and thin walls of redeposited material will break and risk to short devices when the photo resist is removed. To remove the redeposition on already etched walls a cleaning step at high incident angle can be used with some success. This however has its limitations, since structures of a certain height will shadow each other. It will limit the height and density at which structures can be made if a sidewall clean is needed after fabrication.

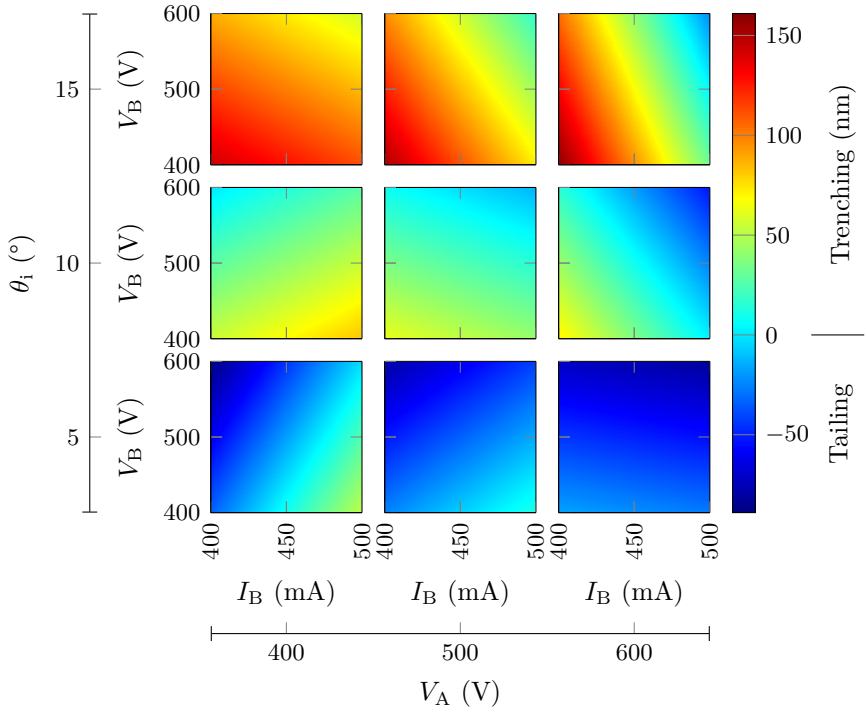

Figure 4.6: The amount of trenching or tailing were highly dependent on the etch parameters. If trenching occurred the value is positive, while a negative value is the same as tailing.

In the literature higher incident angles were used to limit the redeposition, however this will introduce tailing effects [12]. This tailing can be reduced by over etching at lower incident angle.

Etch rate

Ion beam etching of a structure containing multiple layers, like the magnetic stack etched in these experiments, may change the etch rate (R) through the stack depending on the exposed material. In these experiments this effect has been neglected due to the small thickness of the metallic alloys compared to the tantalum oxide insulator. This means that the etch rate calculated is an average for the whole stack and not a value for the single materials in the stack.

Physical sputtering of a material is a slow process as indicated by the etch rates found for the magnetic stack containing tantalum, tantalum oxide, iridium manganese, and permalloy. In table 4.2 the etch rate is around $18\,\mathrm{nm\,min^{-1}}$ (see the intercept value) for the given parameter space. In contrast to expectations the etch rate only shows dependencies on the current and the two voltages, but not on the beam incident angle. Due to the sputter yield dependency on sputter angle, it was expected that the etch rate would also depend on the beam incident angle. From the DoE result there is however no evidence that this is correct.

The etch rate depends on the beam voltage which is a measure of the energy of the

extracted ions that bombard the surface. An increase in beam voltage increases the etch rate as more energy is delivered to the surface. The beam voltage also contributes to the etch rate through interactions with beam current and accelerator voltage. The beam current is proportional to the current density of the beam, for which a higher density is the same as more ions bombarding a given area of the surface. An increase in beam current results in increased sputtering. However, for low beam voltage the current only has a small effect on the etch rate.

The accelerator voltage seems to control the variation of the etch rate for changing beam voltages. For low accelerator voltages a given change in beam voltage will result in a relatively higher change in etch rate, compared to the same scenario with a higher accelerator voltage. This means that if the stability of the etch rate is very important for a given etch, it is preferable to use a high accelerator voltage.

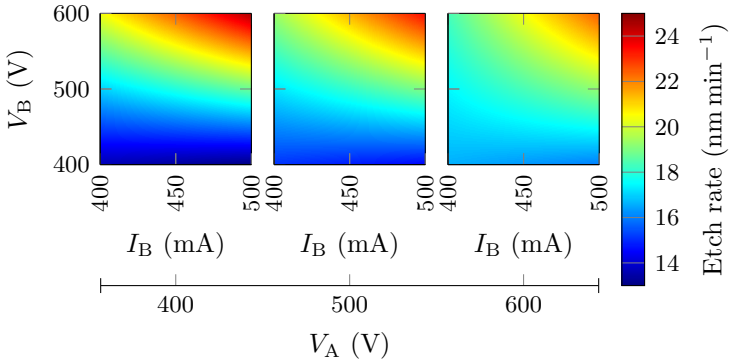

Figure 4.7: The etch rate had a clear dependency on the current and the two voltages, especially the beam voltage had a large influence on the etch rate as expected. However, there was no significant dependency on beam incident angle.

The DoE fit shown in fig. 4.7 gives a great picture of the effects described above. It does however not catch the most extreme cases, as the etch rate for a single set of parameters dropped as low as $10\,\mathrm{nm\,min^{-1}}$. Just as for the trenching model the coefficient of determination, is somewhat low with a value of 82 %. However, the model of the etch rate gives a good estimate that should be tested on the precise structure that is wanted for fabrication.

Electrical measurements

The measurements of sheet resistance did not provide any conclusive results. The measurements were hindered by a burned resist layer on top of the etched structures, limiting the ability to achieve a reliable electrical contact. The same was seen for the measurement from top to bottom layer, where it was not possible to distinguish between good or bad layer separation.

The measurement method should however not be the problem as the setup was tested on some single layer metals that where IBE etched. On these wafers with either gold, titanium, aluminum, or molybdenum it was possible to obtain good measurements of the sheet resistance with the setup. The results from the measurements were also in agreement with the expected values, and the split cross bridges could be used for char-

acterization. Even though these metals were also etched with IBE the etch times were so short that no burning of the photo resist happened. The first couple of measurements on most wafers with single metal layers gave strange results, but if measurements were redone instantly the result was fine. This was ascribed to a thin insulating layer on the contact point which could be removed by short pulses of high power.

4.1.3 Summary

Ion beam etching is ideal for etching of substrates with several stacked layers that need to be structured with exactly the same pattern. The case of a magnetic stack is a good example of how easy it is to etch through several materials without changing any parameters but still obtaining a great result. The etch rate of the purely physical etch will never be able to compete with etch with a chemical component, since the maximum etch rate achieved was $25\,\mathrm{nm\,min^{-1}}$. However, the pure physical nature enables the same etch to structure a wide variety of materials without huge differences in the outcome.

Table 4.3: The listed values will give a good corner definition, and together with a resist thickness calibrated for the etch depth limited redeposition should be possible.

		Optimal etch
Beam current (mA)	I_B	450
Beam voltage (V)	V_B	500
Accelerator voltage (V)	V_A	400
Incident angle (°)	θ_i	10

An unwanted effect of the physical etch is the large dependency on beam incident angle. In these experiments we have not seen any dependence of the etch rate on the incident angle, however the quality of the transfered pattern shows a high dependency on it. Even small changes in the beam incident angle introduced trenching or tailing near the edges of the structures. Redeposition of sputtered material on the resist walls may be a huge problem.

4.2 Steel

Ion beam etching is versatile regarding the materials that can be etched and the etching parameters do not vary much between materials. As part of the exploration of injection molding etching of steel molds has been investigated. Steel is a commonly used material to fabricate tools for injection molding. However when moving into the nano regime with injection molding new techniques are needed if steel is still to be used for tools.

Etching of steel has been investigated in collaboration with the opto-fluidics group at DTU-Nanotech and the company NIL technology. In this section an overview of IBE of steel will be given, largely based on the work of Anas Fahad Al-Azawi, who did all sample preparation. My contribution was mainly the application of IBE for pattern transfer.

4.2.1 Experimental

Wafer preparation was done by Anas and hence a short overview without parameters will be outlined here. 100 mm steel wafers were fabricated by wire-cut electrical discharge machining. On these wafers a MRI7030E resist was patterned by nano imprint lithography with a PDMS stamp cast on a silicon master. The stamp contains some line patterns with different line widths and pitches. The lines used for measurement were either 200 nm or 400 nm wide, with double the pitch.

The steel wafers were mounted on the same sample holder used for silicon wafers, however the wafers were thicker which caused some minor problems with the mounting system. A wafer is fixed to the substrate holder by six thin steel flaps. These flaps are tightened to the substrate by a screw. When a thick steel wafer had been mounted on the substrate holder the flaps had changed their form and they would bend the wrong way for good clamping of a silicon wafer. This could be solved by taking each flap off the holder and bend it back to its correct form, however this is not optimal as it will over time make the flaps more soft.

The structures were transfered to the steel substrate by an etch with standard parameters. The incident angle was varied between 8° and 30°, the beam properties were kept constant in all etches, with a beam current of $I_B = 500\,\mathrm{mA}$, and beam V_B and accelerator voltage V_A fixed to 600 V and 400 V respectively. The argon gas flows where fixed at $Q_N = 5\,\mathrm{sccm}$ and $Q_B = 10\,\mathrm{sccm}$ for neutralizer and plasma respectively.

4.2.2 Results and discussion

Etching of steel by IBE did show some promising results with selectivities of 0.83 between photo resist and steel. The etch rate was not evaluated precisely, since the criteria etching completion was complete removal of the resist layer. However, it was not determined precisely when the resist was removed during etch. Instead one wafer was etched in short steps and unloaded between the steps for visual confirmation. If resist was left on the wafer it was reloaded for further etching. With this method an etch time of 22 min was determined to be sufficient for etch completion. This results in an etch rate less than $10\,\mathrm{nm\,min^{-1}}$ which is considered to be low. Tool steel is a hard type of steel which may explain the low etch rate. A steel surface after etching is seen in fig. 4.8

The selectivity between steel and the resist was seen to increase for increasing incident angle from 8° to 30°. This might suggest increasing etch rates of steel and hence higher sputter yield for angles approaching 30°. It could on the other hand also mean lower etch rates of the polymer resist for increasing incident angles. This is however unlikely since for most materials the sputter yield is known to be highest around 30° to 50° [6]. Most likely it signals a higher increase in etch rate of steel compared to the resist.

The structure height of the 200 nm and 400 nm lines was not the same after etching. The narrow lines with smaller separation were not etched as deep as the wider lines with larger separation. As the aspect ratio is higher for the narrow lines, the mask shadows more of the bottom surface which decreases the etch rate. This effect is more pronounced at high incident angle, but is also present at lower angles.

The pattern transfer from the resist into the wafer is shown in fig. 4.9. The red curve is an AFM scan of the imprint in the resist and the blue curve is the steel structure after etching. The pattern transfer undergoes a reduction of pattern quality in the form of

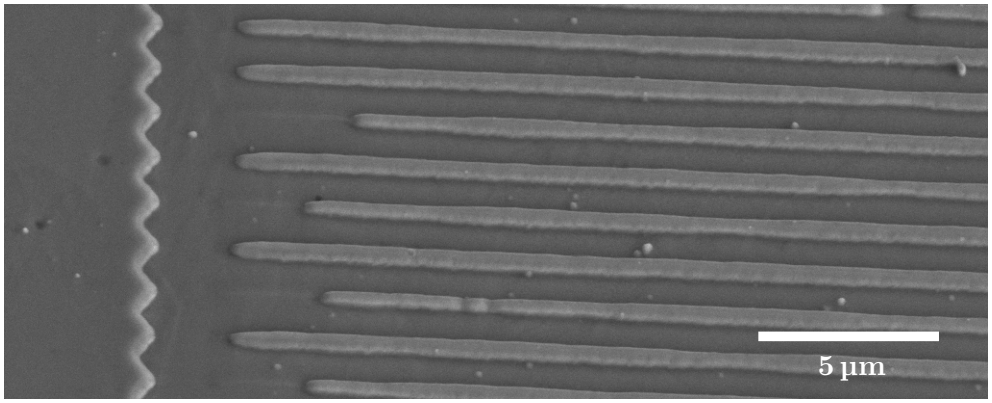

Figure 4.8: Etched lines in a steel substrate. The picture was kindly provided by Emil Søgaard.

more soft edges after etching. The reduced line width is a result of corner erosion of the resist. This is a common problem and becomes more evident with small structures.

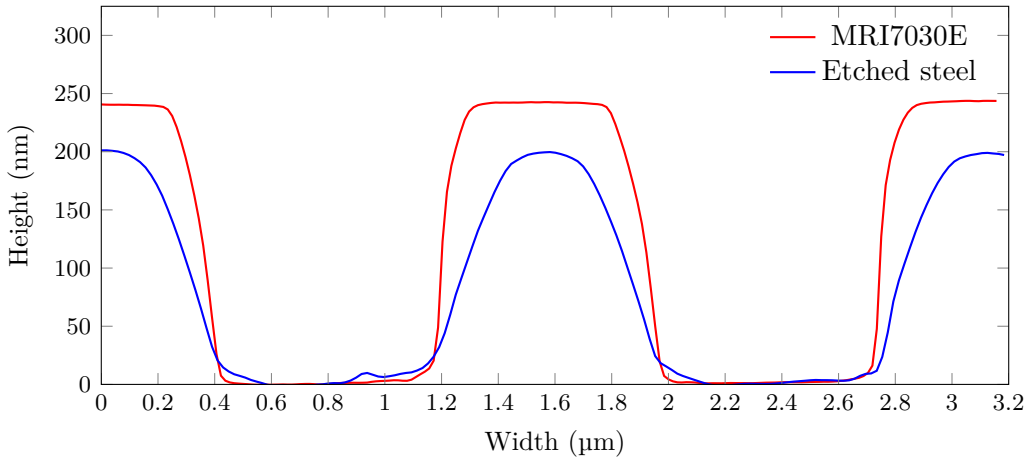

Figure 4.9: The sharp profile of the resist before etching is shown in red. After etching the steel profile (blue) is less sharp due to resist erosion. The selectivity between photo resist and steel is less than 1.

In the case where the etched pattern should be used as an injection molding tool, the rounded corners and the slight angle of the side walls may be an advantage. Separation of tool and device in injection molding is much easier if walls have a slight angle, since the polymer often expands somewhat after the pressure is remove. Hence the inclined sidewalls will facilitate easier demoulding.

4.2.3 Summary

IBE etching of steel has low selectivity and etch rate but the pattern transfer is of acceptable quality. Etch rates around $10\,\mathrm{nm\,min^{-1}}$ can be increased by increasing the beam voltage. This will however increase the substrate heating during etch, which may

be problematic if the resist needs to be removed after the etch. If the structures can be transferred to the substrate without a limit to the depth, meaning that the etch can be allowed to continue until the resist is completely removed, substrate heating is of no consequence and the beam voltage can be increased without consequences.

4.3 Sapphire etching

Patterning of sapphire (Al_2O_3) substrates is difficult since aluminum oxide has an extremely low sputter yield and low chemical etch rate. Sapphire etching can be achieved by use of a chloride based plasma etch [37, 38, 39, 40] and at the DTU-Danchip facilities the ICP-Metal etcher is used for this purpose. These experiments have been done in collaboration with Jakob Harming and Christine Thanner from EV Group in Austria.

4.3.1 Experimental

The sapphire sample wafers were 50 mm wafers prepared and shipped to Denmark by the EV Group. The 50 mm single side polished sapphire wafers have been coated with a silicon containing imprint resist. The resist has been patterned by imprint lithography in a square pattern of circles as shown by the AFM picture in fig. 4.10. The round pillars of resist are approximately 500 nm in diameter with a 900 nm pitch. The master has a structure height of 410 nm which results in an imprint height of 374 nm after resist shrinkage.

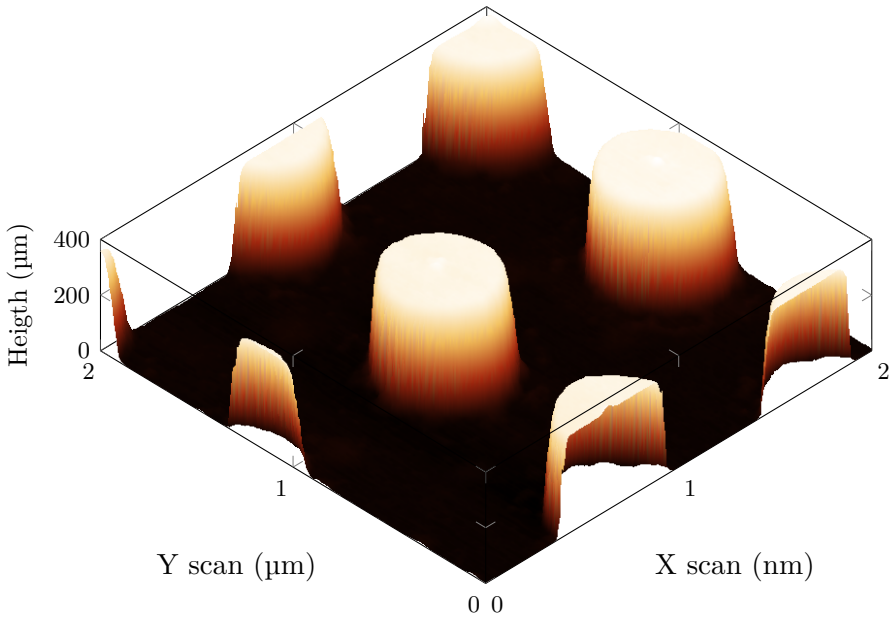

Figure 4.10: A AFM picture of the resist pattern on the sapphire wafers send by EV Group. The resist cones are 374 nm high and around 450 nm wide. This pattern covered all but the outer rim of the 50 mm wafers.

The wafers were ready for etching when I received them. Etch experiments were done in two sessions with a new batch of wafers for each session. The two individual sessions

were used to map two different pressure ranges, a high pressure range between $p_{\mathrm{hp}} = 10\,\mathrm{mTorr} and 20\,\mathrm{mTorr}$ and a low pressure range between $p_{\mathrm{lp}} = 1\,\mathrm{mTorr} and 2\,\mathrm{mTorr}$. DoE was used to map the responses in the two chosen parameter spaces, with four parameters varied in each experimental set. These four parameters are boron trichloride percentage (rest is chlorine) ($\%_{\mathrm{BCl_3}}$), bias power (P_{B}), coil power (P_{C}), and pressure (p). Both set off experiments included 18 experiments include two center points. The low pressure experiments were augmented by four experiments to explain some second order effects and therefore the results are calculated for a total of 22 experiments in the low pressure experiments.

In section 1.2.1 it is mentioned that a chloride or bromide containing plasma results in the best etch rates for sapphire. Bromide has shown to be optimal for anisotropic etching due to low mask erosion. However, the wanted structures for epitaxial growth of gallium nitride are cones with a sharp tip to minimize the stress in the grown layer. For this purpose a chloride based plasma is most optimal. Therefore the plasma constituents will be boron trichloride and chlorine, with a high level of boron trichloride.

From the literature the boron is found to be an oxygen scavenger and hence boron trichloride must be the dominant etch gas. The BCl_3 percentage is therefore varied between 75 % and 85 %. This BCl_3 content interval was used in both sets of experiments.

The bias power was varied in the interval 100 W to 300 W. Just as for the gas composition this range was kept constant for the two separate sets of experiments. Unfortunately it was not possible measure the bias voltage in the system.

The plasma is generated and controlled by the coil power which was in different ranges for the two sets of experiments. For high pressure the coil power was varied between 1 kW and 1.4 kW, while for low pressure it was necessary to reduce the coil power to between 0.8 kW and 1.2 kW. The coil power had to be reduced to enable matching of the plasma.

Two pressure ranges were used. This was done to achieve an understanding of its influence on etching output and especially on the selectivity. The high pressure range was 10 mTorr to 20 mTorr which has been used for etching of other materials in the same system. In the low pressure range the pressure was reduced by a factor ten to between 1 mTorr and 2 mTorr. This range has also been used for etching of some materials in the equipment previously.

The use of a lower pressure has some consequences for the gas flows and as mentioned for the coil power. By reducing the pressure a reduction in the flow rate was necessary to keep the APC valve opening below 50 %. The low valve opening must be used to ensure a stable and correct pressure. The total flow rate for the high and low pressure experiments was set to 100 sccm and 30 sccm respectively. The low total flow rate for the low pressure situation results in a flow rate as low as 4.5 sccm for chlorine. However from monitoring the system no fluctuation for small flow rates were observed.

The etching system is configured for use with 150 mm wafers and a silicon carrier wafer was used. This silicon wafer was prepatterned with recesses for the 50 mm sapphire wafers, the mask is shown in fig. 4.11.

The etch experiments were carried out in random order and the DoE experiments were arranged as described in section 2.3 with the parameters listed in table 4.4. Each wafer was bonded to a carrier by crystal bond which is a polymer design for heat transfer between substrates. A wafer for etch rate measurement with a thicker resist layer was

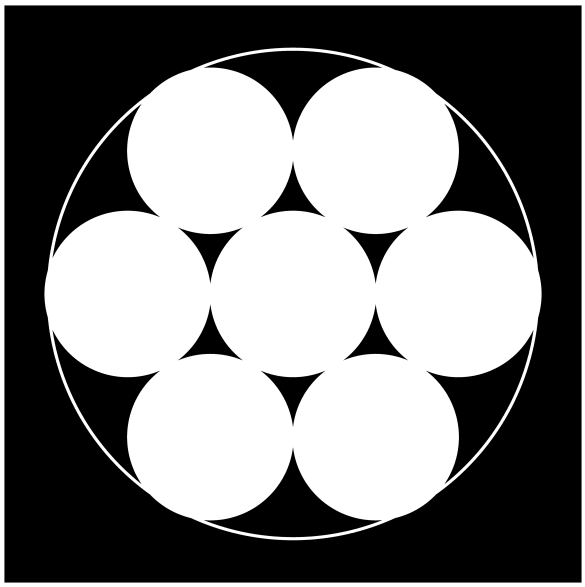

Figure 4.11: The mask for the silicon carrier was printed on a transparent foil which was used to pattern a photo resist in the KS-aligner. The flat on the 150 mm wafers was aligned to keep most of the substrates inside the carrier surface.

also bonded to the carrier. When the carrier was loaded, 5 blank sapphire dummies were placed in the remaining 5 recesses. The wafer was then transfered to the etch chamber for the experiment to start.

Table 4.4: For etching of sapphire four parameters were varied in two separate experimental runs. The values in parenthesis are for the low pressure experiment, if no parameter in parenthesis is shown the same values were used at high and low pressure experiments.

		min		center		max	
Coded value		-1		0		1	
BCl_3 percentage (%)	$\%_{BCl_3}$	75		80		85	
Pressure (mTorr)	p	10	(1)	15	(1.5)	20	(2)
Bias power (W)	P_B	100		200		300	
Coil power (kW)	P_C	1	(0.8)	1.2	(1)	1.4	(1.2)

However, before the etching experiments were done a matching optimization of the coil power was done to obtain the best etch settings. This optimization was done with a silicon wafer in the chamber as matching without sapphire wafers in the chamber did not seem to reduce the usability of the results. For the high pressure situation a different matching point was found for each DoE setting. However, for low pressure the same matching was used for all wafers since it was the only one for which the plasma could be started.

Before starting a new etch a 10 min clean of the chamber and chuck is done in an oxygen plasma. Then a change and check of the etching parameters were done and the

5 min etch was initiated. After the test of the leak-up rate for the backside helium cooling used to ensure a substrate temperature close to 20 °C, an optical emission spectroscopy measurement is initiated to follow the change in emitted plasma light.

The two bonded wafers were separated from the carrier after etch. This was achieved by submerging the carrier with substrates in water and then separated with a razor blade around the edges. The test wafer was washed in water to rinse off residues of crystal bond and then blow dried. The wafer for etch rate measurements was rinsed first in water to remove the crystal bond, then in acetone to remove the photo resist, and finally in water again. After this it was blow dried and then plasma ashed to remove the last residues of photo resist. The carrier wafer was just rinsed in water and then blow dried for later reuse.

The etch height was measured on the plasma ashed wafers placed at the edge of the carrier. This measurement was done in the stylus profilometer mentioned in section 3.7. The profile and etch depth of the device wafer was done by AFM. The area mapped was 3 µm × 3 µm, and from this area the height and profile could be found. A 2 µm × 2 µm area was used for high aspect ratio AFM scans. In addition to this SEM images were taken of the etched wafers to get an idea of the surface after the etch.

4.3.2 Results and discussion

Sapphire is one of the most difficult materials to sputter or etch by plasma, it should therefore be noted that low etch rate and selectivity are expected. The different aspects of sapphire etch will be discussed separately. However, the results for the two sets of experiments will be discussed consecutively in each section.

Etch rate

The etch rate (r) of sapphire is like for every other material relevant with regard to feasible etch depth and control of exact depth. The DoE investigation showed that several parameters and interactions were relevant for the etch rate. In table 4.5 the DoE coefficients are listed for both the low and high pressure etch, and they indicate that the pressure range significantly change the importance of the parameters.

In the high pressure range bias power, coil power, and pressure are all significant, and their contributions are quite large. Bias power has the strongest influence on the etch rate which is due to two important effects in the reaction. The bias power introduces some sputtering on the surface generating active sites where chloride ions will be able to attach. The active etch sites will be low in oxygen content, which is gettered by boron. The generated aluminum chloride has low vapor pressure, however the ion bombardment enhances the desorption. The desorption of aluminum chloride will hence be much faster than the aluminum oxide desorption.

The pressure has an inversely proportional effect on the etch rate for the high pressure range. This is due to a dense plasma where the many plasma particles reduces the energy per ion. This can to some degree be remedied by a high bias power. The interaction between bias power and pressure, as seen in fig. 4.12, clearly shows how pressure reduces the effect of bias power.

If the pressure is low the bias power allows far more control over the etch rate. It is also clear that if the coil power is increased the etch rate is increased. The explanation to

Table 4.5: Sapphire etch rate (r) is dependent on several parameters and interactions. However, the DoE coefficients which are significant depends on whether the pressure is high (hp) or low (lp). At both pressure ranges the bias power (P_B) have the largest influence on the etch rate. At low pressure all the other parameters, coil power (P_C), pressure (p), and ($\%_{BCl_3}$) have large P values and are only included due to their interactions.

$\beta_{i(jk)}$	r_{hp} (nm min^{-1})	P(r_{hp})	r_{lp} (nm min^{-1})	P(r_{lp})
β_i	47.24	$< 10^{-4}$	60.76	$< 10^{-4}$
$\beta_{i(P_B)}$	14.68	$< 10^{-4}$	11.82	$< 10^{-4}$
$\beta_{i(P_C)}$	8.80	$< 10^{-4}$	0.81[a]	0.3709
$\beta_{i(p)}$	-11.04	$< 10^{-4}$	0.12[a]	0.8937
$\beta_{i(\%_{BCl_3})}$	-	-	1.30[a]	0.1577
$\beta_{i(P_C)(p)}$	-4.98	0.0038	2.32	0.0198
$\beta_{i(P_B)(p)}$	-4.87	0.0044	-	-
$\beta_{i(\%_{BCl_3})(P_B)}$	-	-	2.33	0.0222
$\beta_{i(P_B)^2}$	-	-	-6.33	0.0057
R^2		0.96		0.94

[a] DoE coefficient was negligible (P> 0.05) but include due to interactions.

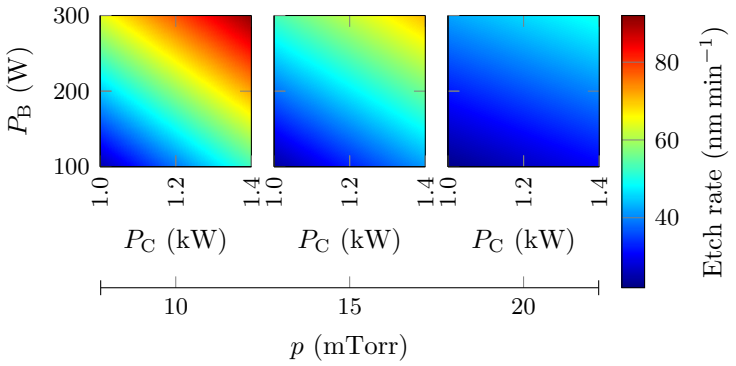

Figure 4.12: The etch rate of sapphire in the high pressure range did not show any dependency on the gas ratio. Low pressure increase the etch rate significantly. Hence the need for a second experimental run at lower pressures.

this is that increased coil power will increase the amount of ions in the plasma. Increased amount of ions negates to some degree the effect of higher pressures since larger fraction the species are accelerated.

If a lower pressure range between 1 mTorr and 2 mTorr was used the etch rate depended in a slightly different manner on the parameters. The bias power is still the parameter which has the largest influence on etch rate, but it was also the only parameter with a P$< 10^{-4}$. The three other main parameters coil power, pressure, and BCl_3 percentage were by themselves not significant. However they must all be included in the model due to interaction between parameters.

From fig. 4.13 the high dependency on bias power is obvious. This is similar as for the

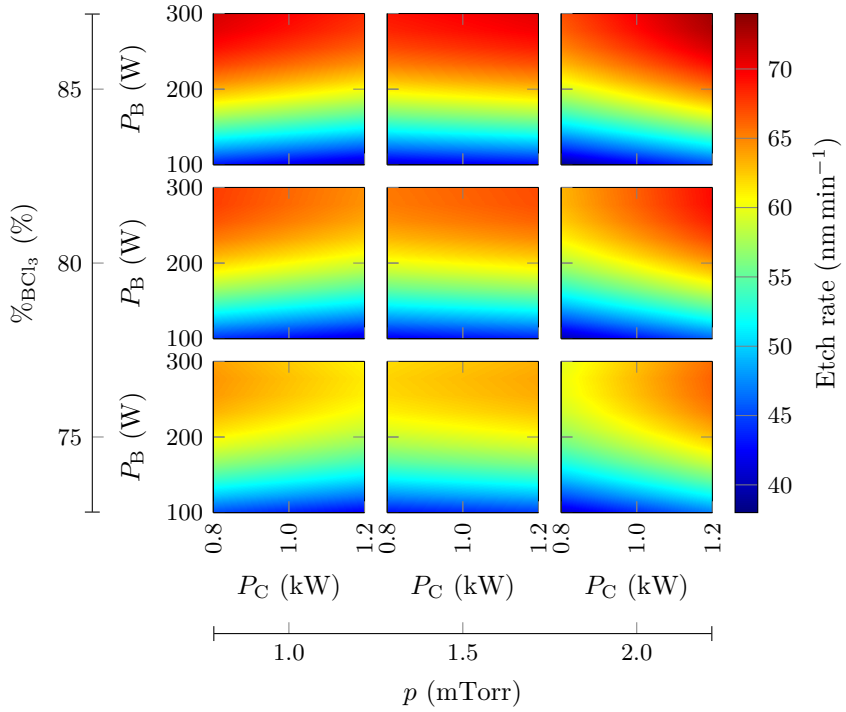

Figure 4.13: The etch rate of sapphire in the low pressures range. For low pressure the BCl_3 percentage does have an influence on the etch rate, however the bias power is the most important parameter for etch rate tuning.

high pressure range due to the increased generation of active sites plus the sputtering of aluminum chloride. Since the pressure range has been reduced significantly no real effect of the pressure and the bias power to pressure interaction are seen. This must be ascribed to the lower density plasma with a higher energy per ion.

However some second order effects in the bias power are seen which may be an indication that a certain energy is needed for onset of etching. Also the interaction between bias power and the BCl_3 percentage is significant. The higher etch rate at high bias power and high BCl_3 percentage is a result of the higher amount of heavy ions, these have a higher energy when impacting with the substrate and therefore generate more damage. At low bias power the amount of BCl_3 does not really influence the etch rate as the heavy ions do not have enough energy to be of significance.

The small effect added by the coil power and pressure interaction is ascribed to changes in the plasma composition. The composition of the plasma is dependent on the pressure and the coil power in a complex way. The amount of different etch species depends on the ionization energies of the different gases, since species can be broken down into small molecules or into atoms.

Selectivity

The low sputter yield and etch rate of sapphire limits the selectivity (S) that can be obtained between any kind of resist and sapphire. The selectivity to the masking layer

is important both with regard to the structure height obtainable and the aspect ratio. If the masks etch too fast small structures are almost impossible to achieve since there is a limit to the aspect ratio of resists. The selectivity was calculated as the etched depth on the sapphire substrate divided by the resist height before etching. Since the resist was completely removed in all etches and the structure height should be constant when the mask has been removed, the over etching should not influence the selectivity results. The goal of this etch optimization has been to reach selectivities of the order 0.5, where the resist only etches twice as fast as sapphire. The resist in use contains silicon which may reduce the selectivity compared to pure polymer resists. A selectivity close to 0.5 has been achieved by a company for EV Group, however they were not willing to disclose the etch settings.

As for etch rate Selectivity was calculated for each of the two pressure ranges used in the experiments. In table 4.6 the DoE fitted parameters are given with respect to the coded values. From the intercept (β_i) it is seen that the selectivity of the two pressure

Table 4.6: Sapphire etch selectivity (S) is dependent on all the parameters. In the low pressure (lp) range the interactions between BCl_3 to Cl_2 ratio ($\%_{BCl_3}$) and pressure (p), and bias power (P_B) and coil power (P_C) becomes significant, but there contributes are smaller than most of the pure parameters.

$\beta_{i(jk)}$	S_{hp}	P(S_{hp})	S_{lp}	P(S_{lp})
β_i	0.092	$< 10^{-4}$	0.201	$< 10^{-4}$
$\beta_{i(P_B)}$	-0.009	$3 \cdot 10^{-4}$	-0.050	$< 10^{-4}$
$\beta_{i(P_C)}$	0.005	0.0090	0.020	0.0081
$\beta_{i(p)}$	-0.017	$< 10^{-4}$	-0.018	0.0121
$\beta_{i(\%_{BCl_3})}$	0.008	$4 \cdot 10^{-4}$	0.006[a]	0.3474
$\beta_{i(\%_{BCl_3})(p)}$	-	-	0.015	0.0328
$\beta_{i(P_B)(P_C)}$	-	-	-0.014	0.0400
R^2		0.92	0.90	

[a] DoE coefficient was negligible (P> 0.05) but include due to interactions.

ranges is quite different. In the high pressure range the selectivity was low and not that variable with the parameters as seen in fig. 4.14.

In the high pressure range the selectivity depends linearly on all four parameters. The pressure is seen to have the larges effect on the selectivity, with low pressure a clear advantage. This increase in selectivity due to reduced pressure can be linked to a higher etch rate of sapphire indicating that the etch rate of the resist does not increase as fast or not at all.

For increased BCl_3 percentage the selectivity also increasesd which cannot be correlated to the etch rate. The resist contains silicon which is known to etch faster in a chlorine plasma than in BCl_3. This explains observation since the resist etch rate lower for high BCl_3 content in the plasma and hence the selectivity is higher.

As for the etch rate, the coil power also increases the selectivity slightly which again is ascribed to an increase in sapphire etch rate without a corresponding increase in resist etch rate. Inversely an increase in bias power decreases the selectivity as the sputter etching of the resist is increased.

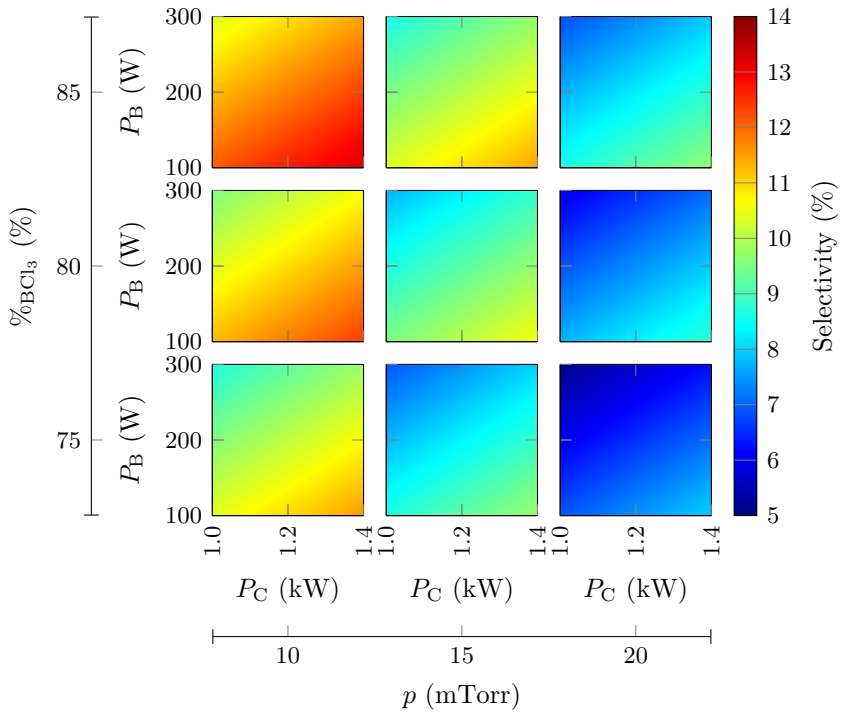

Figure 4.14: Sapphire etch selectivity over the used resist in high pressure range was poor. The results suggest that lower pressures may be the key to increase the selectivity.

The low selectivities found in the high pressure range experiments are to low for many purposes. Hence a lower pressure range has been investigated where the calculated center point value of the selectivity is more than the double compared to the high pressure range. The fitted model from the DoE is shown in fig. 4.15 where it is obvious that some interactions have been introduced.

By comparing fig. 4.14 and fig. 4.15 it is clear that the same overall trends are still present. Especially pressure, bias power, and coil power have the same influence on the selectivity, while BCl_3 percentage only has a minor effect on the selectivity in this range of pressures.

The BCl_3 percentage did however interact with the pressure so for a high pressure it did have an influence on the selectivity. This corresponds nicely with the high pressure range results where the BCl_3 percentage was important. The reason for the smaller influence of BCl_3 at lower pressures is due to the rapid exchange of chemicals in the plasma reducing the amount of different species that are generated. A small interaction between bias and coil power also changes the characteristics of the selectivity.

The coil power was lowered by 200 W to enable etching. However, from the DoE results a higher coil power should improve the selectivity. It might be possible to achieve this if further efforts are put into matching optimization. A reduction of the pressure should also improve the selectivity, but again a matching optimization is needed to start the plasma.

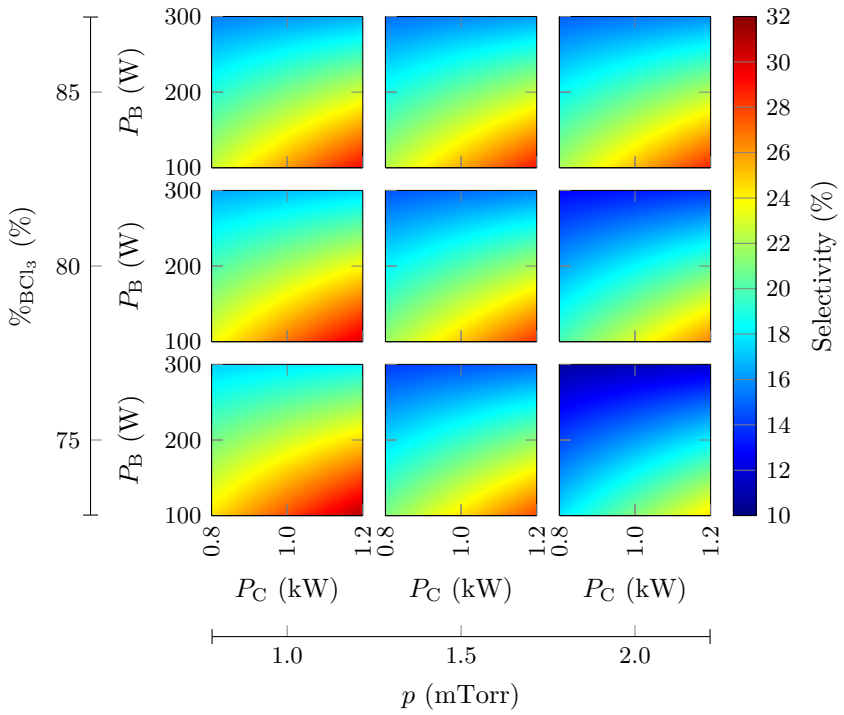

Figure 4.15: The selectivity is considerably improved in the lower pressure range. It is suggested that higher coil power and lower pressure could increase the selectivity further.

Structure replication

The surface morphology of sapphire after etching is expected to replicate the morphology of the imprint resist before etch. However, the exact shape and height of structures differs due to selectivity and mask corrosion at sharp corners. Corner corrosion will be used to transfer a square cylindrical pattern into a cone pattern in the sapphire. The cone shaped pattern is wanted for epitaxial growth of relaxed III-V materials, as mentioned in section 1.2.

The optimal shape for the etched structures is a sharp tipped cone. As seen from fig. 4.16 several shapes can be obtained by etching, from almost cylindrical shape to the cone structure wanted. In the low pressure range AFM profiles shows the same variation in structure shape, see fig. 4.17. If the etch parameters are optimized further the selectivity can be increased and the profile showed by the black curve in fig. 4.17 can be obtained.

Live etch monitoring

The etch system from SPTS used for etching of sapphire has an optical emission spectrometer mounted for measuring the optical emission lines from the generated plasma. This should in principle enable end point detection, since a drop in mask material species or an increase of aluminum species in the plasma should be visible, when the resist is completely removed. The change in aluminum species is impossible to observe, since the chamber is fabricated in aluminum and aluminum oxide. Hence species generated at the

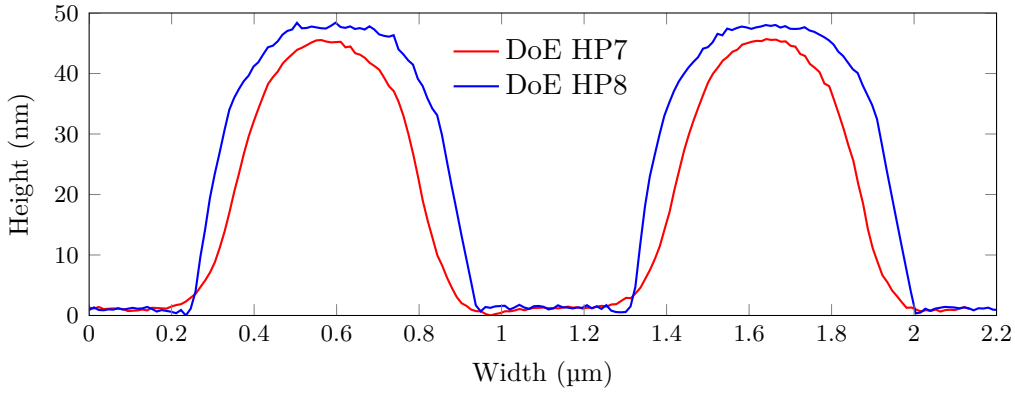

Figure 4.16: Sapphire profile after etching in high pressure range. The profiles vary in top width however they are quite low for all samples due to poor selectivity.

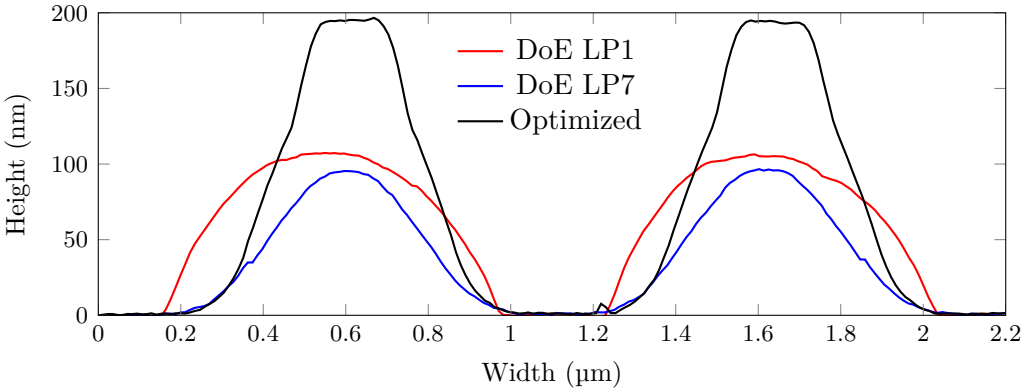

Figure 4.17: At lower pressures the sapphire profiles become higher. Their shape still varies somewhat, however an optimized etch (black curve) with a selectivity of 0.45 shows a promising shape. The optimized etch was done at $p = 0.5$mTorr, $\%_{BCl_3} = 80\%$, $P_B = 50$W, and $P_C = 1200$W.

chamber walls result in high a background of aluminum species in the chamber masking small changes.

In fig. 4.18 it is clear that no significant change can be observed in the two aluminum trend curves. A steady increase or a even level of aluminum and aluminum chloride were present in the chamber. A silicon chloride signal was expected as the imprint resist contains silicon. However, it was also not possible to see a significant change in this signal when the etch should break through the last resist residues.

It could be argued that the etch constituents should change their concentration when the complete resist removal is reached. The main consumer of etch constituents is the chamber due to its large surface area, resulting in no visible change of etch constituents, and in conclusion no change in plasma composition due to resist removal could be observed.

In some cases the end point for etching can be determined by monitoring the plasma, since a change in e.g. matching can signal a change in plasma conditions. The change in

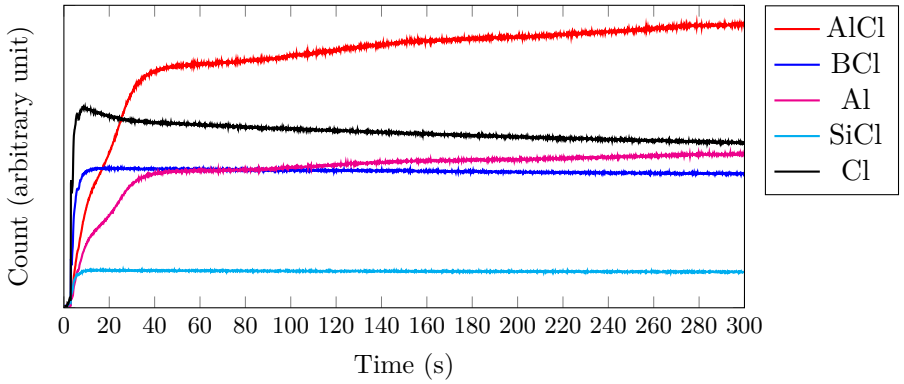

Figure 4.18: Optical emission spectroscopy was used to follow the plasma during etch. However no indication of end point could be observed.

plasma conditions could be a change in plasma constituents, which is not evident from the gas flows as these is fixed. However, in fig. 4.19 no change in either coil or bias matching is observed.

In fig. 4.19 the plasma ignition and matching are seen as peaks in the matching levels. The matching of the plasma should preferable be fast to ensure stable plasma conditions throughout an etch. A fast reaching of steady state ensures that the etch rate is reliable even at short etch times. If the matching settings are wrong it is not possible to ignite the plasma.

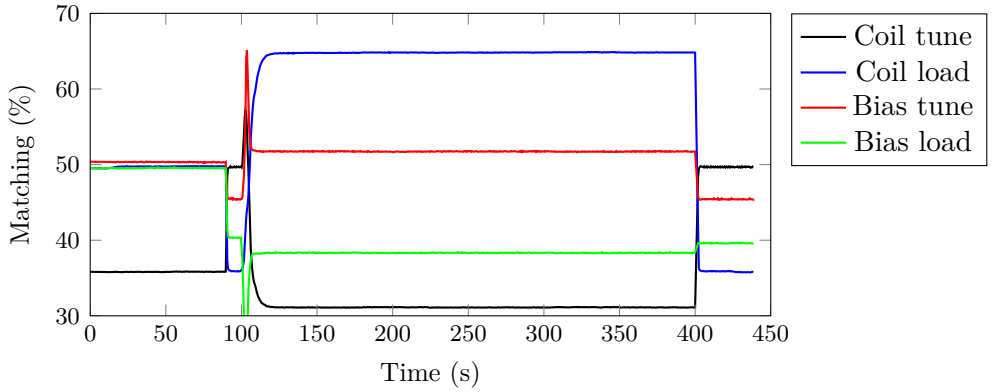

Figure 4.19: ICP coil and platen matching should be fast, and will show jumps if the plasma fails. A fail happen if large changes in the etch environment occurred, however no such jumps were seen. The jump in matching around 100 s is due to plasma ignition and at 400 s the plasma is turned off.

The matching was optimized for plasma ignition and fast reaching of steady state. For the low pressure experimental set, the same setting was used for every experiment to ensure plasma ignition. For the high pressure range, the matching was optimized separately for each set of experiments The final matching values for coil load and tune were found to depend mostly on pressure and coil power. This was expected as the coil

matching is relevant for the plasma ignition which should not depend on the bias power. The absence of a dependency on the BCl_3 percentage may be due to the low change in this parameter. The similar Lennard-Jones potential well depths for Cl_2 and BCl_3 [41] may also be a reason that no dependency on gas ratio is observed.

For the platen matching, which generates the bias power, the bias power was much more significant. However, both pressure and coil power were still significant due to their influence on the plasma composition and hence amount of ions in the plasma. For the platen matching the tune values were in general higher than the load values, while the opposite was true for coil matching.

If a significant change in the plasma composition occurs not only the matching but also a pressure control parameter should change. As pressure is fixed in the recipe the APC position would be where a change in plasma density is seen. However no sudden changes in the APC position was observed when etching sapphire.

4.3.3 Summary

In the sapphire etching outlined above, the wanted structures are almost achieved. If the resist layer can be made around 100 nm higher, the optimized etch with a selectivity of 0.45 will result in fine cones for epitaxial overgrowth. However the obtained etch rates are considerably lower than what is demonstrated in the literature. If a higher etch rate is needed more optimization of the etch must be done, where the results listed here are a good starting point for doing so.

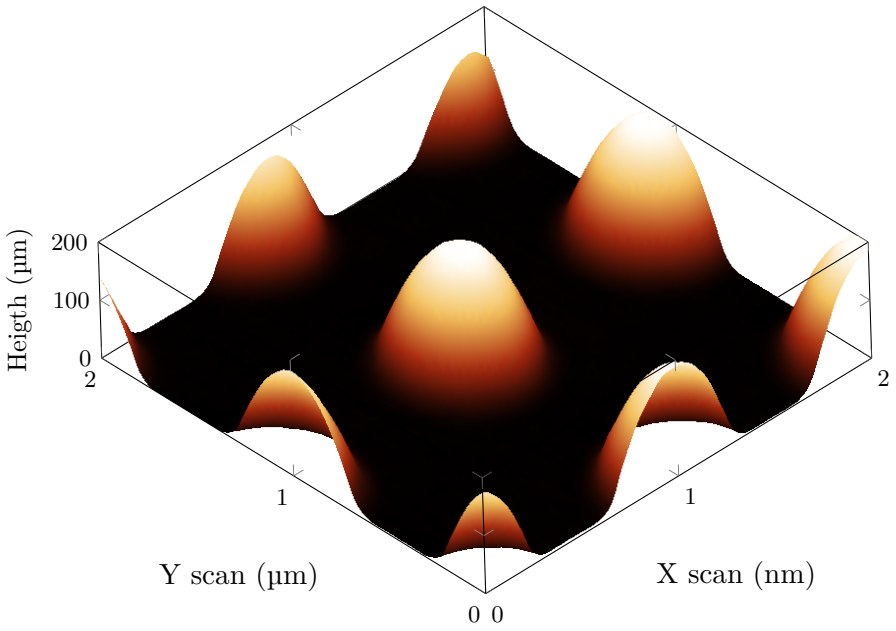

Figure 4.20: A AFM picture of the optimized etched structure. Sharp and well defined cones, which may be used for epitaxial overgrowth of GaN. The optimized etch was done at $p = 0.5$mTorr, $\%_{BCl_3} = 80\%$, $P_B = 50$W, and $P_C = 1200$W.

An AFM scan of a wafer etched with optimized parameters is shown in fig. 4.20. It should be noted that the height of the pattern is lower than for the resist pattern shown

in fig. 4.10. The shape obtained after etch has no crystal planes exposed except at the top, which would be avoided by a thicker resist before etching. The optimized etch parameters used for etching the wafer is shown in fig. 4.20 are listed in table 4.7.

Table 4.7: The etch parameters here, were used for etching of sapphire with a selectivity of 0.45 to the used imprint resist.

		Optimized etch
BCl_3 percentage (%)	$\%_{BCl_3}$	80
Pressure (mTorr)	p	0.5
Bias power (W)	P_B	50
Coil power (kW)	P_C	1.2

The cones obtained by the optimized etch as shown in fig. 4.20 are of a fine quality for epitaxial overgrowth. The sloped sidewalls with no crystal planes exposed will ensure that no epitaxial growth initiates at them. The growth will start at the flat bottom and slowly cover the cones and in the process stress release are achieved.

4.4 Metal and dielectric summary

Etching of metals, metal alloys, and dielectrics can be obtained in several ways. Ion beam etching can always be used to structure a material, no matter its properties. The rate of material removal will however always be low compared to chemical methods. Nonetheless for several purposes the low rate is of not significance compared to the advantages. Such as the ability to structure a sandwich of many different materials without the need to change the etching method. Even structuring of metals that have no known effective dry etch chemistry can be structured, with relatively good sidewall definition.

If a chemical component is added, like in all types of reactive ion etching, the synergistic nature of combined physical and chemical etching allows for faster etch rates, than otherwise possible in pure chemical or physical etching. This has for many years been used for fast, controllable, and anisotropic etching of silicon. However, many materials can benefit from this form for etching. In this project sapphire has been etched at rates that are many times higher than can be obtained by IBE. The etch was isotropic on purpose, however, it should be possible to exchange the chlorine gas with hydrogen bromide to gain both higher rates but also a more anisotropic etching.

Chapter 5

Polymer etching

As polymers become more and more common in micro systems, their etching characteristics also become more relevant. As all polymers are different variation of hydrocarbons they are expected to have several etching characteristics in common. For instance the main plasma etching constituent for all hydrocarbons is oxygen to generate volatile carbon oxide molecules. The oxygen for etching can come from several gases such as O_2, O_3, CO, CO_2, among others. At DTU-Danchip O_2 and CO_2 are available on the designated etch system, the ASE described in section 3.5. Other gases might be added to the plasma to enable removal of trace particles that are present in a specific polymer.

The polymers investigated in this project are SU-8, TOPAS®, PLLA, PCL, and PMMA. Both SU-8 and TOPAS® have been studied in detail while for the three others some preliminary experiments have been done. Therefore the last three polymers are discussed together in one section.

5.1 SU-8

Etching of SU-8 was mainly investigated on request from Letizia Amato, in regards to fabricating thin needle like structures for use in cell measurements. SU-8 is widely used in micro systems due to its easy patterning and excellent properties. However a good understanding of SU-8 etching is not readily available in literature, except that etching can be done by an oxygen plasma sometimes with the addition of fluoride. However the reason for adding of fluoride has never been explained satisfactory. The results of this study have been presented at the 38th International Conference on Micro and Nano Engineering in 2012, appendix A, and published in Microelectronic Engineering, appendix B [94].

5.1.1 Experimental

Etching of SU-8 was done in the ASE system described in section 3.5. At first some initial experiments were done to get a feeling of how SU-8 behaves in a plasma etch. The initial experiments which were done in an oxygen plasma showed severe roughening and XPS analysis was used to check the surface composition. From XPS measurements it was concluded that antimony could be the cause for the roughness and that SF_6 might help eliminate the problem. Initially the objective was to find the etch rate and anisotropy of the SU-8 plasma etching which will be discussed along with surface roughness and antimony surface concentration. Etch rate is simply measured by profilometry, while anisotropy was measured from SEM images.

The experiments were conducted after a design of experiment setup as described in section 2.3. Four important parameters were varied while the remaining parameters were kept constant. The O_2 flow rate (Q_{O_2}) was keep constant at 99 sccm, while the SF_6 flow rate (Q_{SF_6}) was varied between 0 sccm and 20 sccm. The pressure in the etch chamber was controlled to keep the gas density stable. Since the pressure has a pronounced effect on etch characteristics, the pressure (p) was varied between 20 mTorr and 40 mTorr. It should be noted that the system was run in automatic pressure control mode, which continuously adjusts the throttle valve to keep a constant pressure during the etch. The coil power (P_C) was fixed at 1000 W, while the bias power (P_B) was varied between 0 W and 30 W. Finally, the substrate chuck temperature (T) was controlled between 10 °C and 50 °C. This design resulted in a full factorial screening of four parameters, listed in table 5.1, with three center points to check for quadratic curvature. The total number of experiments in this setup is 19, which were etched for 20 min each. The experiments in the design were carried out in random order.

Table 5.1: Parameters used for SU-8 etch optimization. The four parameters were chosen after an evaluation of preliminary experiments.

Parameter		min	center	max
Coded value		-1	0	1
SF_6 flow rate (sccm)	Q_{SF_6}	0	10	20
Pressure (mTorr)	p	20	30	40
Bias power (W)	P_B	0	15	30
Temperature (°C)	T	10	30	50

After completion of the first set of experiments it was evident that curvature was present in the response. To enable data analysis and generation of a valid model for the system, the curvature was addressed by adding eight face centered points with two additional center points to the design. The ten extra experiments were also carried out in random order, and the center points were used to check for variations between the two sets of experiments. The final dataset comprises the 19 initial experiments combined with the 10 additional, giving a total of 29 experiments to characterize.

Samples for SU-8 etching were prepared on 100 mm silicon wafers with a 2 µm thermal oxide on top, following the recipe from Letizia Amato [89]. The wafers were either used directly from the oxidation furnace or baked out in an oven at 250 °C immediately before SU-8 spinning. The bake out was done to remove water from the surface, which may reduce the adhesion of SU-8 to the wafers. On the KS-Spinner, see section 3.2.2, a 25 µm layer of SU-8 2075 resist was spun on the wafers. To acheive the wanted thickness of the resist, the wafers were spun at 1000 rpm for 30 s followed by 120 s at 4000 rpm. The solvent was removed by baking the spun wafers at 50 °C for 1 h on a dedicated hot plate.

For easy measurement of height and width, the properties of SU-8 as a photo resist were used to pattern the wafers with the test mask described in section 3.1. The exposures were done with a dose of 150 mJ cm^{-2} at the I-line and the samples were baked for 2 h at 50 °C. The samples were developed in PGMEA for 5 minutes in a first development tank, followed by 5 min in a second development tank. As cleaning solvent isopropanol was used to remove the developer. Finally, to completely crosslink the polymer, samples were flood exposed with 500 mJ cm^{-2} and hard baked for 15 h at 90 °C on a hot plate.

Each wafer in the initial and in the DoE experiments was etched for 20 min, with chamber conditioning done prior to etching. The chamber conditioning was done by a 20 min chamber clean in an oxygen plasma with a blank silicon wafer loaded. For the cleaning process, the chuck temperature was always set at 20 °C. The chamber cleaning process was considered necessary to ensure stable and predictable conditions in each etch process, since the condition of the chamber walls might affect plasma etching processes. When a new substrate was loaded for etching, the temperature was set to the required value and allowed to stabilize before the etch experiment was started.

Both after sample preparation and etching, samples were characterized with respect to structure depth and width, surface morphology, and composition, see section 3.7. Structure height was measured by profilometry, and SEM images were used to characterize the structure width. Line width was measured in the center of the arrays to eliminate the influence of RIE loading present on outer lines.

The surface composition of samples was characterized using XPS, see section 3.7.4. For each sample a binding energy survey from 0 eV to 1350 eV was performed followed by detailed spectra analysis in the O1s, Sb3d, F1s, and C1s binding energy ranges. O1s and Sb3d binding energy spectra are overlapping in the area around 533 eV. Hence, the ratio and separation of antimony peaks $Sb3d_{3/2}$ and $Sb3d_{5/2}$ were fixed to 0.577 [90] and 9.34 eV [91], respectively. By doing this it was possible to find the surface concentrations of the four main elements in the surface layer: C, O, F, and Sb. Where C1s has a spectrum around 285 eV and F1s spectrum is found at 685 eV.

5.1.2 Results and discussion

The etch outcome was evaluated with four different parameters. Etch rate (r) and anisotropy (A) are important parameters for controlling etch depth and profile in etching. Furthermore, since severe roughening of the surface was observed after etch, root mean square surface roughness (R_{rms}) and surface composition were measured by AFM and XPS. The surface composition was found as the fractional atomic content of carbon [C], oxygen [O], fluorine [F], and antimony [Sb] in the polymer surface layer.

DoE was used to find parameters and interactions with a 0.05 level of significance. Parameters with a significant interaction or quadratic term were always included, even if the P-value was above 0.05. In table 5.2 the P-values are listed for the four measured responses, [Sb], r, A, and R_{rms}, and the calculated DoE coefficients are listed in table 5.3. Some interactions and quadratic terms were insignificant for all responses and are not included in the tables. The coefficients of determination (R^2) for the final models are listed in the last row of table 5.2.

Etch rate

In fig. 5.1 the influence of the four parameters on etch rate (r) is shown. The highest etch rates can be achieved at high bias power and pressure together with a SF_6 flow rate around 11 sccm. The temperature can be increased to gain a small increase in rate but does not have any pronounced effect.

The initial etch experiments showed an ability to thin SU-8 down both vertically and horizontally at reasonable etch rate. From the DoE a dependency of the etch rate on all parameters was seen, see fig. 5.1. Bias power which controls the ion energy during etch

Table 5.2: P-values of the DoE fit. Fitting a model for the responses with DoE results in the following P-values, with parameters that were negligible removed. If no value is given for a parameter or interaction it was excluded from the model. The four measured responses are Sb concentration ([Sb]), etch rate (r), anisotropy (A), and root mean square roughness (R_{rms}).

Term	P([Sb])	P(r)	P(A)	P(R_{rms})
$Q_{\mathrm{SF_6}}$	$< 10^{-4}$	0.6[a]	0.43[a]	$< 10^{-4}$
T	0.1[a]	0.006	-	-
P_{B}	0.005	$< 10^{-4}$	$< 10^{-4}$	$< 10^{-4}$
p	-	$< 10^{-4}$	0.0001	-
$(Q_{\mathrm{SF_6}})(T)$	0.02	-	-	-
$(Q_{\mathrm{SF_6}})(P_{\mathrm{B}})$	0.0007	0.03	0.0005	$< 10^{-4}$
$(Q_{\mathrm{SF_6}})^2$	$< 10^{-4}$	$< 10^{-4}$	-	$< 10^{-4}$
$(P_{\mathrm{B}})(p)$	-	0.0002	0.006	-
$(P_{\mathrm{B}})^2$	-	0.009	0.004	-
R^2	0.94	0.97	0.90	0.93

[a] Included since interactions are significant.

Table 5.3: DoE fit of dependencies. Fitting a model for the responses with DoE gives the following dependencies. Values between columns should not be compared. If no value is given for a parameter or interaction it was excluded from the model. The four measured responses are Sb concentration ([Sb]), etch rate (r), anisotropy (A), and root mean square roughness (R_{rms}).

$\beta_{i(jk)}$	[Sb] ($\%_{\mathrm{atom}}$)	r ($\mathrm{nm\,min^{-1}}$)	A	R_{rms} (nm)
β_i	2.5	0.48	0.56	9.47[a]
$\beta_{i(Q_{\mathrm{SF_6}})}$	-8.1	-0.004	-0.02	-208
$\beta_{i(T)}$	0.9	0.025	-	-
$\beta_{i(P_{\mathrm{B}})}$	1.7	0.146	0.31	144
$\beta_{i(p)}$	-	-0.061	-0.12	-
$\beta_{i(Q_{\mathrm{SF_6}})(T)}$	-1.4	-	-	-
$\beta_{i(Q_{\mathrm{SF_6}})(P_{\mathrm{B}})}$	-2.2	0.019	0.11	-166
$\beta_{i(Q_{\mathrm{SF_6}})^2}$	7.6	-0.19	-	207
$\beta_{i(P_{\mathrm{B}})(p)}$	-	-0.039	0.08	-
$\beta_{i(P_{\mathrm{B}})^2}$	-	-0.05	-0.13	-

[a] Intercept was negligible, but included in model.

had the largest effect on the etch rate. Increased bias power led to faster etching, either due to sputtering on top of the chemical etch by oxygen, or more likely ion-enhanced etching [92], where the ion bombardment of the surface generates active sites for easier initiation of chemical etching. Supporting the hypothesis of ion-enhanced etching, the gain in etch rate was more significant for low bias powers. This might be an indication of a threshold for which the enhanced chemical etching starts. Such a threshold should

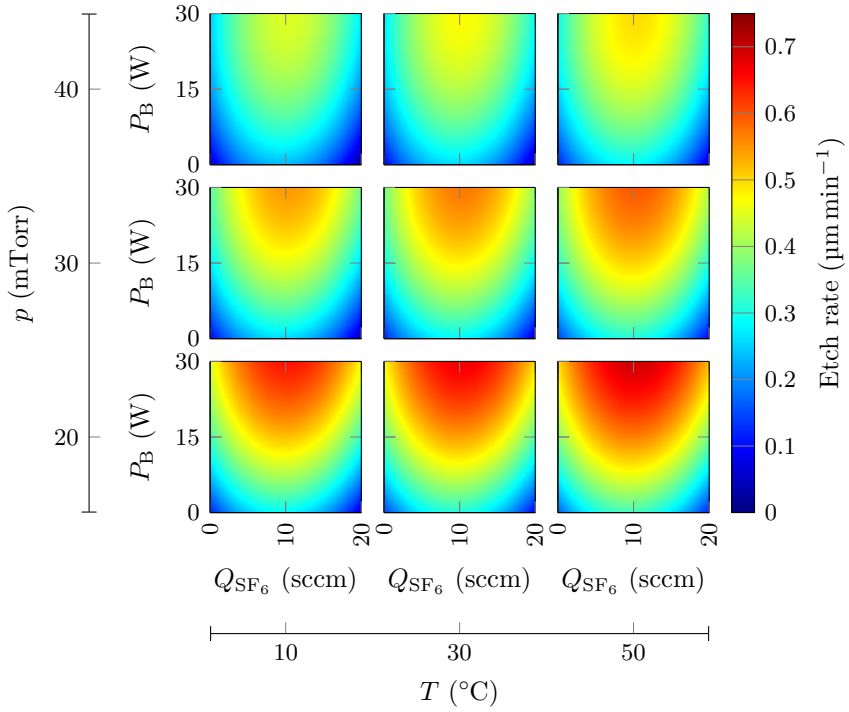

Figure 5.1: Etch rate (r) as a function of etch parameters. Etch rate showed a dependency on all parameters. Q_{SF_6} and P_B both have a strong influence on etch rate. p also affected the etch rate significantly with higher p resulting in lower etch rates. T only slightly influences etch rate and does not interact with any of the other parameters.

however not be given as a bias power, but as bias voltage which translates to an ion energy. The energy of the bombarding ions needs to be above the activation energy of ion enhanced etching. Since no experiments have been done with a bias power between 0 W and 15 W it is not possible to give a precise estimate of the bias power needed to gain ions with a high enough energy.

The SF_6 flow rate to the second order, also significantly affected the etch rate. The response showed curvature with reduced etch rate for both high and low SF_6 flow rates. For low SF_6 flow rates antimony accumulates at the surface, resulting in partial masking of the surface which reduces the etch rate. The decrease in etch rate at higher SF_6 flow rates might be explained by reactions between SF_5 radicals and O, which will reduce the amount of reactive oxygen available for the polymer etch, or a decrease in the ion energy due to more ions at the same bias power.

Higher pressure in general reduced the etch rate, while the interaction with bias power increased the effect. Hence the change in etch rate due to the interaction was most pronounced at high bias powers, while for lower bias power the effect of pressure on etch rate decreased. The decreased etch rate at higher pressures may be due to dilution of plasma species, decreased ion sputtering due to lower ion energy, or a combination.

Finally, the substrate temperature also influenced the etch rate. Higher temperature increased the etch rates due to thermal activation and higher vapor pressures. Temperature was the only parameter on which etch rate exhibited a linear dependency within

the parameter space, while all other parameters interacted with bias power.

Etch anisotropy

In addition to etch rate (A), control of etch anisotropy is important for optimal pattern transfer. For instance etching of SU-8 was explored due to a wish for increasing the aspect ratio of photo lithography defined structures. To achieve this, low anisotropy is wanted to limit the reduction in structure height while getting a thinner structure. However if for instance a second patterning of SU-8 by etching is wanted, it is often preferred to limit the mask under etching i.e. have a high anisotropy. Etch anisotropy (A) is defined as one minus the lateral etch rate (r_L) divided by the horizontal etch rate,

$$A = 1 - \frac{r_L}{r}. \tag{5.1}$$

An anisotropy of 0 is the same as equal lateral and horizontal etch rate, however this means that a thin wall will reduce its thickness at twice the rate of the height reduction.

Bias power had the largest effect on the anisotropy, see fig. 5.2. As expected increased bias power improved the etch anisotropy due to higher ion energy and improved directionality of the ion beam. Pressure and its weak interaction with bias power also

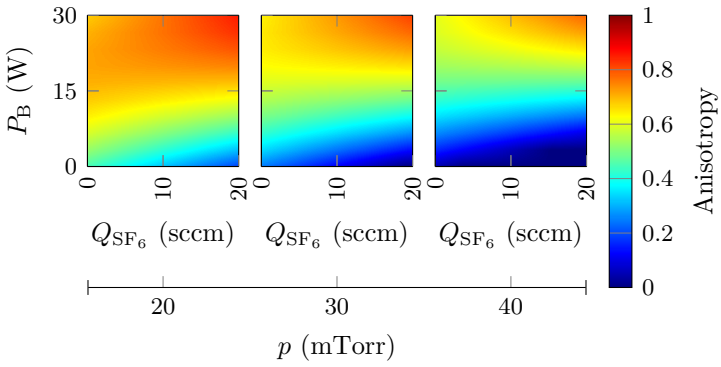

Figure 5.2: Etch anisotropy (A) as a function of etch parameters. The anisotropy showed no dependency on the T, whereas the three other parameters all influenced the outcome. Of notice is the dependency on Q_{SF_6} as both for isotropic and anisotropic etches high Q_{SF_6} gives the best result.

influenced etch anisotropy. At higher pressures the etch was more isotropic due to a reduction directionality.

The interaction between the SF_6 flow rate and the bias power have significant influence on the anisotropy. As seen in fig. 5.2 both for anisotropic and isotropic etching high SF_6 flow rate was optimal. This is because SF_6 can either introduce more directionality by adding heavier, charged particles to the plasma body, or heavy non charged particles, which limit the directionality. Bias power determines the shift from one regime to the other. High bias power is necessary to maintain high anisotropy when the SF_6 flow rate is increased. The temperature did not influence the anisotropy.

Antimony surface concentration

An antimony surface concentration [Sb] estimate was obtained by XPS spectra for each sample, see fig. 5.3. Estimating the surface concentration from XPS can be difficult and there is some uncertainty on the values obtained. For a description of the procedure used to calculate the concentration see section 2.4. XPS survey spectra revealed that C, O, F,

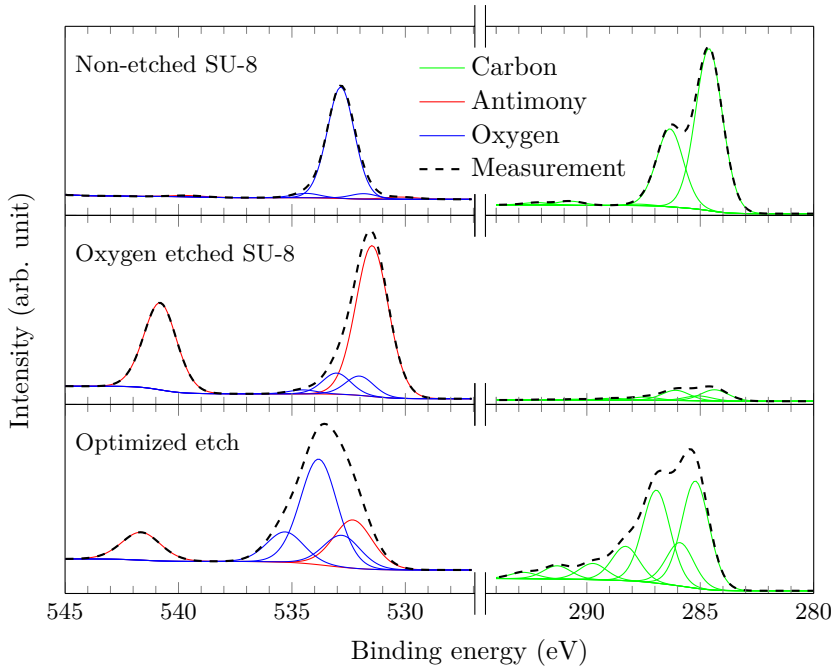

Figure 5.3: XPS measurements on processed SU-8 surfaces. Surveys of all samples showed that C, O, Sb, and F were the only elements in the polymer surface layer. The spectrum analysis showed four different carbon bonds, shown as green curves. Oxygen and antimony were discerned by fixing the ratio of distance and size between the $Sb3d_{5/2}$ peak to the $Sb3d_{3/2}$ peak to fit the $Sb3d_{5/2}$ while O2s was fitted for the remaining area. The oxygen contribution was divided in two types of carbon bonds. Fluorine spectra are not shown, but two bonds for fluorine were used to find the total atomic concentration. Etching of both b) and c) were done at P_C=1000 W, P_B=30 W, and Q_{O_2}=99 sccm For b) p=20 mTorr, T=10 °C, and Q_{SF_6}=0 sccm were used, while for c) p=40 mTorr, T=30 °C and Q_{SF_6}=17 sccm were used.

and Sb were the only measurable elements in the SU-8 surface layer. This is in agreement with the known elemental composition of the photo resist [55], if it is assumed that sulfur reacts in the plasma and leaves the surface during etching. The detailed spectra shown in fig. 5.3 depicts binding energies relevant for C, O, and Sb. The fluorine spectrum is not shown as fluorine shows no direct links to other etch outcomes than antimony. Only traces of antimony were observed in the surface layer of non-etched SU-8 as seen in fig. 5.3. As SU-8 with 5 % photo-initiator contains approximately 0.05 $\%_{atom}$ antimony, antimony is below the detection limit of the XPS system. For etched SU-8, the amount of antimony measured in the surface layer increased significantly, indicating an antimony accumulation during etch.

The XPS measurements of surface elements showed that the antimony surface concentration was highly dependent on the SF_6 flow rate to both first and second order. In fig. 5.4 it is evident that the antimony concentration drastically decreased when SF_6 was added to the plasma. The same tendency is obvious on the contour plots shown in

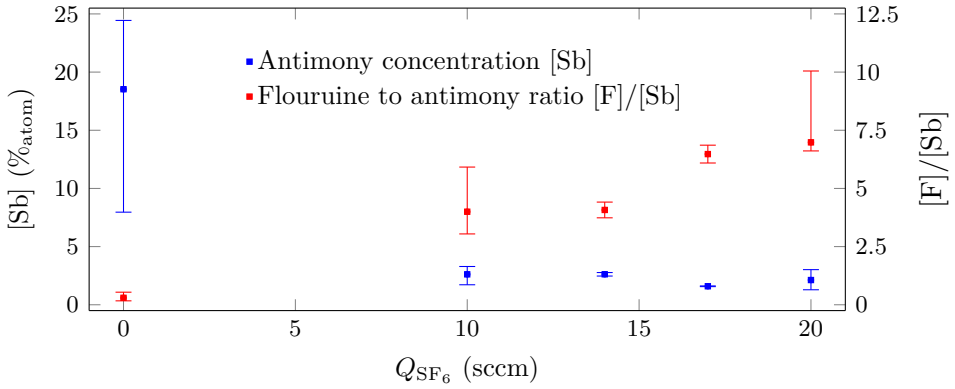

Figure 5.4: [Sb] and [F]/[Sb] ratio were highly dependent on Q_{SF_6}. Low Q_{SF_6} caused high [Sb] while the [F]/[Sb] ratio became low.

fig. 5.5, independent of the other parameters. Moreover the [F]/[Sb] ratio, also shown in fig. 5.4, increased from below one to three or more. This indicates that most fluorine from the photo initiator desorbed from the surface if fluorine was not added to the gas phase.

For samples etched at low SF_6 flow, the [F]/[Sb] ratio was much lower than the expected six that should be present considering the catalyst stoichiometry. The low ratio suggests that the SbF_6^+ ion reacts in the plasma to form other antimony compounds such as atomic antimony or antimony oxides. Atomic antimony and antimony oxide both have high boiling points of 1587 °C and 1425 °C [93]. Hence low vapor pressures of antimony and antimony oxides are expected at the processing temperatures used and antimony is expected to stay on the surface. For samples processed at high SF_6 flow rate, fluorinated compounds are expected on the surface. Antimony trifluoride and pentafluoride have boiling points of 376 °C and 141 °C [93], and in consequence much higher vapor pressures at the processing temperatures. Therefore, these compounds are more likely to evaporate from the surface, resulting in low antimony concentration and a [F]/[Sb] ratio close to the one of the photo-initiator

Bias power as well as first order interaction with SF_6 flow rate also had an effect on the antimony surface concentration, with higher bias power resulting in higher antimony concentrations. This might be ascribed to ion-enhanced etching [92] with more active sites generated on the polymer backbone. Consequently the polymer etch rate may increase more than the antimony etch rate resulting in a faster antimony accumulation. However the increased antimony accumulation rate could be alleviated by adding more SF_6 to the plasma.

Antimony surface concentration only showed a small dependency on temperature. The antimony surface concentration increased at elevated temperatures. This may be explained by an increase in polymer etch rate for higher temperatures. In other words, the rate of antimony removal is slower than the polymer etch rate. The pressure was

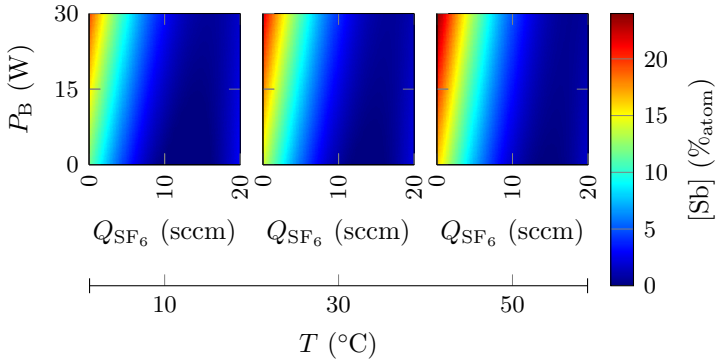

Figure 5.5: Antimony surface concentration ([Sb]) as a function of relevant etch parameters.[Sb] was primarily dependent on Q_{SF_6} but also T and P_B while p did not show any influence on [Sb].

found to not influence the antimony concentration.

Roughness

The surface roughness (R_{rms}) is primarily controlled by the SF_6 flow rate, with decreased roughness as a response to more fluorine in the plasma. Both first and second order of the SF_6 flow rate affects the roughness response. The bias power also influenced the roughness, which increased roughness at higher bias power. Interaction between SF_6 flow rate and bias power led also to an increase in roughness for higher bias powers. The nature of the dependencies on SF_6 flow rate and bias power, indicates that roughness and antimony surface concentration are closely linked. In fig. 5.6 the roughness is plotted against the antimony concentration. It is a clear tendency that if the antimony concentration is kept low, the roughness will also stay low.

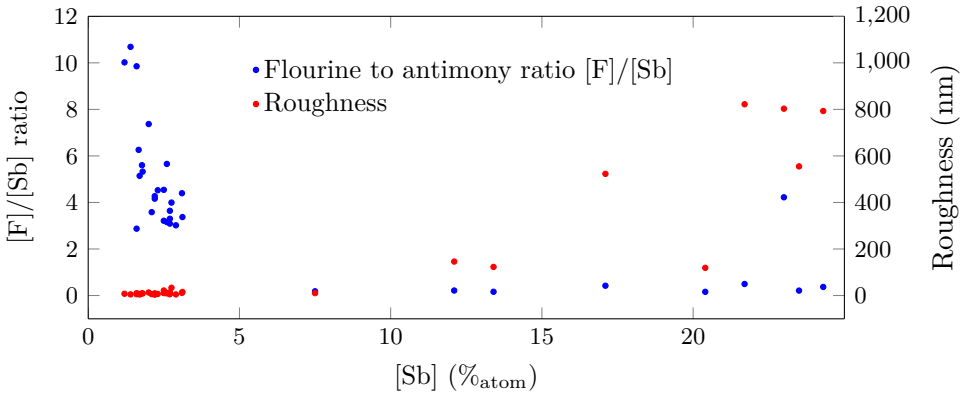

Figure 5.6: Root mean square surface roughness (R_{rms}) and [Sb] concentration correlations. Low [Sb] ensure low R_{rms}, note, that to reach low [Sb] [F] has to be relatively high.

It is worth noticing that for low roughness the [F]/[Sb] ratio in the surface layer is

high. Comparing the [F]/[Sb] ratio with the Sb concentration indicates a threshold at which the amount of fluorine in the surface layer is enough to generate volatile antimony compounds. From fig. 5.6 it seems that a ratio of [F]/[Sb] of 3:1 enables the antimony to start leaving the surface. This correlates fine with the hypothesis that SbF_3 and SbF_5 may be the volatile compounds formed.

The contour plot in fig. 5.7 shows the influence of the different parameters on surface roughness, and the same tendencies as for antimony concentration are seen. However, the interaction between bias power and SF_6 flow rate is more pronounced for roughness than antimony surface concentration. It is evident that the roughness can be quite high if antimony is present on the surface. Note also that the temperature does not influence

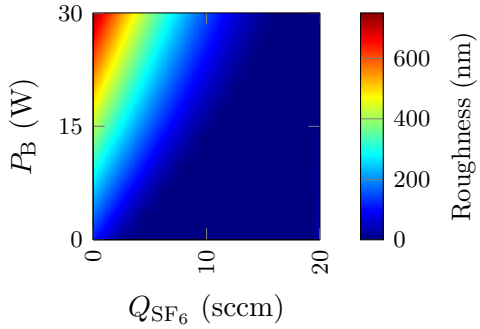

Figure 5.7: Root mean square surface roughness (R_{rms}) as a function of relevant etch parameters. The roughness contour shows similar tendencies as the antimony response, however T did not have and effect on R_{rms}, similar to p.

the roughness and the temperature dependency of antimony surface concentration was also limited.

The high surface roughness was visible by eye as a dull surface, and in SEM images it is readily identified. Figure 5.8b shows a sample etched in a pure oxygen plasma with a high roughness both at the top surface and sidewalls. Panel b and c of fig. 5.8 shows two samples etched with optimized parameters for low roughness are shown. The two etch processes were optimized for different anisotropy; in fig. 5.8c the anisotropy is 0.9 while in fig. 5.8d the anisotropy is 0.3. This gives a good indication that relatively smooth surfaces can be obtained with both high and low anisotropy etches.

Sidewall and edge roughness as seen in fig. 5.8c were linked directly to the bias power, with generation of edge roughness when a non zero bias power was applied. The dependency on bias power suggests that sidewall roughness is an effect of plasma directionality. For highly anisotropic etches antimony fluoride desorption on vertical surfaces is not assisted by ion bombardment. The ion bombardment hence seem to be necessary to initiate removal of antimony. For samples etched with no bias power the absence of roughness can be explained by the lower etch rate for these samples. Samples with rough sidewalls always showed rough edges due to the faster etching of corners, as they are attacked from two directions.

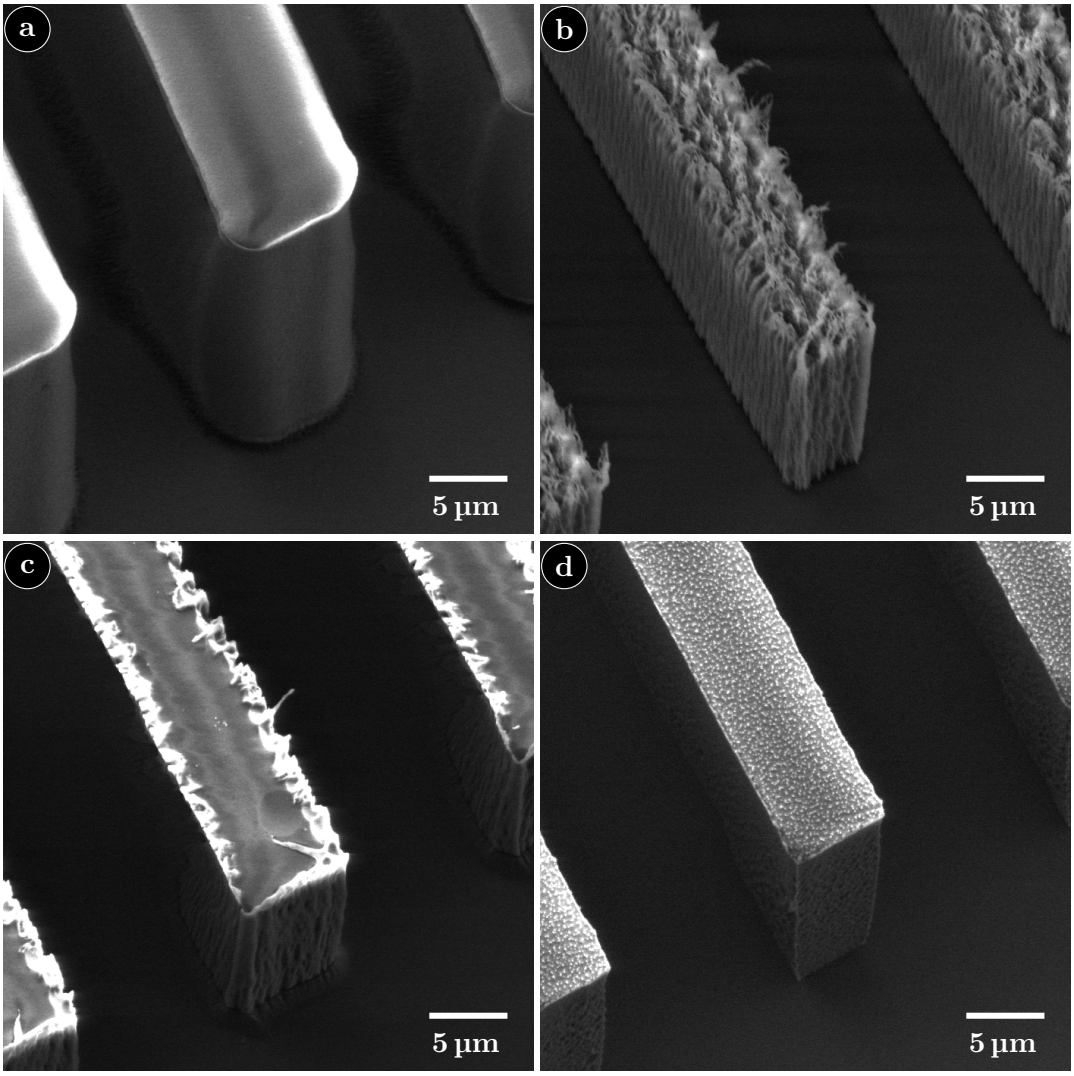

Figure 5.8: Surface topology of etched samples. a: A sample that has not been etched. b: The pure oxygen plasma (P_B=30 W, T=10 °C, p=20 mTorr, Q_{SF_6}=0 sccm) causes a high roughness. c: Optimized etch (P_B=30 W, T=30 °C, p=40 mTorr, Q_{SF_6}=17 sccm) with high anisotropy at reasonable etch rate and with a smooth surface. d: Optimized etch (P_B=0 W, T=10 °C, p=20 mTorr, Q_{SF_6}=14 sccm) at low anisotropy with moderate etch rate and a smooth surface.

Thinning of SU-8 pillars

From the DoE experiments outlined above it should be possible to thin down SU-8 pillars to obtain a higher aspect ratio than possible with photo lithography. With an isotropic etch the width can be reduced and pillars with a width smaller than 1 µm could be made, see fig. 5.9. Experiments have shown that if the height is reduced significantly at the same time the adhesion to the carrier is reduced. In fig. 5.9 three cases for which the pillars have been thinned down are shown. All the pillars were 5 µm in width before etching was started. However in the first two images only a width reduction was desired,

while for the last image a reduction in height was also wanted. If only a width reduction is wanted it is seen that pillars stand quite stable after etching, while if the height is reduced faster than the width the pillars are only loosely bound to the carrier surface.

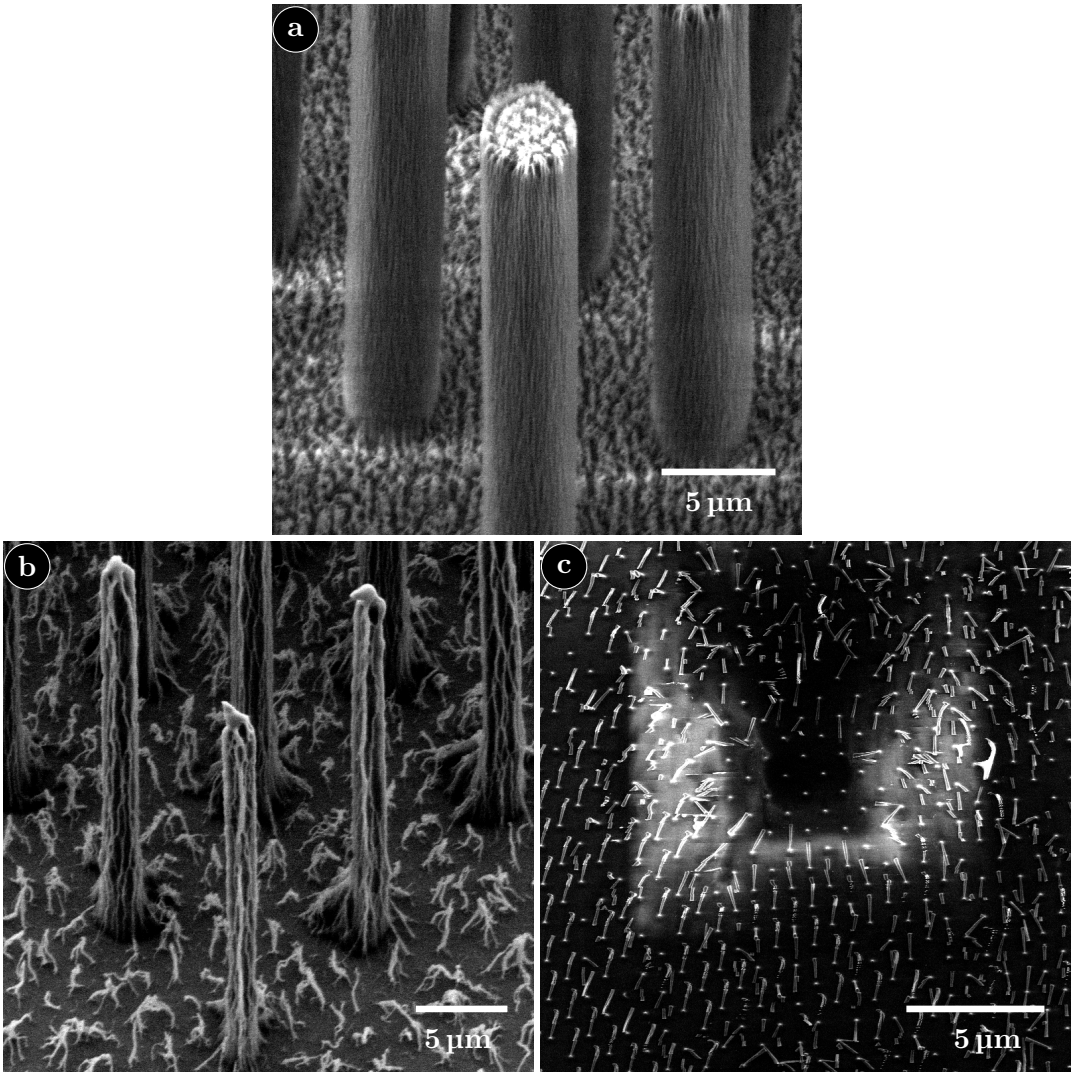

Figure 5.9: Pillars of SU-8 either etched fine or their adhesion to the carier became poor. a and b shows two different ratios of thinning are shown, without any problems except the roughening of surfaces these were etch with an isotropic etch. c show pillars etched with an anisotropic etch, which resulted in poor adhesion to the surface, with pillars detaching when zooming in the SEM microscope.

The loosely bounded pillars are detached and scattered by the SEM microscope when zooming in on the structures. The reason for the easy detachment is an effect of fast etching which introduces stresses in the pillars and might introduce more damage around the base of the pillars. On the other hand the pillars which are primarily thinned have a good adhesion and thin pillars below 1 µm in diameter can easily be obtained.

5.1.3 Summary

A DoE study of SU-8 plasma etching enabled improved control of surface properties of the polymer. For a pure oxygen plasma, high antimony concentration, high roughness, and low etch rate were observed. The amount of antimony accumulated at the surface could be reduced to a few percent by addition of SF_6 to the oxygen plasma, which directly lowered the surface roughness. Reasonable etch rates up to $0.8\,\mu m\,min^{-1}$ could be obtained at high anisotropy, while optimizing for an isotropic etch will inevitable cause a reduction of the etch rate, since the bias power must be lowered. Parameters for a high and a low anisotropic etch are listed in table 5.4.

Table 5.4: The etch parameters here are optimized for either low or high anisotropy.

		High anisotropy	Low anisotropy
Bias power (W)	P_B	30	0
Temperature (°C)	T	30	10
Pressure (mTorr)	p	40	20
SF_6 flow rate (sccm)	Q_{SF_6}	17	14

The high concentration of antimony accumulated at the surface must be considered when SU-8 devices are to be used for biological application. For short plasma treatments the antimony concentration will not increase much, but if samples are processed for longer time it will definitely be an issue. For complete SU-8 stripping, antimony surface accumulation results in a contaminated surface. However, adding SF_6 to the plasma chemistry can minimize the residue level and improve the usability of SU-8 as sacrificial mask.

5.2 TOPAS®

The etching behavior of TOPAS® was investigated on request of several people including Nikolaj Ormstrup Christiansen and Morten Bo Mikkelsen at DTU Nanotech. Since little knowledge is available on etching of TOPAS® some preliminary tests were made. These pawed the way for a set of DoE experiments with focus on etch rate and surface roughness. In this process the masking method was seen to have a high influence on the result. These results have been presented at the 39th International Conference on Micro and Nano Engineering in 2013 and the abstract and poster are included in appendix C. The TOPAS® results are currently in the process of being prepared for publication.

5.2.1 Experimental

The TOPAS® used for these experiments was the same as what is used for injection molding in the DTU Danchip facility. That means that it was bought in pellet form and had to be dissolved before it could be spun on silicon wafers. Several solvents can be used, however, Morten Bo Mikkelsen advised the use of o-xylene, with which he has obtained good results. However, TOPAS® does not readily dissolve in o-xylene so heat and stirring had to be used to obtain the thick TOPAS® paste.

The dissolved TOPAS® was made by mixing 8 g of TOPAS® 6013 in 32 g of o-xylene. The mixture was heated to 60 °C and magnetic stirring were applied to speed up the dissolution. The mixture was left for 24 h after which the pellets were completely dissolved. If the solution thickened before use a short period of magnetic stirring was introduced to regain the viscous solution.

The dissolved TOPAS® was spin coated onto silicon wafers, either on the old tabletop spinner or the new manual spinner, for more information see section 3.2.2. The parameters used for spin coating were the same for both spinners to obtain the same film thickness at all times. First a wafer was placed on the spinner so it was centered on the vacuum holder. Hereafter a pool of TOPAS® with a 2 cm diameter was deposited in the center of the wafer, by use of a syringe with a mounted filter. The wafer with resist was spun at 2500 rpm for 1 min with a 5 s spin up and down. These spin settings result in a film thickness of around 2 µm.

To remove the solvent from the spun resist films each wafer was baked on a hotplate at 150 °C for 10 min. This baking time and temperature ensure that the o-xylene solvent is evaporated from the TOPAS®. Furthermore stress in the TOPAS® are relaxed as the temperature is above the glass transition temperature of 143 °C for TOPAS® 6013.

As a hard mask, 50 nm of either aluminum or silicon were deposited on the TOPAS® surface, see fig. 5.10. Aluminum was deposited by e-beam evaporation while silicon was sputter deposited, both processes are described in section section 3.3. All experiments in the DoE setup and the preliminary test were made with aluminum as a hard mask. However, a small number of experiments with silicon as the hard mask were made to achieve a better edge definition in the photo lithography.

Figure 5.10: Etching of TOPAS® was done without removing the resist from the hard mask. The hard mask was used to ensure masking even if the photo resist was completely removed. The hard mask material were either aluminum or silicon.

Both with aluminum and silicon a standard AZ5214e photo resist was used for patterning. However as mentioned in section section 3.2, aluminum is etched by the developer resulting in poor edge definition of the pattern. To overcome this problem, silicon can be used instead since silicon is not attacked by the developer. A breakthrough in the form of a silicon etch was then done in the ASE before polymer etching was initiated.

Design of experiments was used to investigate the etch dependencies on the etch settings. A setup with variations of the three parameters; CO_2 percentage, bias power, and pressure was used, see table 5.5. The total gas flow was fixed to $Q_{\text{total}} = 100$ sccm, while the CO_2 percentage ($\%_{CO_2}$) was varied between 0 % and 100 % as a single parameter with O_2 as the other gas. The bias power (P_B) which introduces a physical etch aspect was varied between 0 W and 30 W and the chamber pressure (p) was varied between 20 mTorr and 40 mTorr. The pressure was controlled by automatic pressure control (APC), which changes the pump opening to keep a constant chamber pressure during

the etching.

Table 5.5: For TOPAS® the following parameters were used in DoE experiments. The first set of experiments excluded the coil power, which however was included by augmenting the DoE.

		min	center	max
Coded value		-1	0	1
CO_2 percentage (%)	$\%_{CO_2}$	0	50	100
Pressure (mTorr)	p	20	30	40
Bias power (W)	P_B	0	15	30
Coil power (W)	P_C	800	900	1000

The DoE setup with three parameters and an additional 2 center-points gives a total number of experiments of 10, that were performed in random order. The initial 10 experiments were augmented by another 10 experiments with coil power (P_C) lowered to 800 W from 1000 W to gain more knowledge about the uniformity. These combined 20 experiments were again augmented by 8 face-centered points and two extra center points to account for curvature seen in the data. All other variables in the system were kept constant to ensure the data would be accurate. Other parameters such as the substrate temperature (20 °C) might have an influence on the etch, however this was not investigated, since it should be possible to obtain good etch results at most temperatures around room temperature. All samples in the DoE setup were etched for 300 s after which they were characterized by different means.

Etch rate and selectivity were measured by a combination of three measurements of the structure height by use of the Dektak 8 profilometer. First the height of the photo resist was measured after development but before polymer etching. After the polymer etching the height was measured both before and after resist stripping, to obtain a measure of the reduction in photo resist thickness, in addition to the TOPAS® etch depth. All these height measurements were done both in the center and at the edge of each sample wafer, to allow for a uniformity calculation.

AFM of the samples was done on a flat part of the etched TOPAS® to measure the roughness introduced by the etch. The roughness measurements were made in 10 µm × 10 µm field of view. The data from the AFM measurements was processed by the free software package Gwyddion [86] to extract the measures for roughness.

As a final step SEM images were taken of the etch profile. The SEM images were taken by tilting the samples to 35° and a corner of the etched structure was observed. The SEM images used for under-etch determination were mainly taken of samples etched with a silicon hard mask, and only at specific etch settings.

5.2.2 Results and discussion

The analysis of the 10 initial experiments was first completed on the three etch characteristics etch-rate, uniformity, and roughness. However the 10 experiments were not able to explain the small variations in uniformity. Since etch uniformity is influenced by the local density of the plasma, and the pressure alone was not able to describe uniformity, a variation of coil power was introduced to the DoE setup. In the 10 new experiments

the coil power was lowered by 200 W, for all experiments except the center points. The center point experiments were run at the new center point coil power of 900 W, the mean of the old and new coil power. This however made them different from the first two center points, which changes the math for calculation slightly.

Taking coil power into account made it possible to predict the uniformity, even though some curvature was observed in the data. This curvature was both seen in the selectivity and etch rate data, and to address the curvature 8 face-centered points with 2 extra center points were added to the DoE. The total DoE thus ends up with 30 experimental runs, describing four parameters and their second order interactions.

Etch rate

An etch rate (r) expectation value equation was fitted by help of the DoE for all three sets of experiments. In the 10 first experiments, coil power was not varied and can hence not be included in the model. All primary factors influence the etch rate, together with all interactions with carbon dioxide percentage. The three main factors and two interactions result in a model with a coefficient of determination of 0.99, see table 5.6. Even though the model predicts the values well, the model is recalculated with a varied coil power, as this is needed for the uniformity calculation, see more below.

Table 5.6: The TOPAS® etch rate (r) DoE coefficients were calculated for 10, 20, and 30 experiments. In the 10 first experiments the coil power (P_C) was not included (NA), and it does not influence the rate much if more experiments were done. For the full set of experiments it is evident that the second order effects for bias power (P_B) and CO_2 percentage ($\%_{CO_2}$) both influence the etch rate.

$\beta_{i(jk)}$	r_{10} (nm min^{-1})	P(r_{10})	r_{20} (nm min^{-1})	P(r_{20})	r_{30} (nm min^{-1})	P(r_{30})
β_i	155.96	$< 10^{-4}$	151.82	$< 10^{-4}$	152.07	$< 10^{-4}$
$\beta_{i(P_B)}$	93.34	$2 \cdot 10^{-4}$	89.91	$< 10^{-4}$	88.64	$< 10^{-4}$
$\beta_{i(\%_{CO_2})}$	-54.59	0.0017	-55.33	$< 10^{-4}$	-55.64	$< 10^{-4}$
$\beta_{i(p)}$	-38.26	0.0063	-32.66	$< 10^{-4}$	-32.93	$< 10^{-4}$
$\beta_{i(P_C)}$	NA	NA	-	-	6.05	0.0382
$\beta_{i(\%_{CO_2})(P_B)}$	-29.31	0.0159	-28.73	$< 10^{-4}$	-28.73	$< 10^{-4}$
$\beta_{i(\%_{CO_2})(p)}$	22.19	0.0385	19.3	10^{-4}	19.3	$< 10^{-4}$
$\beta_{i(P_B)(p)}$	-	-	-11.91	0.0049	-11.91	$8 \cdot 10^{-4}$
$\beta_{i(P_B)^2}$	-	-	-	-	-18.57	0.0099
$\beta_{i(\%_{CO_2})^2}$	-	-	-	-	16.2	0.0219
R^2		0.99		0.99		0.99

With the coil power added to the experiments, as explained in section 5.2.1, the five parameter and interactions found to be significant with 10 experiments are still significant. It is, however, clear that due to the additional experiments the estimates become more precise, as seen by lower P values. The estimated parameters are approximately unchanged, even though the interaction between bias power and pressure is now deemed significant. Just as for the model without coil power included the coefficient of determination is 0.99, and the predictions should hence be of high quality. This model was again

augmented by face centered points, to better describe the selectivity which includes some second order interactions, see below for more information.

The etch rate from the complete set of 30 experiments is found to be dependent on all four parameters, also the coil power. However, the P value for the coil power and the small DoE coefficient indicates that its influence on the etch rate is small. The small change in the estimated parameters for contributions found significant without face centered points, shows the quality of fit without face centered points.

However, the increased number of experiments again decreases the P values, and enables the identification of small contributions from the second order interactions of bias power and carbon dioxide percentage. The second order effects are small compared to the first order effects, when it is taken into account that fitting is done in coded parameter space.

In fig. 5.11 a contour plot of the etch rate, with respect to all four parameters, is shown. From fig. 5.11 and table 5.6 it is obvious that increasing the pressure reduces the etch rate. This can be explained by a decrease in ion energy due to more ions are accelerated by the same power. The lower energy of the ions bombarding the surface of the etch sample means less sputtering.

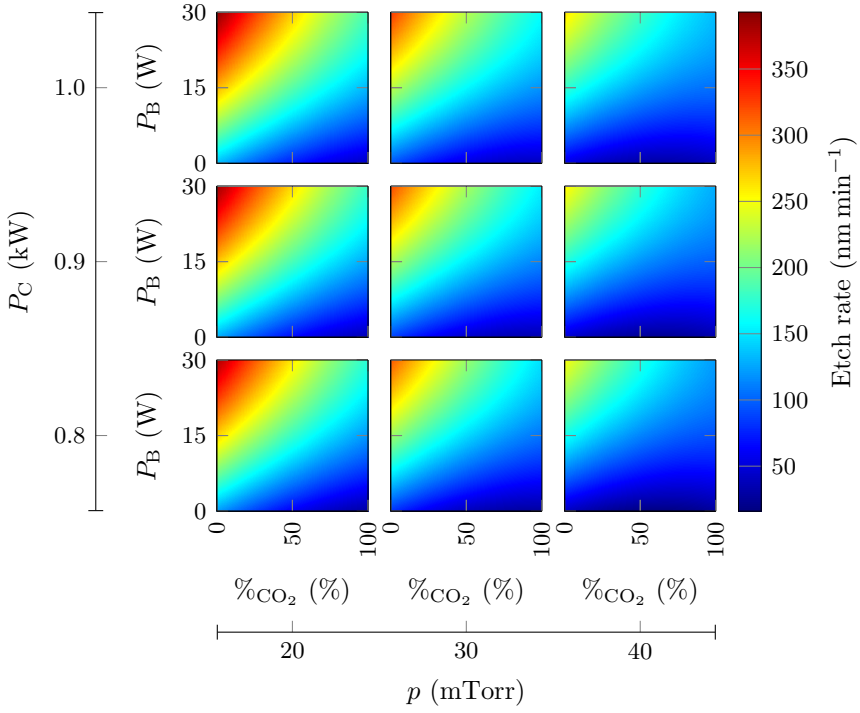

Figure 5.11: The etch rate of TOPAS®, is highly dependent on bias power, pressure, and the CO_2 percentage, and the interactions between these. The highest etch rate is achieved at high bias power, high O_2 plasma content, and low pressure. The coil power has a slight influence on the etch rate, with lower coil powers giving higher etch rates.

In contrast to higher pressures reducing the etch rate, higher bias power increases the etch rate. However, from table 5.6 it is clear that bias power does not increase the etch linearly, as bias power to the second order is also significant. This second order term

indicates that the highest gains in etch rate by increasing the bias power are obtained, when the etch rate is low. The interaction between bias power and pressure also decreases the etch rate.

Both pressure and bias power interact with the carbon dioxide percentage. The interaction between the CO_2 percentage and pressure is due to a change in the amount and mass of the ions generated, while the interaction between CO_2 percentage and bias power is an indication of a change in plasma density and the energy of the ions due to the changed mass.

However, the direct effect of CO_2 percentage on etch rate is that for more oxygen in the plasma the etch rate is increased. This can be due to two effects: the first is that oxygen may be a better etchant of the polymer, the second is that oxygen is ionized more easily by the plasma. If more atomic and ionized oxygen are generated in the plasma the amount of etchants are increased.

Finally the only parameter that shows a linear influence on the etch rate is coil power, as there does not seem to be any influence from interactions between coil power and any other parameter. The coil power only shows a small influence according to DoE, where increased coil power gives slightly higher etch rates. This is due to a small increase in the number of atomic oxygen and oxygen ions, giving a slightly higher etch yield.

Selectivity

The selectivity (S) between photo resist and TOPAS® for the first set of 10 experiments could not be fitted with a meaningful interpretation. This was due to second order terms that could not be distinguished from each other, see table 5.7. Since the second order terms were more significant than some of the other parameters, no conclusion could be drawn from the data. The experiments were first augmented by the inclusion of coil power to enable calculation of the uniformity, see more below.

As expected, inclusion of coil power in the design, did not remove the inseparable second order terms. The pressure seems to be insignificant in this set of experiment, in contradiction to the first 10 experiments. However, no conclusion can be drawn without inclusion of the additional face centered points that have been measured. Fo a single substrate the photo resist was completely removed in the etch, exposing the hard mask beneath, the selectivity for this substrate was not calculated.

With face centered points included the selectivity between TOPAS® and photo resist shows a dependency on all parameters but coil power. The bias power shows the highest influence on the selectivity. This is explained by the increase in the energy transfered ti the surface by ion bombardment. This energy can either cause sputtering or it can generate active sites. Both of these processes need different activation energies for the different polymers and hence influence the etch rates of TOPAS® and photo resist in different ways. The second order of bias power also significantly influences the selectivity.

The carbon dioxide percentage has an small effect on the selectivity, as the etch chemistry is changed by the composition. Different etchants like oxygen radicals and carbon monoxide radicals will attack different kind of bonds in the polymers with different efficiency. From fig. 5.12 it is observed that a carbon dioxide plasma results in higher selectivity. This means that for a carbon dioxide plasma the etch rate of TOPAS® is higher than the etch rate for photo resist.

Table 5.7: The TOPAS® selectivity (S) DoE coefficients were calculated for 10, 20, and 30 experiments. In the 10 first experiments the coil power (P_C) was not included (NA), and it was found to have high P values for 20 and 30 experiments. The selectivity could not be explain without face centered points, since the second order effects of both bias power (P_B) and pressure (p) are significant.

$\beta_{i(jk)}$	S_{10}	P(S_{10})	S_{20}	P(S_{20})	S_{30}	P(S_{30})
β_i	1.03	$< 10^{-4}$	1.02	$< 10^{-4}$	1.01	$< 10^{-4}$
$\beta_{i(P_B)}$	0.12	$< 10^{-4}$	0.11	$< 10^{-4}$	0.10	$< 10^{-4}$
$\beta_{i(\%_{CO_2})}$	-	-	-0.016	0.0439	0.019	0.0329
$\beta_{i(p)}$	-0.024	0.0379	-0.013[a]	0.1066	-0.0083[a]	0.3253
$\beta_{i(P_B)(p)}$	0.026	0.028	0.030	0.0017	0.034	0.0013
$\beta_{i(\%_{CO_2})(P_B)}$	-	-	0.019	0.0239	0.023	0.0207
$\beta_{i(\%_{CO_2})(p)}$	-	-	-0.018	0.0324	-0.021	0.0278
Second order terms		0.0016		$< 10^{-4}$		
$\beta_{i(P_B)^2}$					-0.073	10^{-4}
$\beta_{i(p)^2}$					-0.038	0.0203
R^2		0.99		0.99		0.96

[a] Intercept was negligible, but included in model.

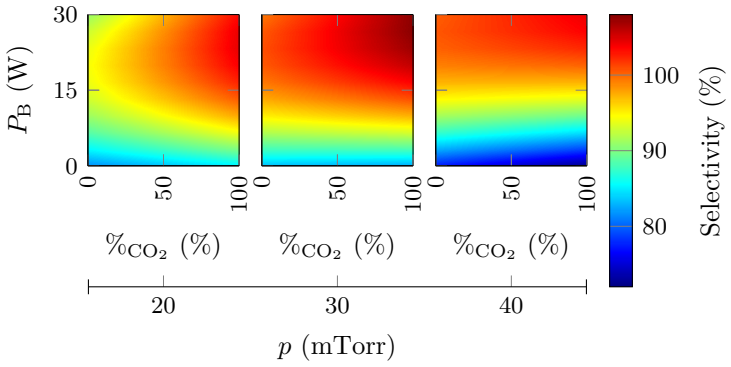

Figure 5.12: TOPAS® etch selectivity to photoresist is controlled by bias power, CO_2 percentage, and pressure. TOPAS® needs a higher bias power than photoresist for sputter activation of the ion enhanced reactive ion etching effects. On the contrary TOPAS® seems to etch faster in CO_2 than photoresist, although the etch rate is still lower than for oxygen plasma.

However, at high pressure the interaction between the CO_2 percentage and pressure eleminates the effects of CO_2 percentage. This might be a result of a lower etch rate of TOPAS® at high pressure, without a corresponding change in the photo resist etch rate. The interaction between bias power and CO_2 percentage makes it possible to obtain the same selectivity at two different bias powers.

Uniformity

In etching of TOPAS® a uniform etch rate over the whole sample surface is wanted, as to not remove more material at the edge compared to the center of the wafer. The uniformity (U) is a measure for the difference in etch rate between two or more places on a single wafer. The uniformity measure used in this thesis is calculated as the Center-Edge uniformity, given as

$$U = 1 - \frac{r_c - r_e}{r_c + r_e}, \tag{5.2}$$

r_c and r_e denotes the etch rate at the center and edge. The goal is 1 for best uniformity. The uniformity was calculated for each wafer in the DoE, which gives a clear overview of which parameters are important for the uniformity of the etch.

Fitting of the uniformity from the first 10 experiments, does not indicate any significant parameters. This lack of significance is because coil power has the largest effect on the outcome. To generate a meaningful model for the uniformity, the design was augmented with experiments at lower coil power, as described in section 5.2.1.

Table 5.8: From the first 10 experiments for TOPAS® etching it was not possible to generate a response surface for the uniformity. The inclusion of coil power (P_C) enabled estimation of DoE coefficients for uniformity. Coil power (P_C) and pressure (p) are the two variable for which the DoE coefficients can be estimated with highest significance, and also have the largest influence on the uniformity.

$\beta_{i(jk)}$	U_{20}	P(U_{20})	U_{30}	P(U_{30})
β_i	0.86	$< 10^{-4}$	0.87	$< 10^{-4}$
$\beta_{i(P_C)}$	-0.036	$< 10^{-4}$	-0.035	$< 10^{-4}$
$\beta_{i(p)}$	0.026	10^{-4}	0.027	$< 10^{-4}$
$\beta_{i(\%_{CO_2})}$	0.015	0.0089	0.014	0.0062
$\beta_{i(P_B)}$	0.01[a]	0.0613	0.01	0.0481
$\beta_{i(\%_{CO_2})(p)}$	0.014	0.0146	0.014	0.0126
$\beta_{i(P_B)(p)}$	0.014	0.0146	0.014	0.0126
R^2		.90		0.84

[a] Intercept was negligible, but included in model.

By adding the coil power to the experimental design, it is possible to give a descriptive model for the uniformity. It should be noticed that bias power is insignificant but included since the interaction between bias power and pressure is significant. If the face centered points are added to the experimental setup the expectation parameters do not change. However the P values for some of the parameters are lowered, indicating that the increased number of experiments lowers the error on the estimates. In particular the bias power is shown to be significant by itself with face centered points included. The final data analysis is done on the full experimental setup.

In fig. 5.13 and from table 5.8 it is obvious that the coil power has the largest influence on uniformity. The uniformity was found to increase when the coil power was lowered. This indicates that the coil power has influence on the uniformity of the plasma, and a high coil power generates a plasma that is more dense in the center. The coil power

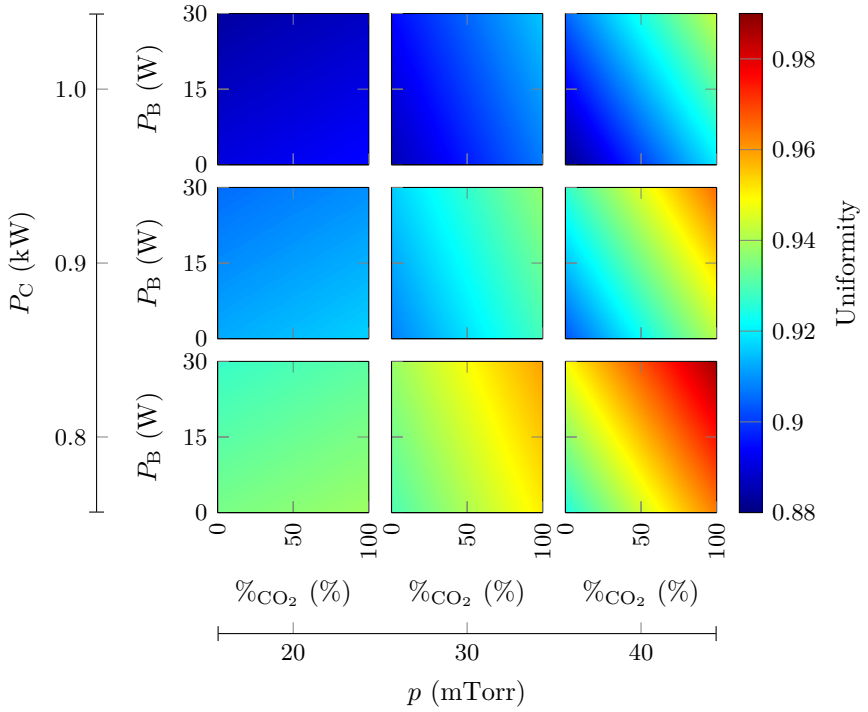

Figure 5.13: TOPAS® etch uniformity is highly dependent on coil power and pressure, with higher pressure and lower coil power resulting in a more uniform etch of a 100 mm wafer.

does not seem to influence the uniformity through interactions with other parameters, which makes it easier to optimize the uniformity.

Even though coil power has the largest influence on uniformity, the three other parameters also influence the outcome. Pressure is the second most influential parameter, where an increase in pressure results in an increase in the uniformity due to a more evenly spread plasma. Two interactions with pressure give a slight contribution to the uniformity. Both the interaction between carbon dioxide percentage and pressure, and the bias power and pressure interactions are significant. The contribution from interaction with bias power is however small.

The interaction with the CO_2 percentage is larger and the CO_2 percentage is by itself a significant contributor to uniformity. The more carbon dioxide in the plasma the more uniform is the etch. However, for high etch rates oxygen is the preferred plasma gas and the uniformity must be increased using other settings.

Surface properties

The surface properties of the etched wafers are of importance for the intended use. Often a surface with the same properties as before or a surface that is more or less hydrophilic after etching is wanted. The surface properties tested for the TOPAS® before and after etch are roughness and the surface composition. The roughness was measured by AFM in a 10 µm × 10 µm area of etched surface, see section 5.2.1. The surface composition

was measured by XPS on a area of etched surface, and on a dummy sample that was not etched.

The roughness was found to be low independent of the plasma conditions, and the DoE showed that all roughness measurements was within statistical uncertainty. However, if the hard mask beneath the photo resist were exposed to the plasma during etching, roughness increased drastically. This is ascribed to local masking by sputtered and redeposited particles from the hard mask onto the surrounding surface. The hard mask is used to ensure that if all photo resist is removed the etch still only attacks the non masked areas. Instead of a resist process, a hard mask can be deposited on the polymer through a shadow mask. This will however leave the hard mask exposed to the plasma.

Another option is to use silicon for hard masks, since silicon is not etched by the developer and hence must be removed after development. The use of a sputtered silicon as hard mask result as for aluminum in local masking, if the mask is exposed to the plasma. However with a silicon hard mask under the photo resist it is possible to obtain a better edge definition. The increased edge definition makes it easier to observe under-etching in SEM images. In fig. 5.14 two SEM images of wafers etched with the same settings, but different hard masks are shown. It is apparent that the silicon hard mask results in better edges, while aluminum even introduces a rough surface of the non etched material at the edge. The round corners of the structure are a result of the photo lithography.

It is not only the roughness of the surface that has an influence interactions with other materials In this respect the surface composition of the polymer is as important for interactions with solids and fluids. The amount of oxygen or hydrogen in the surface layer can drastically alter the wetting and bonding abilities of the polymer.

XPS measurements have been used to calculate the surface composition, however this technique cannot discern hydrogen atoms. For this reason the given surface composition of carbon and oxygen may add up to 100 % even when it is known that hydrogen is present in the surface layer. From the XPS measurements it was found that traces of aluminum and fluoride were present in the surface layer. The amount measured of these two traces was low, and for aluminum a small increased was seen for two samples where the photo resist was removed completely during etch. The etch chamber is made of alumina and the system is used for fluorine containing etches, which will leave fluorine on the chamber walls, which may deposit on the wafers in small amounts.

In figure fig. 5.15 the XPS spectra of a non-etched and an etched sample are shown. From the peak heights it is clear that more oxygen is present on the etched sample. This was true for all samples, with correspondingly less carbon present on the etched samples.

The carbon peak was split in four different contributions, depending on the type of bonds on the carbon molecule. The polymer is mostly rich in carbon to carbon bonds with a binding energy of around 285 eV depending on charging of the sample. The three other identified carbon peaks are characterized as carbon with oxygen bound to it. Carbon with an oxygen bound by a single bond has a binding energy which is 1.7 eV higher than the primary peak, while carbon atoms with two bonds to oxygen are identified as having a binding energy 3.1 eV higher than the primary peak. For an carbon with a oxygen bound by a single bond and an oxygen bound by a double bond to it, the binding energy is 4.5 eV higher than the primary peak.

The carbon oxygen bonds outline in table 5.9 result in three different configuration

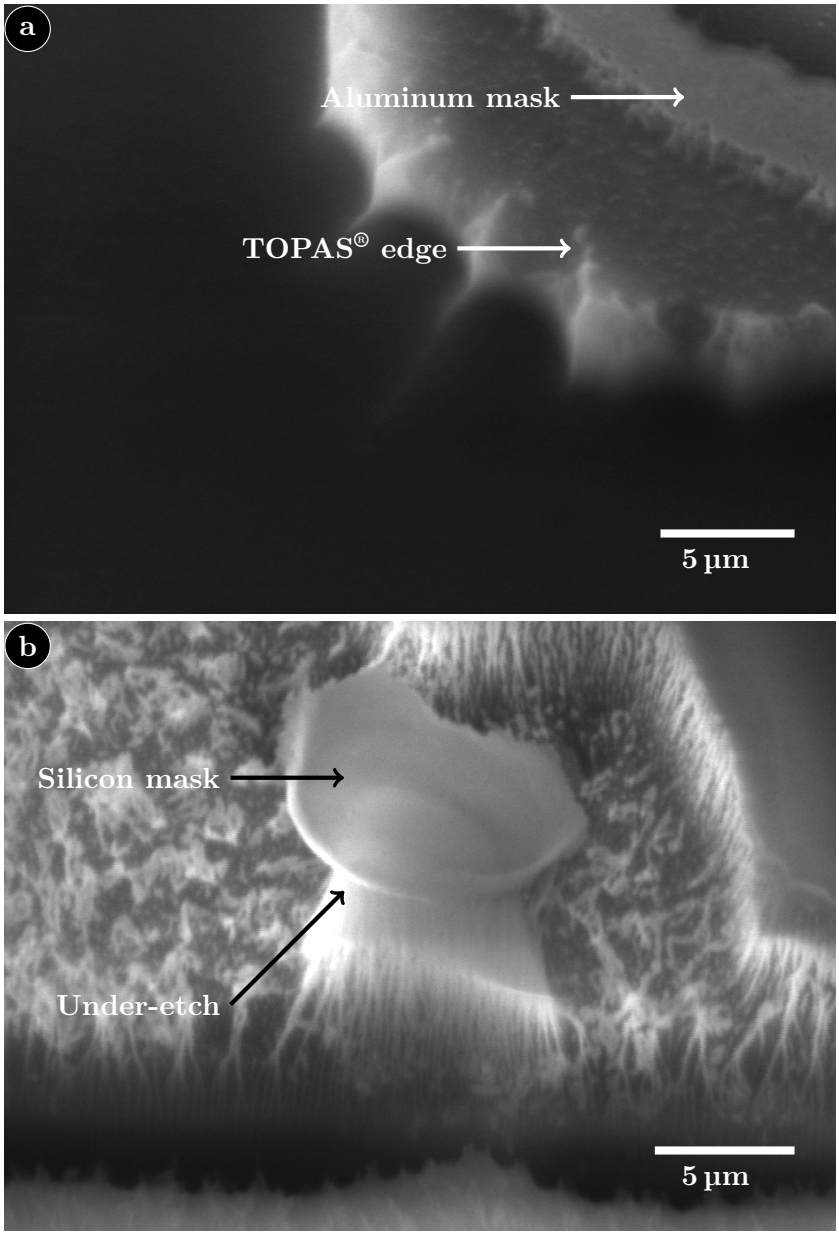

Figure 5.14: TOPAS® edge definition is much better if silicon (b) is used as hard mask instead of aluminum (a). a: For the aluminum wafer no under etch can be seen, because of the poor aluminum edge definition before etch. b: For silicon it is clear that a certain amount of under etching has been done. The wafers are etched with a high etch rate, the only difference is the hard mask material.

of oxygen. When an oxygen is bound by a double bond to carbon it cannot bond to anything else. However an oxygen bound by a single bond to carbon can either be attached to a hydrogen or it can be bound to another carbon. These three kinds of oxygen cannot be distinguished from each other in the XPS measurement at the peak around 533 eV. There was no indication that peroxy groups were generated during the

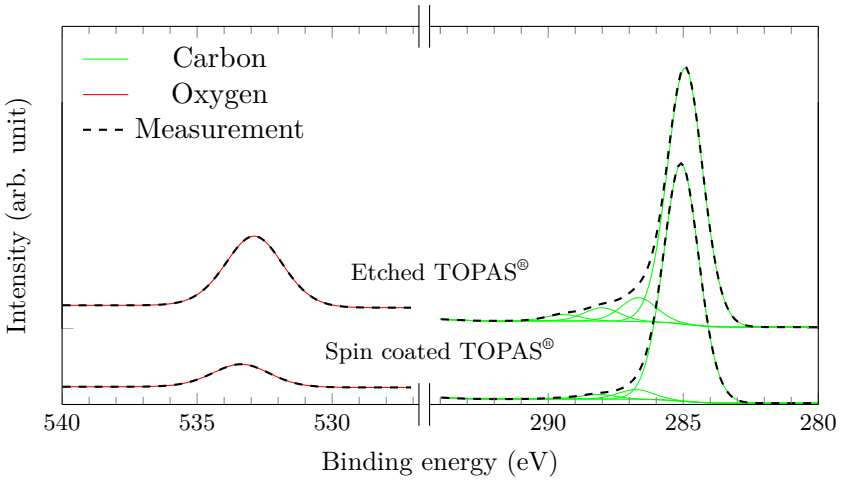

Figure 5.15: XPS measurements on TOPAS® before and after etching showed an increase in surface oxygen.

Table 5.9: The expected binding energies for C1s carbon atoms and O1s oxygen atoms, the binding energies are associated with the * marked atoms. The three kinds of oxygen which are expected have the same binding energy.

Carbon	E_{binding} (eV)	Oxygen	E_{binding} (eV)
$C^\star - C$	285.0	$O^\star - C$	533.1
$C^\star - O$	286.7	$O^\star = C$	533.1
$O - C^\star - O$ or $C^\star = O$	288.1	$C - O^\star - C$	533.1
$O - C^\star = O$	289.5	$O^\star - O$	535.3

etch, as oxygen bound to one carbon and one oxygen has a higher binding energy than oxygen only bound to carbon.

The increase in oxygen after etch was expected, and is in itself an indication of changed surface properties. From the data it is clear that the likelihood of carbon having one oxygen bond is higher than for the carbon to have two or three bonds to oxygen. Hence there is roughly half the amount of carbon with two bonds to the oxygen, compared to carbon with a single bond to oxygen. Also the amount of carbon with three bonds to oxygen is lower than the to other carbon types. This can be explained by carbon leaving the polymer surface, when all four bonds from carbon are attached to oxygen hence generating CO_2.

The amount of carbon and oxygen at the surface after etch did not show a correlation to etching parameters. The difference between different etches was small, but a significant change was seen compared to a non etched surface. The small increase in aluminum seen in cases where the photo resist was fully removed before the end of etching, could also be correlated to a slight increase in roughness.

5.2.3 Summary

ICP-RIE has shown to be an excellent tool for etching of TOPAS®, with the possibility to control etch rate and uniformity while keeping the roughness low. Low surface roughness after etching is, however, not universal since it depends on the masking material. Photo resist is a polymer and hence etched at comparable rates as TOPAS®. This limits the depth obtainable with this kind of masking material. If instead a hard mask is used the selectivity is drastically increased, this however is at the cost of a more rough surface.

Obtaining good center to edge uniformity is possible with quite different etch parameters. If the center to edge uniformity is the most important factor, and the etch rate is only of limited interest, then a plasma containing carbon dioxide is recommended. However, the use of carbon dioxide in the plasma will lower the etch rate more than what can be compensated by an increase in by bias power.

Etch rates of $150\,\mathrm{nm\,min^{-1}}$ to $350\,\mathrm{nm\,min^{-1}}$ can be obtained with carbon dioxide in the plasma, while a pure oxygen plasma can give rates above $500\,\mathrm{nm\,min^{-1}}$. The fast etching oxygen plasma can still keep the center to edge uniformity above 95.5 %, enabling etch depths of several microns with short processing times. Some optimized and tested etch parameters have been listed in table 5.10, it should however be noted that the etch rates depend on pattern coverage. For shallow etches a low etch rate is wanted to keep control of the etch depth while depending on the need for uniformity a faster etch can be chosen.

Table 5.10: Optimal etching parameters for TOPAS® are listed for three different etches. The etch rate can be varied in a large interval with small change of the center to edge uniformity.

		Slow etch rate	Medium etch rate	Fast etch rate
CO_2 percentage (%)	$\%_{CO_2}$	50	50	0
Pressure (mTorr)	p	40	40	40
Bias power (W)	P_B	30	60	60
Coil power (W)	P_C	660	800	720
Etch rate ($\mathrm{nm\,min^{-1}}$)		200	344	503
Center to edge uniformity (%)		96.5	97.7	95.5

5.3 Other polymers

Some initial work on several other polymers than SU-8 and TOPAS® was carried out. Among these were polycaprolactone (PCL), poly L-lactic acid (PLLA), and poly methyl methacrylate (PMMA). PLLA and PCL are biopolymers which are interesting for use in for example drug delivery [77]. These polymers showed some of the same problems as TOPAS®, and the polymer layers also have some of the same characteristics. TOPAS® and the three mentioned polymers do not contain any photo catalyst as SU-8 does. The absence of photo a catalyst ensures that the polymers are free from metals and other, in an etch perspective, unpleasant elements. Experiments with all three polymers were

prepared almost identically. For PCL and PLLA some experiments were done on actual device wafers kindly provided by Johan Nagstrup from DTU Nanotech

5.3.1 Experimental

Even through the three polymers have different properties and different structures, as seen in fig. 5.16, the sample preparation was very similar. There was a difference in the solvent used, and the parameters for spin coating. However this is only small changes in the general procedure. The etching experiments were all done on the ASE system, see

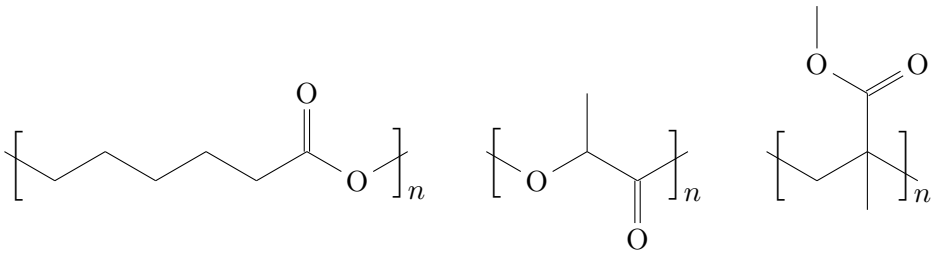

Figure 5.16: Structure of PCL, PLLA, and PMMA. They do all contain a double bonded oxygen atom and a oxygen in the carbon chain. However the chain length differs between the three polymers.

section 3.5, with similar parameters. For PCL and PMMA only preliminary experiments have been done, hence no DoE data are available for these experiments.

The polymers were spun onto silicon wafers on one of three manual spinners. Different spinners were used because of their availability and decommission during the project. The change of spinner should not have a large effect on the resulting polymer layer, as long as the same spinning parameters have been used.

When spinning the resist onto silicon wafers, a clean wafer was placed on the vacuum chuck and centered. Then polymer was added with a syringe at the center of the wafer until a pool of roughly 3 cm in diameter was poured on. Spinning was started as fast as possible after adding the polymer to reduce the solvent evaporation to a minimum. Some of the solvents used, evaporate fast enough for the polymer to dry before the 1 min spin time was completed.

The bake of wafers spun with a polymer is done for two reasons. The wafers are baked to get the solvent out of the polymer matrix. If the polymer dries fast, the solvent evaporation will introduce tension in the polymer layer. The tension can result in polymer release from the surface, and to minimize this risk the wafers are baked at a temperature above their glass transition temperature (T_g), or for PCL above the melting temperature. The polymer solvent, glass transition temperature, and spinning parameters are listed in table 5.11.

The prepared wafers were masked by a layer of e-beam evaporated aluminum, which was either structured by photo lithography or by evaporation through a shadow mask. If a photo resist was used, the aluminum was etched in photo resist developer. When spinning photo resist on the substrates a recipe without baking was used for PCL to ensure no reflow of the polymer and a low mixing with aluminum. The wafers were

Table 5.11: Coating parameters for PCL, PLLA, and PMMA. Coating parameters depends much on the viscosity of the polymer blend. DCM is short for dichloromethane.

Polymer	PCL	PLLA	PMMA
Solvent	DCM	DCM/Acetone	Anisole
Concentration (wt%)	15	20	15
T_g (°C)	-60	55	105
Melting point (°C)	60	180	160
Acceleration (rpm/s)	200	400	800
Spin speed (rpm)	800	2000	2500
Bake out temperature (°C)	100	65	110
Bake out time (min)	60	10	10

instead left for solvent evaporation for some days. The resulting resist pattern after development was of an acceptable quality.

The shadow mask used was made of silicon with holes etched through the wafer in KOH, however fabrication of a shadow mask by laser dicing a thin aluminum wafer was also investigated. Laser dicing of aluminum resulted in some very rough edges in the diced areas. As the use of shadow masking was investigated to obtain a better pattern transfer on low T_g polymers, the rough edges could not be accepted.

As mentioned all etching was done in the ASE system with a chamber clean on a dummy wafer between each etch. For PCL and PMMA only small sets of experiments were done, while for PLLA a more thorough testing was performed. For PLLA two sets of DoE experiments were carried out one with O_2, CO_2, and SF_6 the other with O_2, CO_2, and Ar, none of which has been augmented by face centered points, even though the results indicated a curvature. In the experiments with SF_6 18 experiments were used, and for the Ar as additive gas 10 experiments were used in the DoE. The paramters for the two sets of DoE done on PLLA are listed in table 5.12. Be aware that the temperature has only been varied in the etch with SF_6.

Table 5.12: Parameters used for DoE design when etching PLLA. Center denotes the value used for center points and face centered points.

		min	center	max
Coded value		-1	0	1
CO_2 percentage (%)	$\%_{CO_2}$	0	50	100
Bias power (W)	P_B	0	75	150
Additive gas (sccm) (either SF_6 or Ar)	$Q_{SF_6/Ar}$	0	14	28
Temperature (°C) (only for SF_6 etch)	T	0	10	20

The PLLA samples were etched for 10 min with a total flow of CO_2 and O_2 of $Q_{CO_2+O_2} = 50$ sccm, a coil power (P_C) of 600 W, and a pressure (p) of 40 mTorr. For the argon containing etch the temperature was fixed at $T = 0$ °C for all experiments. In all cases the pressure was fixed so the APC angle was varied during the experiments to keep the pressure stable. Either SF_6 or argon was added at flow rates between $Q_{SF_6/Ar} = 0\,\text{sccm} and 14\,\text{sccm}$. The additive gases were chosen to test if inert argon or

reactive fluoride had a influence on the etch.

For PMMA and PCL some initial experiments have been done to get a feeling of the etch rates obtainable and possible problems. For both polymers oxygen and carbon dioxide have been tried as etch gases but at lower pressures. The coil power, temperature and, total flow rate were the same as for PCL, and the bias power was tested at different values.

On these polymers the etch rate measured by a contact profilometer is the primary result. The surfaces after the etch have been visualized by SEM imaging to get a picture of roughness and edge definition. Anisotropy and uniformity of the etches have not been tested due to the poor quality of a pattern transfered by the photo resist and aluminum hard mask combination, which was discussed in section 5.2.2.

5.3.2 Results and discussion

The etching results for PLLA, PCL, and PMMA will be presented with discussion of the results for PLLA which is based on the most complete set of experiments. This will then be linked to the few results for PCL and PMMA and the challenges with etching of these. The focus will be on etch rate and surface roughness with etch parameters for PCL and PMMA listed when discussed.

Etch rate of PLLA

The etch rate (r) of PLLA was fitted to find the dependency of the rate on the input parameters. The results however showed curvature in the response and the number of experiments were not sufficient to determine the specific parameters introducing this. Nonetheless by comparing the measurements and the curves fitted with different second order terms included, it was concluded that the most important second order terms were related to bias power. This is not the standard procedure but the measurements and calculated expectation values are in good agreement. The augmentation of the design was skipped due to time limitations.

The bias power has the largest effect on etch rate and if the curvature is ascribed to bias power to, the other parameters only result in minor changes. As expected increased bias power directly increases the etch rate. In fig. 5.17 the second order term seems to introduce a maximum etch rate with a bias power in between 75 W and 150 W. However only values of 0 W, 75 W and 150 W have been tested and it is more likely that an energy level must be overcome and a linear increase in etch rate is seen for higher bias powers. This however is not possible to confirm with the polynomial fit used in the DoE.

The energy level that must be overcome is related to bond breaking in the polymer for generation of active sites for etchant attack. An estimate of the energy will not be given as the ASE etching system cannot measure the bias voltage and hence the energy of the ions is not known.

The same tendencies as seen for SF_6 are seen if argon is added to the plasma. However the interaction between bias power and the diluting gas seems to disappear, maybe because argon can only be ionized but not increase the number of reactive particles in the plasma. On the other hand the interaction between the etch gas oxygen or carbon dioxide with argon is significant, even if it is small.

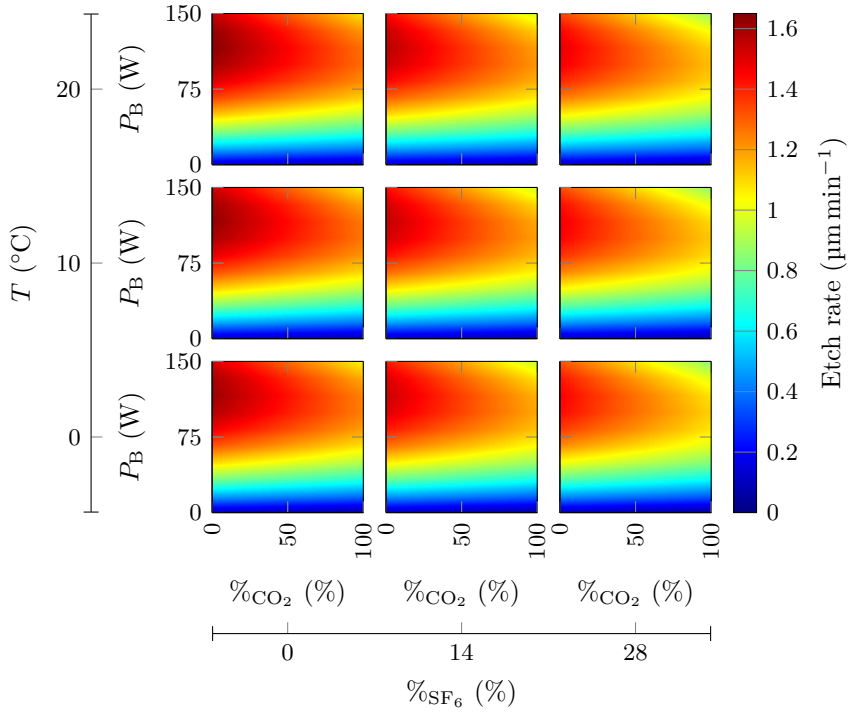

Figure 5.17: The etch rate of PLLA with SF_6 added to the plasma. SF_6 did not change anything for the etch rate except diluting the plasma, resulting in slightly lower rates. Oxygen is the fastest etchant while a bias power is needed for the etch to proceed.

In fig. 5.17 the obtained results for PLLA etching are shown with the second order term fitted to bias power. Both the temperature and amount of SF_6 in the plasma have a small influence on the etch rate. The temperature was found to be significant, however from table 5.13 it is obvious that the contribution is small compared to the other parameters.

SF_6 as a parameter alone and its interaction with bias power reduces the etch rate when more is added. This indicates that SF_6 does not have a role in the etch chemistry but merely dilutes the plasma. The best option for etching of PLLA and most other polymers is to not use SF_6 if no specific compound in the polymer should be removed by it.

The carbon dioxide percentage had as expected a significant influence on the etch rate. For a carbon dioxide plasma a lower etch rate was found compared to an oxygen plasma. This is explained by a lower ratio of oxygen radicals in the plasma; oxygen radicals are chemically more active than carbon monoxide radicals. A small interaction between CO_2 percentage and bias power is also seen which increases the etch rate for an oxygen plasma. This indicates either more charged particles or less scattering of charged particles in the oxygen plasma. As more heavy particles will be present in a carbon dioxide plasma the main reason for this is more scattering.

Table 5.13: PLLA etch rate with SF_6 or Ar in the plasma. When Ar was used as additive gas the temperature (T) was not varied. All DoE coefficients for the parameters bias power (P_B), CO_2 to O_2 ratio ($\%_{CO_2}$), and additive gas ratio ($\%_{SF_6}$ or $\%_{Ar}$) without interactions were significant. All interactions except one, included bias power for both additive gases.

$\beta_{i(jk)}$	r_{SF_6} ($nm\,min^{-1}$)	$P(r_{SF_6})$	r_{Ar} ($nm\,min^{-1}$)	$P(r_{Ar})$
β_i	1.239	$< 10^{-4}$	0.809	$< 10^{-4}$
$\beta_{i(P_B)}$	0.565	$< 10^{-4}$	0.612	$< 10^{-4}$
$\beta_{i(\%_{CO_2})}$	-0.128	$< 10^{-4}$	-0.164	$< 10^{-4}$
$\beta_{i(\%_{SF_6})}$ or $\beta_{i(\%_{Ar})}$	-0.052	$< 10^{-4}$	-0.029	0.0016
$\beta_{i(T)}$	0.015	0.0067	NA	NA
$\beta_{i(P_B)(\%_{CO_2})}$	-0.107	$< 10^{-4}$	-0.111	$< 10^{-4}$
$\beta_{i(P_B)(\%_{SF_6})}$ or $\beta_{i(P_B)(\%_{Ar})}$	-0.047	$< 10^{-4}$	-	-
$\beta_{i(\%_{CO_2})(\%_{Ar})}$	-	-	0.033	0.001
$\beta_{i(P_B)^2}$	-0.603	$< 10^{-4}$	-0.08	$8 \cdot 10^{-4}$
R^2		1.00		1.00

Etch rate of PCL and PMMA

As mentioned PCL and PMMA were not investigated as thoroughly as PLLA. However, an indication of the etch rate for a specific set of parameters can be given. More interestingly an indication of the influence of some plasma parameters can be deduced. First of all it should be noted that these experiments were done at a significantly lower pressure than for PLLA. PCL is a polymer that also has an usability in the biological applications and is discussed first.

With PCL some invistigation on the plasma composition was done, using either oxygen or carbon dioxide, with either SF_6, argon, or nothing added. Ethcing of PCL in a plasma generated from carbon dioxide has less than half the etch rate compared to in an oxygen plasma. Even a plasma with 50 % argon and 50 % oxygen gives a higher etch rate than the carbon dioxide plasma. The etch rates obtained with a bias power of 150 W were between $0.45\,\mu m\,min^{-1}$ and $1.4\,\mu m\,min^{-1}$ for CO_2 and O_2 respectively.

The bias power also has an influence on the etch with 50 % oxygen and 50 % argon. If a bias power of only 15 W the etch does not remove much material and the etch rate is close to zero. This is indicative of a threshold energy required for removal of material from the surface.

For PMMA an etch rate of $200\,nm\,min^{-1}$ was obtained with a mixture of oxygen and carbon dioxide at a low bias power of 15 W. PMMA is often spun on wafers in thin layers and hence no optimization for higher etch rate was carried out. Both for PCL and PMMA the highest etch rates can be obtained in a pure oxygen plasma.

Surface roughness

The surface roughness of PMMA has not been investigated as the used layers were etched too little to show any significant roughening. However both for PLLA and PCL

a surface roughening was seen after etch. Especially in the etch tests with a pattern defined in a aluminum hard mask with photo resist on top. Both polymers will be treated simultaneously in the following discussion.

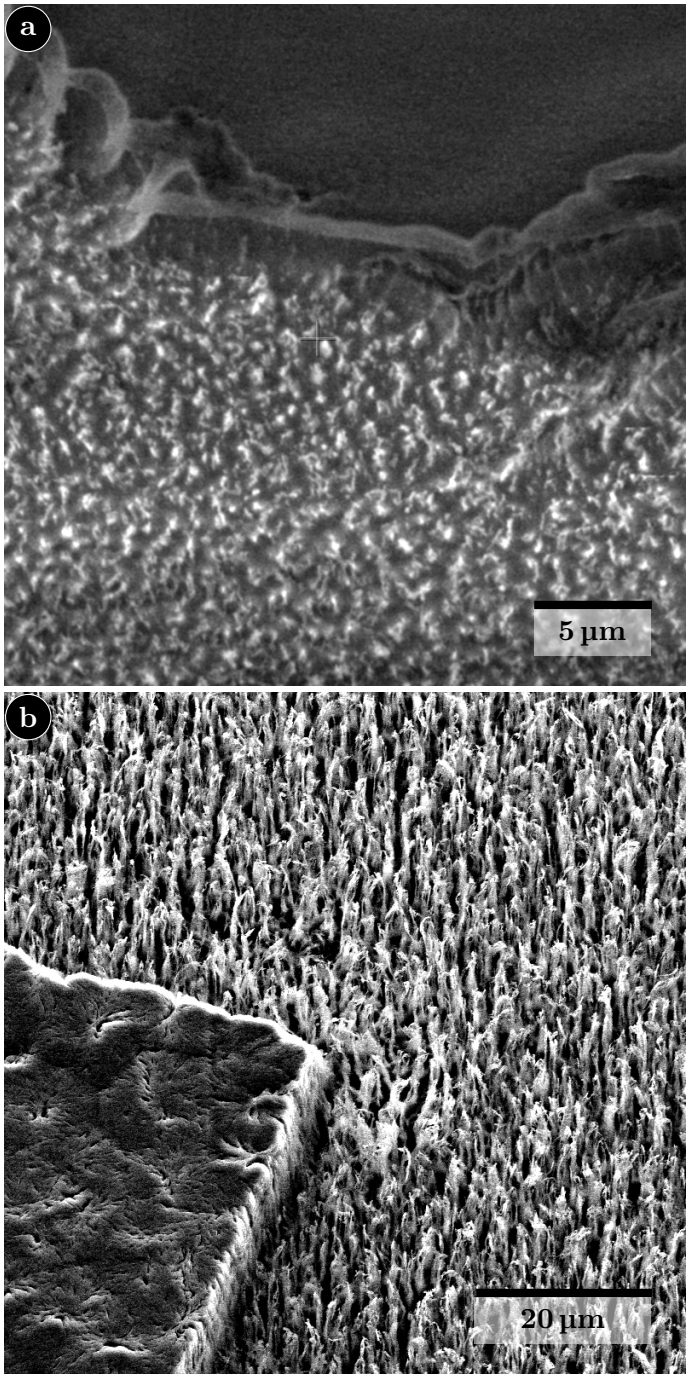

Figure 5.18: Etched PLLA (a) and PCL (b) with a hard mask shows severe surface roughening due to redeposition of the mask material. For PCL etching with a shadow mask roughness approach what was seen for SU-8 etching in an oxygen plasma.

In fig. 5.18a and fig. 5.18b shows etched PLLA and PCL respectively. Some surface roughening of PLLA is seen, as small bumps on the surface. This can be due to several things. As for TOPAS® it may be introduced by local masking from redeposited shadow mask aluminum. However, if an imprinted structure in PLLA without any masking was etched the surface also became rough as seen in fig. 5.19a.

For the PCL, shown in the right panel of the figures, a large difference in the roughness is seen. In fig. 5.18b high hair-like structures are seen, while only a low amount of roughness is seen on the imprinted and etched structure in fig. 5.19b. This is almost certainly an effect of local masking by redeposited mask material. It is however also indicative of some anisotropy of the etch, since the structures are not just under-etched and removed. PLLA appear to have a higher anisotropy than PCL, seen by in the thickness of the sidewalls left, see fig. 5.19. The etched structures had approximately the same thickness. The difference in height is because of different thicknesses of the spin-coated layer.

In the etch of PLLA as seen in fig. 5.19a cracking of the thick polymer layer occurred. This cracking is a consequence of thermal effects during etching. The heat conductivity of polymers is not high, and for a thick polymer etching will heat the layer a lot. This introduces thermal stresses in the material and ends up in cracking of the polymer. The effect can be reduced if a reduction of the heating during etch can be achieved. This will however reduce the etch rate and as seen in fig. 5.19a only larger areas have the problem. So if only smaller structures on the wafer are needed, it may be unimportant. Johan Nagstrup needed the round containers shown in the figures and hence the cracking of the surrounding material was of little importance.

5.3.3 Summary

The result presented here can be used as a guideline and starting point for further investigations with these polymers. Etch rates for PLLA, PCL, and PMMA can be varied quite a lot by changing the bias power or diluting the plasma with chemically inactive species. All the way from a couple of hundreds of $\mathrm{nm\,min^{-1}}$ up to tens of $\mathrm{\mu m\,min^{-1}}$ is possible to obtain without problems. The use of CO_2 instead of or as a supplement to O_2 lowers the etch rate and no improvement in surface roughness was seen. Hence I would recommend the use of pure O_2 as etch gas.

Some problems with etches was seen, in the form of surface roughness and polymer cracking. These problems may need to be addressed to obtain a polymer surface of a usable quality after etching. The amount of cracking might be reduced by ensuring less heating of the polymers during etching. This can either be done by reducing the polymer thickness or to etch parameters which will introduce less heating at the cost of a high etch rate.

5.4 Polymers summary

As outlined above etching of different polymers have many characteristics in common between the different polymers. However, there are also important differences such as varying etch rates and anisotropies. In general a high dependency on bias power was observed, and if no bias power was applied during etching the etch rate would be

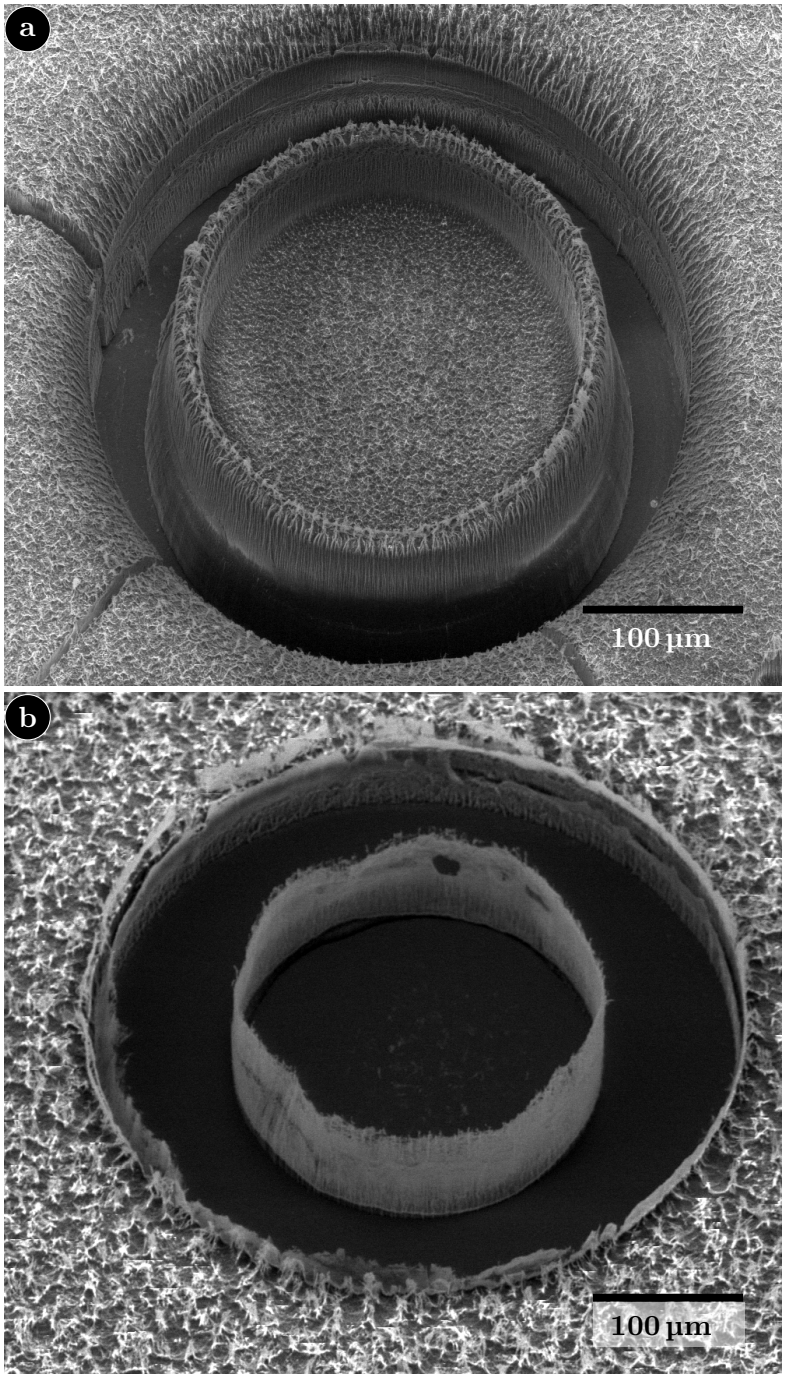

Figure 5.19: Etch of imprinted PLLA (a) and PCL (b) had slightly less rough surfaces after etching compared to samples with a shadow mask. However some roughening was seen especially on PCL. Cracking of the polymer was evident on thick polymer layers due to heat transfer problems.

negligible. This indicates that some energetic ions are needed to overcome a certain threshold for etching to begin.

It was also common for all etched polymers, that oxygen based plasmas resulted in higher etch rates compared to carbon dioxide based plasmas. If other gases were added to the plasma they in general lowered the etch rate by diluting the reactive species. However for SU-8 it was clear that adding SF_6 could increase the etch rate, since antimony would otherwise accumulate in the surface. Hence adding of additional gases is discouraged unless the specific gas is added to remove components of the polymer not removed by oxygen.

Selectivity and uniformity have not been investigated for all polymers. However, since photo resist is a polymer just like the etched materials, the selectivity is expected to be around 1. The uniformity on the other hand is highly dependent on the plasma density. The density in turn is dependent on coil power, pressure, and gas combination, among others. These parameters also have a large influence on the etch rate, which for some polymers easily reached tens of micrometer per minuter.

Chapter 6

Conclusion and outlook

In this project dry etching of a long list of materials have been investigated. For some materials only a limited number of experiments have be done, while etching of other materials have been explored more in depth. The materials investigated and some etch rates are listed in table 6.1. Ion beam etching of a magnetic structure containing several

Table 6.1: The minimum and maximum etch rates listed is the rates obtained in this process. The IBE processes are much slower than the ICP-RIE processes.

Etched Material	Process	Minumun Etch rate ($nm\,min^{-1}$)	Maximum Etch rate ($nm\,min^{-1}$)
Magnetic stack	IBE	13	25
Steel	IBE	8	12
Sapphire	ICP-RIE	38	74
SU-8	ICP-RIE	50	750
TOPAS®	ICP-RIE	25	375
PLLA	ICP-RIE	60	1500
PCL	ICP-RIE	450	1400
PMMA	ICP-RIE	200	200

different metals and of steel substrates have been undertaken. From etching of the magnetic structure problems with material redeposition at sidewalls was observed. This introduced shorts between two layers which was intended to electrically insulated from each other. However this could be remedied by means of a sidewall etch at the cost of structure quality. For the steel structures no such problem as redeposition was observed. The etch rate of steel was lower than what were seen for most other materials. The IBE etch rate for any material are quite low, on the order of $10\,nm\,min^{-1}$ to $40\,nm\,min^{-1}$, limiting the feasible depth that can be obtained by this method.

Etching of sapphire in inductively coupled plasma reactive ion etching with reasonable rates could be obtained considering the difficulties usually related to sapphire etching. For the use of sapphire as a prepatterned substrate for growth of LED's the structures should be almost cone like. This was achieved in a boron chloride and chlorine plasma, however the structures still had a flat surface at the top which is unwanted. If possible the best solution for this is to increase the resist height as the resist is completely removed during etching. For the same reason the height of the resist also determine the structure height and with the specific resist a selectivity of maximum 0.45 was obtained.

If etching of a polymer is wanted instead, a plasma rich in oxygen species must be used.

An oxygen plasma can be generated from several different gases, such as O_2 or CO_2, where the more oxygen rich O_2 plasma has a considerable faster etch rate. For SU-8 a plasma only containing oxygen has shown to be problematic, as the photo initiator contains antimony which accumulates at the surface. For removal of antimony SF_6 can be added to the plasma, which enables the generation of antimony fluoride molecules with relatively high vapor pressures. The removal of antimony is important to obtain a smooth surface in the etching. However, reactive gas species should not be added to the plasma if they are not needed as shown for PLLA.

PLLA, PCL, and PMMA can all be structured with good etch rates in an oxygen plasma. They do however all have a tendency to have more rough surfaces after etching, and this phenomenon is only increased if a hard mask material is exposed to the plasma. This can limit the etch depths that are feasible since the selectivity to photo resist is low due to their similar composition. TOPAS® also has poor selectivity to photo resist and surface roughness is present if the hard mask is exposed to the plasma. The etch rates of TOPAS® were found to be lower than for some of the other polymers. One of the reasons for this is the relatively low bias power used in the experiments. The bias power had a large influence on etch rate for all polymers, with increased etch rates for higher bias powers.

Bibliography

[1] H. Conrads and M. Schmidt. "Plasma generation and plasma sources". In: *Plasma Sources Sci. Technol* 9.4 (2000), pp. 441–454.

[2] G. Jackson. "R.F. sputtering". In: *Thin Solid Films* 5.4 (1970), pp. 209–246.

[3] R. A. Dugdale, J. T. Maskrey, S. D. Ford, P. R. Harmer, and R. E. Lee. "Glow discharge beam techniques". In: *J. Mater. sci.* 4.4 (1969), pp. 323–335.

[4] E. G. Spencer and P. H. Schmidt. "Ion-beam techniques for device fabrication". In: *J. Vac. Sci. Technol.* 8.5 (1971), S52–S70.

[5] N. Laegreid and G. K. Wehner. "Sputtering yields of metals for Ar^+ and Ne^+ Ions with Energies from 50 to 600 eV". In: *J. Appl. Phys.* 32.3 (1961), pp. 365–369.

[6] P. G. Glöersen. "Ion-beam etching". In: *J. Vac. Sci. Technol.* 12.1 (1975), p. 28.

[7] M. E. Walsh, Y. Hao, C. A. Ross, and H. I. Smith. "Optimization of a lithographic and ion beam etching process for nanostructuring magnetoresistive thin film stacks". In: *J. Vac. Sci. Technol. B* 18.6 (2000), pp. 3539–3543.

[8] G. Betz. "Alloy sputtering". In: *Surf. Sci.* 92.1 (1980), pp. 283–309.

[9] K. Naito, H. Hieda, M. Sakurai, Y. Kamata, and K. Asakawa. "2.5-inch disk patterned media prepared by an artificially assisted self-assembling method". In: *IEEE T. Magn.* 38.5 (2002), pp. 1949–1951.

[10] R. C. Sousa and P. P. Freitas. "Influence of ion beam milling parameters on MRAM switching". In: *IEEE T. Magn.* 37.4 (2001), pp. 1973–1975.

[11] S. Takahashi et al. "Ion-beam-etched profile control of MTJ cells for improving the switching characteristics of high-density MRAM". In: *IEEE T. Magn.* 42.10 (2006), pp. 2745–2747.

[12] K. Sugiura et al. "Ion beam etching technology for high-density spin transfer torque magnetic random access memory". In: *Jpn. J. Appl. Phys.* 48.8 (2009), 08HD02.

[13] H.-W. Ra, K. S. Song, and Y.-B. Hahn. "Submicron patterning of Ta, NiFe, and Pac-man type Ta/NiFe/Ta magnetic elements". In: *Korean J. Chem. Eng.* 22.5 (2005), pp. 793–796.

[14] K. Kinoshita, H. Utsumi, K. Suemitsu, H. Hada, and T. Sugibayashi. "Etching magnetic tunnel junction with metal etchers". In: *Jpn. J. Appl. Phys.* 49.8 (2010), 08JB02.

[15] T. Kato, K. Suzuki, S. Tsunashima, and S. Iwata. "Magnetic domain structure of NiFe and MnIr/NiFe elements patterned by focused ion beam". In: *Jpn. J. Appl. Phys.* 41.Part 2, No. 10A (2002), pp. L1078–L1080.

[16] H. N. Yu, R. H. Dennard, T. H. P. Chang, C. M. Osburn, V. Dilonardo, and H. E. Luhn. "Fabrication of a miniature 8K-bit memory chip using electron-beam exposure". In: *J. Vac. Sci. Technol.* 12.6 (1975), pp. 1297–1300.

[17] J. A. Bondur. “Dry process technology (reactive ion etching)”. In: *J. Vac. Sci. Technol.* 13.5 (1976), pp. 1023–1029.

[18] S. Somekh. “Introduction to ion and plasma etching”. In: *J. Vac. Sci. Technol.* 13.5 (1976), pp. 1003–1007.

[19] “Method of anisotropically etching silicon”. 5501893. F. Laermer and A. Schilp. 1996.

[20] “Method for anisotropic etching of silicon”. 6284148. F. Laermer and A. Schilp. 2001.

[21] “Method of anisotropic etching of silicon”. 6531068. F. Laermer and A. Schilp. 2003.

[22] M. Iio, M. Goto, H. Toyoda, and H. Sugai. “Relative cross sections for electron-impact dissociation of SF_6 into SF_x (x = 1−3) neutral radicals”. In: *Contrib. Plasma Phys.* 35.4-5 (1995), pp. 405–413.

[23] G. Kokkoris, A. Panagiotopoulos, A. Goodyear, M. Cooke, and E. Gogolides. “A global model for SF_6 plasmas coupling reaction kinetics in the gas phase and on the surface of the reactor walls”. In: *J. Phys. D: Appl. Phys.* 42.5 (2009), p. 055209.

[24] R. W. Boswell and R. K. Porteous. “Large volume, high density rf inductively coupled plasma”. In: *Appl. Phys. Lett.* 50.17 (1987), pp. 1130–1132.

[25] A. J. Perry and R. W. Boswell. “Fast anisotropic etching of silicon in an inductively coupled plasma reactor”. In: *Appl. Phys. Lett.* 55.2 (1989), pp. 148–150.

[26] D. C. Flanders, L. D. Pressman, and G. Pinelli. “Reactive ion etching of indium compounds using iodine containing plasmas”. In: *J. Vac. Sci. Technol. B* 8.6 (1990), pp. 1990–1993.

[27] G. Zorpette. “Let there be light [gallium nitride LED]”. In: *IEEE Spectrum* 51.9 (2002), pp. 70–74.

[28] S. Nakamura. “III–V nitride based light-emitting devices”. In: *Solid State Commun.* 102.2-3 (1997), pp. 237–248.

[29] C. I. H. Ashby, C. C. Mitchell, J. Han, N. A. Missert, P. P. Provencio, D. M. Follstaedt, G. M. Peake, and L. Griego. “Low-dislocation-density GaN from a single growth on a textured substrate”. In: *Appl. Phys. Lett.* 77.20 (2000), p. 3233.

[30] H. Gao, F. Yan, Y. Zhang, J. Li, Y. Zeng, and G. Wang. “Enhancement of the light output power of InGaN/GaN light-emitting diodes grown on pyramidal patterned sapphire substrates in the micro- and nanoscale”. In: *J. Appl. Phys.* 103.1 (2008), p. 014314.

[31] W.-K. Wang, D.-S. Wuu, S.-H. Lin, P. Han, R.-H. Horng, T.-C. Hsu, D. T.-C. Huo, M.-J. Jou, Y.-H. Yu, and A. Lin. “Efficiency improvement of near-ultraviolet InGaN LEDs using patterned sapphire substrates”. In: *IEEE J. Quantum Elect.* 41.11 (2005), pp. 1403–1409.

[32] J.-H. Lee, J. T. Oh, Y. C. Kim, and J.-H. Lee. “Stress reduction and enhanced extraction efficiency of GaN-based LED grown on cone-shape-patterned sapphire”. In: *IEEE Photon. Tech. L.* 20.18 (2008), pp. 1563–1565.

[33] M. A. Mastro, B.-J. Kim, Y. Jung, J. K. Hite, C. R. Eddy, and J. Kim. “Gallium nitride light emitter on a patterned sapphire substrate for improved defectivity and light extraction efficiency”. In: *Curr. Appl. Phys.* 11.3 (2011), pp. 682–686.

[34] K. Grigoras, L. Sainiemi, J. Tiilikainen, A. Säynätjoki, V.-M. Airaksinen, and S. Franssila. “Application of ultra-thin aluminum oxide etch mask made by atomic layer deposition technique”. In: *J. Phys.: Conf. Ser.* 61 (2007), pp. 369–373.

[35] X. Dongzhu, Z. Dezhang, P. Haochang, X. Hongjie, and R. Zongxin. “Enhanced etching of sapphire damaged by ion implantation”. In: *J. Phys. D: Appl. Phys.* 31.14 (1998), pp. 1647–1651.

[36] D.-J. Kang, I.-S. Kim, J.-H. Moon, and B.-T. Lee. “Inductively coupled plasma reactive ion etching of sapphire using C_2F_6- and NF_3-based gas mixtures”. In: *Mater. Sci. Semicond. Process.* 11.1 (2008), pp. 16–19.

[37] Y. Sung, H. Kim, Y. Lee, J. Lee, S. Chae, Y. Park, and G. Yeom. “High rate etching of sapphire wafer using $Cl_2/BCl_3/Ar$ inductively coupled plasmas”. In: *Mater. Sci. Eng. B* 82.1-3 (2001), pp. 50–52.

[38] C. H. Jeong, D. W. Kim, K. N. Kim, and G. Y. Yeom. “A study of sapphire etching characteristics using BCl_3-based inductively coupled plasmas”. In: *Jpn. J. Appl. Phys.* 41.Part 1, No. 10 (2002), pp. 6206–6208.

[39] C. Jeong, D. Kim, J. Bae, Y. Sung, J. Kwak, Y. Park, and G. Yeom. “Dry etching of sapphire substrate for device separation in chlorine-based inductively coupled plasmas”. In: *Mater. Sci. Eng. B* 93.1-3 (2002), pp. 60–63.

[40] Y. Hsu, S. Chang, Y. Su, J. Sheu, C. Kuo, C. Chang, and S. Shei. “ICP etching of sapphire substrates”. In: *Opt. Mater.* 27.6 (2005), pp. 1171–1174.

[41] E. Meeks, P. Ho, A. Ting, and R. J. Buss. “Simulations of $BCl_3/Cl_2/Ar$ plasmas with comparisons to diagnostic data”. In: *J. Vac. Sci. Technol. A* 16.4 (1998), pp. 2227–2239.

[42] C. Jeong, D. Kim, H. Lee, H. Kim, Y. Sung, and G. Yeom. “Sapphire etching with BCl_3/HBr/Ar plasma”. In: *Surf. Coat. Technol.* 171.1-3 (2002), pp. 280–284.

[43] D. Kim, C. Jeong, K. Kim, H. Lee, H. Kim, Y. Sung, and G. Yeom. “High rate sapphire (Al_2O_3) etching in inductively coupled plasmas using axial external magnetic field”. In: *Thin Solid Films* 435.1-2 (2003), pp. 242–246.

[44] L. Sha and J. P. Chang. “Plasma etching selectivity of ZrO_2 to Si in BCl_3/Cl_2 plasmas”. In: *J. Vac. Sci. Technol. A* 21.6 (2003), pp. 1915–1922.

[45] H.-K. Kim, J. W. Bae, T.-K. Kim, K.-K. Kim, T.-Y. Seong, and I. Adesida. “Inductively coupled plasma reactive ion etching of ZnO using BCl_3-based plasmas”. In: *J. Vac. Sci. Technol. B* 21.4 (2003), pp. 1273–1277.

[46] J. Shoeb and M. J. Kushner. “Mechanisms for plasma etching of HfO_2 gate stacks with Si selectivity and photoresist trimming”. In: *J. Vac. Sci. Technol. A* 27.6 (2009), pp. 1289–1302.

[47] F. D. Egitto. “Plasma etching and modification of organic polymers”. In: *Pure Appl. Chem.* 62.9 (1990), pp. 1699–1708.

[48] K. Tsougeni, N. Vourdas, A. Tserepi, E. Gogolides, and C. Cardinaud. "Mechanisms of oxygen plasma nanotexturing of organic polymer surfaces: from stable super hydrophilic to super hydrophobic surfaces". In: *Langmuir* 25.19 (2009), pp. 11748–11759.

[49] C. Zhang, C. Yang, and D. Ding. "Deep reactive ion etching of commercial PMMA in O_2/CHF_3, and O_2/Ar-based discharges". In: *J. Micromech. Microeng.* 14.5 (2004), pp. 663–666.

[50] E. Occhiello and F. Garbassi. "Halofluorocarbon plasma treatments of polystyrene and poly(methyl methacrylate) surfaces". In: *Polymer* 29.12 (1988), pp. 2277–2284.

[51] Y. S. Jung and C. A. Ross. "Orientation-controlled self-assembled nanolithography using a polystyrene−polydimethylsiloxane block copolymer". In: *Nano Lett.* 7.7 (2007), pp. 2046–2050.

[52] J. Garra, T. Long, J. Currie, T. Schneider, R. White, and M. Paranjape. "Dry etching of polydimethylsiloxane for microfluidic systems". In: *J. Vac. Sci. Technol. A* 20.3 (2002), pp. 975–982.

[53] S. J. Hwang, D. J. Oh, P. G. Jung, S. M. Lee, J. S. Go, J.-H. Kim, K.-Y. Hwang, and J. S. Ko. "Dry etching of polydimethylsiloxane using microwave plasma". In: *J. Micromech. Microeng.* 19.9 (2009), p. 095010.

[54] B. Lamontagne, O. M. Küttel, and M. R. Wertheimer. "Etching of polymers in microwave/radio-frequency O_2–CF_4 plasma". In: *Can. J. Phys.* 69.3-4 (1991), pp. 202–206.

[55] "Photoresist composition and printed circuit boards and packages made therewith". 4882245 (US). J. D. Gelorme, R. J. Cox, and S. A. R. Gutierrez. 361/379; 361/412; 428/195; 428/201; 428/209; 428/220; 428/332; 428/901; 430/14; 430/18; 430/271; 430/275; 430/280; 522/170; 74/685. 1989.

[56] Momentive Specialty Chemicals Inc. *EPON™ Resin SU-8 (a.k.a. EPIKOTE™ 157)*. Momentive.com - EPON Resin SU-8. 2001. URL: http://www.momentive.com/Products/TechnicalDataSheet.aspx?id=3603 (visited on 01/08/2013).

[57] K. Y. Lee, N. LaBianca, S. A. Rishton, S. Zolgharnain, J. D. Gelorme, J. Shaw, and T. H. P. Chang. "Micromachining applications of a high resolution ultrathick photoresist". In: *J. Vac. Sci. Technol. B* 13.6 (1995), pp. 3012–3016.

[58] L. Guerin, M. Bossel, M. Demierre, S. Calmes, and P. Renaud. "Simple and low cost fabrication of embedded micro-channels by using a new thick-film photoplastic". In: *Transducers 97*. 1997 International Conference on Solid State Sensors and Actuators. Vol. 2. Chicago: IEEE, 1997, pp. 1419–1422.

[59] R. J. Jackman, T. M. Floyd, R. Ghodssi, M. A. Schmidt, and K. F. Jensen. "Microfluidic systems with on-line UV detection fabricated in photodefinable epoxy". In: *J. Micromech. Microeng.* 11.3 (2001), pp. 263–269.

[60] K. B. Mogensen, J. El-Ali, A. Wolff, and J. P. Kutter. "Integration of Polymer Waveguides for Optical Detection in Microfabricated Chemical Analysis Systems". In: *Appl. Opt.* 42.19 (2003), pp. 4072–4079.

[61] S. Balslev, A. M. Jorgensen, B. Bilenberg, K. B. Mogensen, D. Snakenborg, O. Geschke, J. P. Kutter, and A. Kristensen. “Lab-on-a-chip with integrated optical transducers”. In: *Lab Chip* 6.2 (2005), pp. 213–217.

[62] M. Nordström, S. Keller, M. Lillemose, A. Johansson, S. Dohn, D. Haefliger, G. Blagoi, M. Havsteen-Jakobsen, and A. Boisen. “SU-8 cantilevers for bio/chemical sensing; fabrication, characterisation and development of novel read-out methods”. In: *Sensors* 8.3 (2008), pp. 1595–1612.

[63] P. M. Dentinger, W. Clift, and S. H. Goods. “Removal of SU-8 photoresist for thick film applications”. In: *Microelectron. Eng.* 61-62 (2002), pp. 993–1000.

[64] G. Hong, A. Holmes, and M. Heaton. “SU8 resist plasma etching and its optimisation”. In: *Microsys. Technol.* 10.5 (2004), pp. 357–359.

[65] H. Mischke, G. Gruetzner, and M. Shaw. “Plasma etching of polymers like SU8 and BCB”. In: *Micromachining and Microfabrication Process Technology VIII*. Ed. by J. Yasaitis, M. PerezMaher, and J. Karam. Vol. 4979. Proceedings of the society of photo-optical instrumentation engineers (SPIE). Conference on Micromachining and Microfabrication Process Technology VIII, SAN JOSE, CA, JAN 27-29, 2003. 1000 20TH ST, PO BOX 10, Bellingham, WA 98227-0010 USA: SPIE, 2003, pp. 372–381.

[66] M. F. L. De Volder, R. Vansweevelt, P. Wagner, D. Reynaerts, C. Van Hoof, and A. J. Hart. “Hierarchical carbon nanowire microarchitectures made by plasma-assisted pyrolysis of photoresist”. In: *ACS Nano* 5.8 (2011), pp. 6593–6600.

[67] T. Gebel. “Arsenic and antimony: comparative approach on mechanistic toxicology”. In: *Chem. Biol. Interact.* 107.3 (1997), pp. 131–144.

[68] K. Kuroda, G. Endo, A. Okamoto, Y. S. Yoo, and S.-i. Horiguchi. “Genotoxicity of beryllium, gallium and antimony in short-term assays”. In: *Mutat. Res. Lett.* 264.4 (1991), pp. 163–170.

[69] L. Bregoli, F. Chiarini, A. Gambarelli, G. Sighinolfi, A. M. Gatti, P. Santi, A. M. Martelli, and L. Cocco. “Toxicity of antimony trioxide nanoparticles on human hematopoietic progenitor cells and comparison to cell lines”. In: *Toxicology* 262.2 (2009), pp. 121–129.

[70] R. Lamonte and D. McNally. “Cyclic olefin copolymers”. English. In: *Adv. Mater. Processes* 159.3 (2001), pp. 33–36.

[71] C. Markos, A. Stefani, K. Nielsen, H. K. Rasmussen, W. Yuan, and O. Bang. “High-T_g TOPAS microstructured polymer optical fiber for fiber Bragg grating strain sensing at 110 degrees”. In: *Opt. Express.* 21.4 (2013), pp. 4758–4765.

[72] G. Palmer, Changfang Zhu, T. Breslin, Fushen Xu, K. Gilchrist, and N. Ramanujam. “Comparison of multiexcitation fluorescence and diffuse reflectance spectroscopy for the diagnosis of breast cancer (March 2003)”. In: *IEEE T. Bio-Med. Eng.* 50.11 (2003), pp. 1233–1242.

[73] T. Nielsen, D. Nilsson, F. Bundgaard, P. Shi, P. Szabo, O. Geschke, and A. Kristensen. “Nanoimprint lithography in the cyclic olefin copolymer, Topas®, a highly ultraviolet-transparent and chemically resistant thermoplast”. In: *J. Vac. Sci. Technol. B* 22.4 (2004), pp. 1770–1775.

[74] S.-J. Hwang, M.-C. Tseng, J.-R. Shu, and H. Her Yu. "Surface modification of cyclic olefin copolymer substrate by oxygen plasma treatment". In: *Surf. Coat. Technol.* 202.15 (2008), pp. 3669–3674.

[75] T. I. Wallow et al. "Reactive ion etching of 193-nm resist candidates: current platforms and future requirements". In: *Proc. SPIE.* Advances in Resist Technology and Processing XV. Vol. 3333. Santa Clara, CA, USA: Will Conley, 1998, pp. 92–101.

[76] F. Wang, C. Bertelsen, G. Skands, T. Pedersen, and O. Hansen. "Reactive ion etching of polymer materials for an energy harvesting device". In: *Microelectron. Eng.* 97 (2012), pp. 227–230.

[77] J. Nagstrup, S. Keller, K. Almdal, and A. Boisen. "3D microstructuring of biodegradable polymers". In: *Microelectron. Eng.* 88.8 (2011), pp. 2342–2344.

[78] J. R. Coupland, T. S. Green, D. P. Hammond, and A. C. Riviere. "A study of the ion beam intensity and divergence obtained from a single aperture three electrode extraction system". In: *Rev. Sci. Instrum.* 44.9 (1973), pp. 1258–1270.

[79] H. Jansen, M. d. Boer, R. Legtenberg, and M. Elwenspoek. "The black silicon method: a universal method for determining the parameter setting of a fluorine-based reactive ion etcher in deep silicon trench etching with profile control". In: *J. Micromech. Microeng.* 5.2 (1995), pp. 115–120.

[80] D. C. Montgomery. *Design and analysis of experiments.* English. 7th ed. Hoboken, NJ: Wiley, 2009.

[81] M. Repoux. "Comparison of background removal methods for XPS". In: *Surf. Interface Anal.* 18.7 (1992), pp. 567–570.

[82] M. Buehler and C. Hershey. "The split-cross-bridge resistor for measuring the sheet resistance, linewidth, and line spacing of conducting layers". In: *IEEE T. Electron Dev.* 33.10 (1986), pp. 1572–1579.

[83] A. Walton. *Microelectronic test structures.* English. Dordrecht: Kluwer, 1998.

[84] *Ion Beam System - Ionfab 300Plus - Oxford Instruments.* URL: http://www.oxford-instruments.com/products/etching-deposition-and-growth/tools/ion-beam-etch-deposition-systems/ion-beam-system-ionfab-300plus (visited on 01/16/2013).

[85] S. Jensen. "Inductively coupled plasma etching for microsystems". English. Ph.D. Thesis. MIC - Department of Micro- and Nanotechnology: Technical University of Denmark, 2004. 125 pp.

[86] D. Nečas and P. Klapetek. "Gwyddion: an open-source software for SPM data analysis". In: *Cent. Europ. J. Phys.* 10.1 (2011), pp. 181–188.

[87] B. Dalslet, M. Donolato, and M. Hansen. "Planar Hall effect sensor with magnetostatic compensation layer". In: *Sensor Actuat. A-Phys.* 174 (2012), pp. 1–8.

[94] K. H. Rasmussen, S. S. Keller, F. Jensen, A. M. Jorgensen, and O. Hansen. "SU-8 etching in inductively coupled oxygen plasma". In: *Microelectron. Eng.* 112 (2013), pp. 35–40.

[89] L. Amato, S. S. Keller, A. Heiskanen, M. Dimaki, J. Emnéus, A. Boisen, and M. Tenje. "Fabrication of high-aspect ratio SU-8 micropillar arrays". In: *Microelectron. Eng.* 98 (2012), pp. 483–487.

[90] T. Honma, R. Sato, Y. Benino, T. Komatsu, and V. Dimitrov. "Electronic polarizability, optical basicity and XPS spectra of Sb_2O_3–B_2O_3 glasses". In: *J. Non-Cryst. Solids* 272.1 (2000), pp. 1–13.

[91] J. F. Moulder and J. Chastain. *Handbook of x-ray photoelectron spectroscopy: a reference book of standard spectra for identification and interpretation of XPS data.* English. Eden Prairie, Minn.: Physical Electronics Division, Perkin-Elmer Corp., 1992.

[92] J. D. Plummer, M. Deal, and P. B. Griffin. *Silicon VLSI technology: fundamentals, practice and modeling.* English. Upper Saddle River: Prentice Hall, 2000.

[93] W. M. Haynes. *CRC handbook of chemistry and physics: a ready-reference book of chemical and physical data.* English. 94th ed. Boca Raton, Fla.: CRC Press/Taylor & Francis, 2013.

Appendix A

MNE 2012

Results from the experiments with SU-8 was first presented at the 38th International Conference on Micro and Nano Engineering. The conference was held in Toulouse, France, in September 2012 Below the abstract and the poster that were presented are shown.

Surface properties of plasma etched SU-8

Kristian Hagsted Rasmussen [a], Stephan S. Keller [a], Ole Hansen [a],
Anders M. Jorgensen [b], Flemming Jensen [b]

[a] DTU Nanotech, Technical University of Denmark, Kongens Lyngby, DK-2800, Denmark
[b] DTU Danchip, Technical University of Denmark, Kongens Lyngby, DK-2800, Denmark
e-mail: kristian.rasmussen@nanotech.dtu.dk

Keywords: Plasma etching, SU-8, RIE, surface composition, XPS.

The epoxy based photo resist SU-8 has many applications in microtechnology, due to its easy manufacturing and many good properties such as chemical stability. The as coated SU-8 has a smooth surface, see fig. 1. And as seen from the XPS measurement in fig. 2 it is primarily containing carbon, oxygen and hydrogen, but with traces of antimony from the cross-linker. Oxygen plasma treatment is used for cleaning and surface activation of SU-8, but composition of the surface SU-8 layer will change by this treatment. Controlled etching of SU-8 can also be obtained by oxygen plasma, e.g. to obtain structures with higher aspect ratio than what is possible by i-line photo lithography. This increase in aspect ratio can be achieved by an isotropic plasma etching process of the lithographically defined structures. The goal of this study is to reach an understanding of changes in surface roughness and composition depending on etching parameters.

The samples were prepared on silicon wafers with a 2 µm grown silicon dioxide, whereon 25 µm of SU-8 2075 was spin coated. The SU-8 was exposed through a mask and developed in PGMEA to define a pattern for measurement of height and line width reductions. Etching was done in an ASE etcher from STS, with SF_6 and O_2 as etch gasses, while CO_2 is also available on the system it has not been used in the current study. SEM, AFM, and XPS have been used to characterize the surface in terms of visual surface topology, surface roughness, and surface composition, respectively. Design of Experiments with varying SF6 flow rate, chamber pressure, chuck temperature, and platen power has been used to screen for the optimal etching conditions. While the coil power used for plasma generation and the O_2 flow rate have been kept constant.

Several groups have observed that oxygen plasma introduces severe surface roughness [1, 2, 3]. Recently De Volder et.al [2] has mentioned antimony as a potential reason for generation of this rough polymer surface. In our current work we can confirm the hypothesis that the antimony present in SU-8 (in the photo-initiator required for cross linking) has a significant effect on etching characteristics. In fig. 3 severe surface roughness can be seen after etch, and from the XPS spectrum in fig. 4 the atomic content of antimony is found to around 20%. The antimony from the cross linker will accumulate at the surface during etching, where it will act as local mask resulting in increased surface roughness. Surface roughness might not be the only issue, since antimony is toxic to cells. SU-8 surfaces that have been plasma treated are not suitable for biological applications without further treatment to remove the antimony.

We have found that changing the composition of the plasma by addition of fluorine reduces the antimony concentration at the surface and prevents generation of a rough surface unlike the pure oxygen plasmas. In fig. 5 the surface after etching in a plasma containing 5% fluorine is seen to be less rough than a surface etched in pure oxygen. This is confirmed by the XPS spectrum in fig. 6 which estimates the atomic antimony content to around 4%. Furthermore, other parameters such as platen temperature, platen power, and chamber pressure do also have an influence on the surface properties, and can be tuned to reduce the antimony concentration at the surface even further.

[1] F. Chollet. "su-8: Thick photo-resist for mems". http://memscyclopedia.org/su8.html, May 2009.
[2] M. F. L. De Volder, R. Vansweevelt, P. Wagner, D. Reynaerts, C. Van Hoof, and A. J. Hart, ACS Nano, 5(8) (2011) 6593-6600.
[3] G. Hong, A. Holmes, and M. Heaton, Microsystem Technologies, 10 (2004) 357-359.

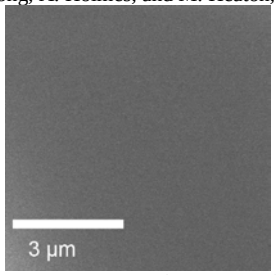

Figure 1. SEM picture of SU-8 surface after development and hard bake, the surface is smooth.

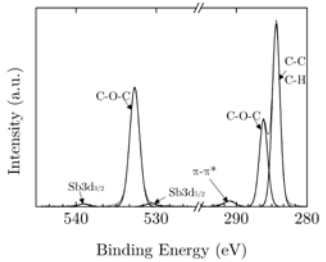

Figure 2. XPS spectrum for O, C and Sb in SU-8 surface after development and hard bake. Only a weak trace of antimony is observed, less than 1% in atomic content.

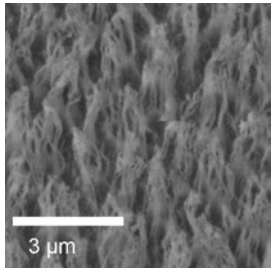

Figure 3. SEM picture of SU-8 surface after exposure to oxygen plasma for 30 min. Very high thin structures are covering the surface giving a high surface roughness.

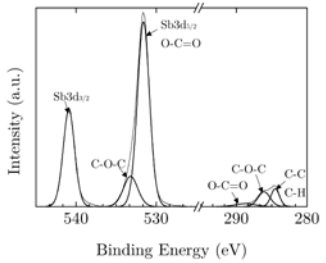

Figure 4. XPS spectrum of SU-8 surface after exposure to oxygen plasma for 30 min. The antimony concentration in the surface is very high, approx 20% of atomic content.

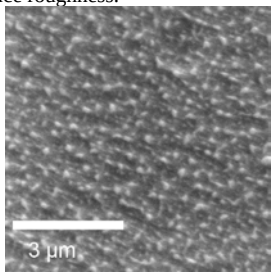

Figure 5. SEM picture of SU-8 surface after exposure to oxygen plasma with 5% SF_6 for 30 min. The surface roughness is considerably reduced compared to Fig 3.

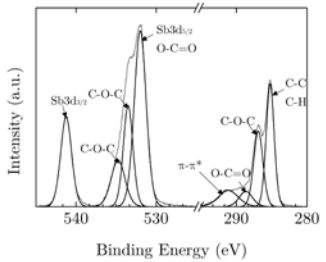

Figure 6. XPS spectrum of SU-8 surface after exposure to oxygen plasma with 5% SF_6 for 30 min. The antimony to carbon ratio is significantly decreased, resulting in a surface composition close to that of non etched SU-8, with only 4% of antimony in surface.

DTU Nanotech
Department of Micro- and Nanotechnology

Surface properties of plasma etched SU-8

Kristian Hagsted Rasmussen*†, Ole Hansen†, Flemming Jensen‡, Stephan S. Keller†, and Anders M. Jorgensen‡

Oxygen plasma etching of cross linked SU-8 results in severe surface roughening and antimony contamination. Design of Experiments (DoE) was used to optimize etch settings for improved surface morphology and composition control.

Experiments

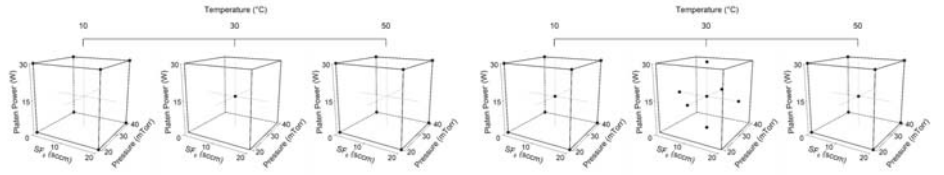

Design of Experiments was used to get an overview of the influence from the different etch parameters. This resulted in 19 experiments for 4 parameters arranged as a full factorial with 3 center points, as shown above.

In the first experiments curvature was observed which was investigated by adding 8 facial points with two extra center points. Above the final set of experiments are shown including the first 19 experiments.

25 µm SU-8 was spin coated on oxidized silicon wafers, exposed, developed, and RIE etched. DoE was used to vary pressure, temperature, platen power, and SF_6 flow rate in the RIE etch. All other factors e.g. oxygen flow rate and coil power were held constant. Samples were characterized using profilometery, SEM, AFM, and XPS.

SU-8 etch rate

Both high etch rate and high anisotropy are easily obtained simultaneously, however roughness will increase slightly. High isotropy results in lower etch rate since physical etch is minimized.

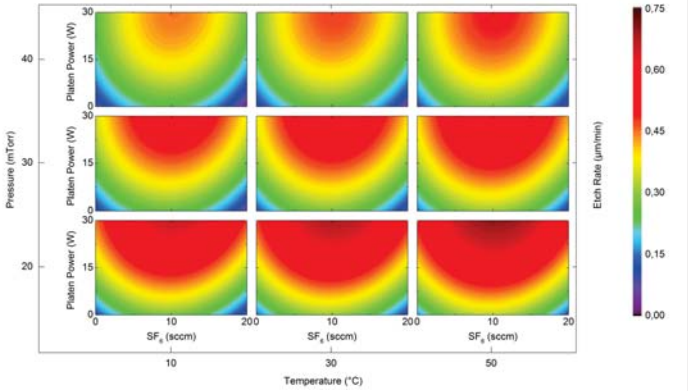

The etch rates dependency on reactive species in the plasma and surface bombardment, give rise to a dependency on all four parameters. Pressure and SF_6 flow rate will change the concentration of reactive species. While increased platen power will increase the ion flux density and the temperature will increase the volatility, both will result in increased etch rate.

Surface roughness and antimony contamination

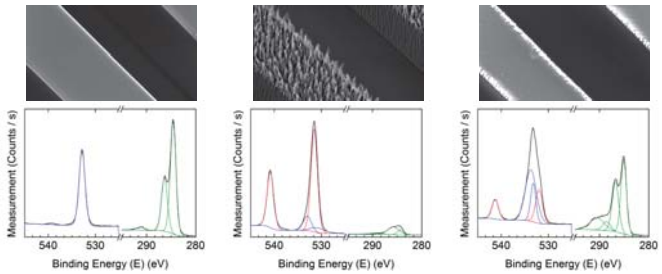

SEM images of SU-8 lines with the corresponding XPS spectra below, from left to right: as prepared SU-8, SU-8 etched in pure Oxygen, and SU-8 etched with SF_6 added and at high temperature. In the XPS spectra the black curves are the measurements, blue, red, and green curves represents peak fits for oxygen, antimony, and carbon peaks respectively. As seen by comparing SEM images and XPS peak fits, roughness and antimony concentration are correlated.

The surface roughness of SU-8, RIE etched in oxygen, approach 15% of the etched depth. The roughness can be reduced by reducing antimony surface contamination through optimization of SF_6 flow rate and platen power. XPS shows that increased SF_6 flow rate increases fluorine but reduces antimony contamination in the surface. This imply that excess fluorine in the plasma enables formation of volatile SbF_5, instead of nonvolatile Sb or SbO_x.

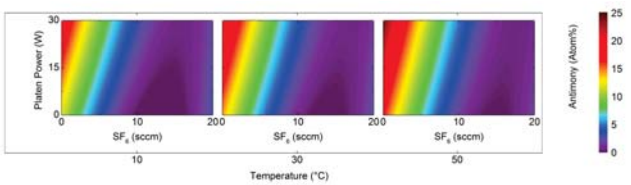

Antimony is inherent in small concentrations in SU-8 as part of the photo initiator. When SU-8 is exposed to an oxygen plasma antimony accumulate on the surface. SF_6 added to the plasma helps to reduce surface antimony by volatilizing $SbF_{(3-5)}$. Low platen power also reduces the surface concentration since the etch rate is reduced.

Etch anisotropy

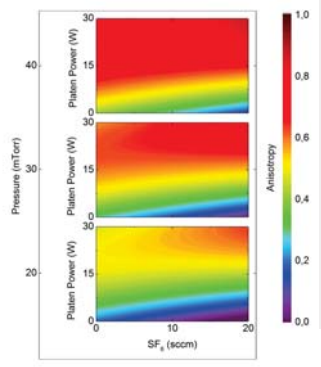

The anisotropy of the etch depends on SF_6 flow rate, platen power and pressure, where both higher platen power and pressure increase the anisotropy, while increased SF_6 flow rate decreases the anisotropy at low platen power and increases it for high platen power.

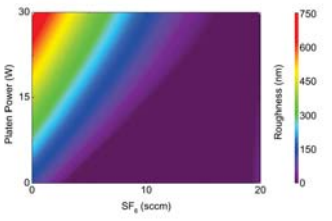

Both the antimony surface concentration and the roughness decreases with increased SF_6 flow rate and decreased platen power. Neither temperature nor pressure contribute to the roughness.

The two extremes of anisotropy are obtained by setting the SF_6 flow rate high and both pressure and platen power either high or low.

We have shown that a high degree of control of etched SU-8 surface morphology and composition can be obtained by choosing optimized etch parameters.

†DTU Nanotech, Technical University of Denmark
Oersteds Plads, building 345E
DK-2800 Kongens Lyngby, Denmark

‡DTU Danchip, Technical University of Denmark
Oersteds Plads, building 347
DK-2800 Kongens Lyngby, Denmark

*Presenting author: Kristian Hagsted Rasmussen
kristian.rasmussen@nanotech.dtu.dk

Appendix B

Article

The SU-8 results was later submitted to Microelectronic Engineering, and accepted for publication the 16 May 2013. The paper was available only in the beginning of June, and will be published in the December number of the journal. Published:

K. H. Rasmussen, S. S. Keller, F. Jensen, A. M. Jorgensen, and O. Hansen. "SU-8 etching in inductively coupled oxygen plasma". In: *Microelectron. Eng.* 112 (2013), pp. 35–40.

Microelectronic Engineering 112 (2013) 35–40

Contents lists available at SciVerse ScienceDirect

Microelectronic Engineering

journal homepage: www.elsevier.com/locate/mee

SU-8 etching in inductively coupled oxygen plasma ☆

Kristian Hagsted Rasmussen [a,*], Stephan Sylvest Keller [a], Flemming Jensen [b], Anders Michael Jorgensen [b], Ole Hansen [a,c]

[a] Department of Micro- and Nanotechnology, Technical University of Denmark, DTU Nanotech Building 345E, DK-2800 Kgs. Lyngby, Denmark
[b] DTU Danchip, Technical University of Denmark, Oersteds Plads Building 347, DK-2800 Kgs. Lyngby, Denmark
[c] CINF – Center for Individual Nanoparticle Functionality, Technical University of Denmark, DK-2800 Kgs. Lyngby, Denmark

ARTICLE INFO

Article history:
Received 1 February 2013
Received in revised form 9 April 2013
Accepted 16 May 2013
Available online 7 June 2013

Keywords:
Dry etching
ICP-RIE
SU-8
Antimony
Roughness
SF_6

ABSTRACT

Structuring or removal of the epoxy based, photo sensitive polymer SU-8 by inductively coupled plasma reactive ion etching (ICP-RIE) was investigated as a function of plasma chemistry, bias power, temperature, and pressure. In a pure oxygen plasma, surface accumulation of antimony from the photo-initiator introduced severe roughness and reduced etch rate significantly. Addition of SF_6 to the plasma chemistry reduced the antimony surface concentration with lower roughness and higher etch rate as an outcome. Furthermore the etch anisotropy could be tuned by controlling the bias power. Etch rates up to 800 nm min^{-1} could be achieved with low roughness and high anisotropy.

© 2013 The Authors. Published by Elsevier B.V. All rights reserved.

1. Introduction

SU-8 is an epoxy based, photo sensitive polymer developed by IBM in the late 1980s [1]. SU-8 negative photo resist is derived from EPON™resin [2], where the monomer consists in average of eight epoxy groups and eight aromatic benzene groups as indicated by the name. The viscous polymer contains between 5% and 10% photo-initiator enabling cross linking by standard I-line lithography. The photo-initiator used for the SU-8 resin is based on triarylsulfonium–hexafluoroantimonium, adding fluorine, sulfur, and antimony to the carbon, hydrogen, and oxygen from the monomers as elements in the SU-8 resin.

SU-8 in microtechnology was developed for use in LIGA[1] [3] where the polymer is used to define a structured mold. Furthermore, SU-8 was interesting as etch mask, due to the patterning by standard photolithography. The chemical resistance of SU-8, however, complicates the removal of the resist in both applications, with plasma removal as one of the only reliable option. Therefore, the most thoroughly discussed subject in SU-8 etching is complete removal of SU-8 after its use as masking material.

More recently, SU-8 has been used as a device layer rather than a sacrificial layer. Fabrication of devices in SU-8 can in general be accomplished by photo-lithography, for a large number of applications. Lab on a chip (LOC) systems with microfluidic channels made in SU-8 [4,5], have advantages such as biological compatibility and easy fabrication. Devices for optical applications such as polymer waveguides [6] and optical transducers [7] have been shown. Furthermore, the mechanical properties of SU-8 make it an obvious choice for cantilever sensors [8].

Plasma treatment of all of these devices can be used for several purposes. Probably the most relevant cases of plasma treatment of SU-8, in addition to removal, is functionalization or activation of a surface. This can for example be used to tune the hydrophobicity of a surface or change the surface termination to alter the bonding capabilities [9]. For some applications further patterning of the SU-8 after the initial photo-lithography in the form of etching might be interesting. For instance an isotropic etch can be used to increase the aspect ratio or decrease the line width of lithographically defined structures.

In the scarce literature on SU-8 etching available, most authors agree on the need for fluorine in the plasma chemistry. However, there has not been offered a satisfying explanation for this observation.

Dentinger et al. [10] presented a study on different methods for SU-8 removal, including removal using solvents, chemical removal

☆ This is an open-access article distributed under the terms of the Creative Commons Attribution License, which permits unrestricted use, distribution, and reproduction in any medium, provided the original author and source are credited.

* Corresponding author. Address: Building 344, Room No. 208, Oersteds Plads, DK-2800 Kgs. Lyngby, Denmark. Tel.: +45 4525 5848; fax: +45 4588 7762.
E-mail addresses: khara@nanotech.dtu.dk, kristian.rasmussen@nanotech.dtu.dk (K.H. Rasmussen).

[1] Lithographie, Galvanoformung, Abformung.

0167-9317/$ - see front matter © 2013 The Authors. Published by Elsevier B.V. All rights reserved.
http://dx.doi.org/10.1016/j.mee.2013.05.011

in different plasma etching configurations, and other more exotic methods. For our study the chemical removal in any type of plasma setting is interesting. Both, results from reactive ion etching (RIE) as well as downstream chemical etching (DCE) can increase the understanding of the different mechanism involved in the process. Etch rates of 1–4 μm min^{-1} were obtained in RIE using a mixture of CF_4/O_2 in approximately equal proportions [10].

In DCE, Dentinger et al. observed that only 2–4% of CF_4 was needed to obtain etch rates as high as 10 μm min^{-1}. However, to obtain such high rates the temperature was elevated to 275 °C. Such high temperatures will introduce thermal stress in the polymer, increasing the risk of cracking and peeling. It will also cause compatibility problems with some materials in practical applications. Furthermore, surface contamination with antimony was observed after complete SU-8 removal. Dentinger et al. ascribed the surface antimony contamination to residues left from the photo initiator.

The influence of fluorine on etching of cured SU-8 is also discussed by Hong et al. [11] and Mischke et al. [12]. Mischke et al. used CF_4 just as Dentinger et al. did, while Hong et al. added SF_6 as fluorine source to the plasma. Hong et al. limit the discussion to etch rate and anisotropy without discussing chemical composition. However Mischke et al. [12] used Energy-dispersive X-ray spectroscopy (EDX) on etched SU-8 surfaces to identify antimony and fluorine in addition to the expected carbon and oxygen. Mischke et al. conclude that fluorine is introduced by the etch chemistry, neglecting the fact that the photo initiator in SU-8 is triarylsulfonium hexafluorantimonium which includes SbF_6^+ ions.

De Volder et al. [13] used plasma etching to produce nanowires in SU-8. Their process is basically an oxygen plasma etch where they also see an accumulation of antimony at the surface; the antimony is believed to act as local masking agent and starting point of the nanowires. X-ray photoelectron spectroscopy (XPS) analysis of the surface shows up to 19%$_{atom}$ antimony surface concentration in their experiments. Similar to Mischke et al. no external source for antimony was present, and the antimony must hence originate from the SU-8 photo-initiator. For removal of SU-8 this will result in rough surfaces and low etch rates and should be avoided.

The presence of antimony in plasma treated surfaces is a problem for biological applications since antimony is toxic. This does not only apply to samples structured by plasma etching, but also surfaces cleaned or primed in an oxygen plasma will have increased concentrations of antimony in the surface after a shallow etch. Small amounts of antimony may not be critical since the toxicity is weaker than e.g. that of arsenic [14,15]. However, since etching generates thin hairlike structures it can be assumed that the antimony present in the surface is on nanometer scale, for which Bregoli et al. [16] has evaluated the toxicity and found it poisonous. It is important to minimize the antimony concentration to achieve relevant results for biological experiments performed on SU-8 chips.

In this work we will discuss structuring of SU-8 in an ICP-RIE oxygen plasma with varying SF_6 content. Control of antimony concentration and surface roughness will be discussed, together with measurements of etch anisotropy and rate. We will in more detail discuss the influence of antimony on the surface quality obtained and link it to the etch chemistry.

2. Experimental

All SU-8 etching experiments were done in a turbo pumped, inductively coupled plasma (ICP) system, Advanced Silicon Etcher (ASE HC250M) from STS, refitted for polymer etching. The system is fitted with two RF power supplies; the main power supply, the Coil Power, controls the intensity of the plasma, while the secondary power supply, the Bias Power, controls the ion energy of the ion flux to the etched substrate. In the experiments reported here, the feed gasses oxygen (O_2) and sulfur hexafluoride (SF_6) were used at flow rates controlled using mass flow controllers. The pressure in the etch chamber is controlled by a throttle valve and measured using a pressure gauge. All sample preparation and characterization except XPS was carried out in a cleanroom environment.

Since plasma etching, in general, is a very complicated process involving many parameters, Design of Experiments (DoE) was used to reduce the number of experiments necessary to identify the most important parameter relations in etching of SU-8.

2.1. Design of experiments

The number of experiments conducted was reduced by selecting the four most important parameters for variation, Table 1 while the remaining parameters were kept constant. The O_2 flow rate (Q_{O_2}) was keep constant at 99 sccm, while the SF_6 flow rate (Q_{SF_6}) was varied between 0 and 20 sccm. The pressure in the etch chamber was controlled to keep the gas density stable. Since the pressure has a pronounced effect on etch characteristics, the pressure (p) was varied between 20 and 40 mTorr. It should be noted that the system was run in automatic pressure control mode, which continuously adjusts the throttle valve to keep a constant pressure during etch. The coil power (P_C) was fixed at 1000 W, while the bias power (P_B) was varied between 0 and 30 W. Finally, the substrate chuck temperature (T) was controlled between 10 and 50 °C. This design resulted in a full factorial screening in four parameters, where three center points were used to check for quadratic curvature, where the quadratic term of a parameter is needed to generate a valid model. The total number of experiments in this setup is 19, which were processed for 20 min each. The experiments in the design were carried out in random order.

After completion of the first set of experiments it was evident that curvature was present in the response. To enable data analysis and generation of a valid model for the system, the curvature was addressed by adding eight face centered points with two additional center points to the design. A face centered point is a center point with one parameter value at min or max. The ten extra experiments were also carried out in random order, and the center points were used to check for variations between the two sets of experiments. The final dataset comprises the 19 initial experiments combined with the 10 additional, giving a total of 29 experiments to characterize.

2.2. Sample preparation

Samples were prepared by spinning 25 μm SU-8 2075 resist on 100 mm silicon wafers with a 2 μm thick thermal silicon dioxide followed by 1 h of baking on a hotplate at 50 °C [17]. The samples were exposed with 150 mJ cm^{-2} at the I-line, through a test mask with line arrays of different widths, and baked for 2 h at 50 °C on a hotplate, followed by development in PGMEA. Finally, to completely crosslink the polymer, samples were flood exposed

Table 1
Parameters used for DoE design. Center denotes the value used for center points and face centered points.

Parameter		Min	Center	Max
Coded value		−1	0	1
SF_6 flow rate (sccm)	Q_{SF_6}	0	10	20
Pressure (mTorr)	p	20	30	40
Bias power (W)	P_B	0	15	30
Temperature (°C)	T	10	30	50

with 500 mJ cm^{-2} at the I-line and baked for 15 h at 90 °C in an oven. The sample patterning by photo lithography facilitated characterization of the subsequent etch. Prior to each etch experiment the chamber was conditioned using a 20 min chamber clean in an oxygen plasma with a blank silicon wafer loaded. For the cleaning process, the chuck temperature was always set at 20 °C. The chamber cleaning process was considered necessary to ensure stable and predictable conditions in each etch process, since the condition of the chamber walls might affect plasma etching processes. When a new substrate was loaded for etching, the temperature was set to the required value and allowed to stabilize before the etch experiment was started.

2.3. Characterization

Before and after etching, the samples were characterized with respect to etched depth, structure width, surface morphology, and composition. The height of the structures was measured before and after etching using a Dektak 8 stylus profiler from Veeco. Scanning electron microscopy (SEM) images were used to characterize the structure width and the appearance of the surfaces. The width of the structures found from SEM images and the known line pitch in the line array were used to characterize line width reduction during the etch process. For line width measurements, lines in the center of the arrays were chosen to eliminate influence of RIE loading effects on the line width. The roughness was measured using atomic force microscopy (AFM) after etching.

The surface composition of the samples was characterized using XPS. The analysis was carried out in a Thermo K-Alpha XPS instrument with a monochromatic Al–Kα-source and charge compensation. For each sample a binding energy survey from 0 to 1350 eV was performed followed by detailed spectra analysis in the O1s, Sb3d, F1s, and C1s binding energy ranges. The atomic concentrations of surface elements were extracted using the software package Advantage provided by Thermo. In the calculations for the O1s and Sb3d peaks, the ratio and separation of antimony peaks $Sb3d_{3/2}$ and $Sb3d_{5/2}$ were fixed to 0.577 [18] and 9.34 eV [19], respectively. By doing this it was possible to find the surface concentrations of the four main elements in the surface layer: C, O, F, and Sb.

3. Results and discussion

The etch outcome was evaluated on four different parameters. Etch rate (r) and anisotropy (A) are important parameters for controlling etch depth and profile in etching. Furthermore, since severe roughening of the surface was observed after etch, root mean square surface roughness (R_{rms}) and surface composition were measured by AFM and XPS. The surface composition was found as the fractional atomic content of carbon [C], oxygen [O], fluorine [F], and antimony [Sb] in the polymer surface layer. All results outlined below are extracted from the total set of 29 experiments.

The DoE was used to find parameters and interactions with a 0.05 level of significance. Parameters with a significant interaction or quadratic term were always included, even if it's P-value was above 0.05. In Table 2 the P-values are listed for the four measured responses, [Sb], r, A, and R_{rms}. Some interactions and quadratic terms were insignificant for all responses and are not included in the tables. The coefficients of determination (R^2) for the final models are listed in the last row of Table 2.

The etch outcome can be estimated for a response y by a DoE fitted model as,

$$y_i = \beta_i + \sum_j \beta_{ij} x_j + \sum_{j,k} \beta_{ijk} x_j x_k. \quad (1)$$

Table 2
P-values of the DoE fit. Fitting a model for the responses with DoE results in the following P-values, with parameters that were negligible removed. If no value is given for a parameter or interaction it was excluded from the model. The four measured responses are Sb concentration ([Sb]), etch rate (r), anisotropy (A), and root mean square roughness (R_{rms}).

Term	P ([Sb])	P (r)	P (A)	P (R_{rms})
Q_{SF_6}	$< 10^{-4}$	0.6[a]	0.43a	$< 10^{-4}$
T	0.1a	0.006	–	–
P_B	0.005	$< 10^{-4}$	$< 10^{-4}$	$< 10^{-4}$
p	–	$< 10^{-4}$	0.0001	–
$(Q_{SF_6})(T)$	0.02	–	–	–
$(Q_{SF_6})(P_B)$	0.0007	0.03	0.0005	$< 10^{-4}$
$(Q_{SF_6})^2$	$< 10^{-4}$	$< 10^{-4}$	–	$< 10^{-4}$
$(P_B)(p)$	–	0.0002	0.006	–
$(P_B)^2$	–	0.009	0.004	–
R^2	0.94	0.97	0.90	0.93

[a] Included since interactions are significant.

x and y denotes the DoE coded parameters and the response respectively, and $\beta_{i(jk)}$ denotes the estimated coefficients listed in Table 3. The index i denotes the response, while indices j and k denote the parameters.

3.1. Antimony surface concentration

The antimony surface concentration was estimated by XPS spectra of each sample, see Fig. 1. XPS survey spectra revealed that C, O, F, and Sb were the only measurable elements in the SU-8 surface layer, which is in agreement with the known elemental composition of the photo resist [1], if it is assumed that S reacts in the plasma and leaves the surface during etch. The detailed spectra shown in Fig. 1 are therefore shown for binding energies relevant for these elements. Only traces of antimony were observed in the surface layer of non-etched SU-8. SU-8 with 5% photo-initiator contains approximately 0.05%$_{atom}$ antimony which is below the detection limit. For etched SU-8, the amount of antimony measured in the surface layer increased significantly, indicating an antimony accumulation during etch.

The XPS measurements of surface elements showed that the antimony surface concentration was highly dependent on the SF_6 flow rate to both first and second order. In Fig. 2a it is evident that the antimony concentration drastically decreased when SF_6 was added to the plasma. The same tendency is obvious on the contour

Table 3
DoE fit of dependencies. Fitting a model for the responses with DoE gives the following dependencies. Values between columns should not be compared. If no value is given for a parameter or interaction it was excluded from the model. The four measured responses are Sb concentration ([Sb]), etch rate (r), anisotropy (A), and root mean square roughness (R_{rms}).

$\beta_{i(jk)}$	[Sb] (%$_{atom}$)	r (μ min^{-1})	A	R_{rms} (nm)
β_i	2.5	9.57	0.56	9.47[a]
$\beta_{i(Q_{SF_6})}$	−8.1	−0.08	−0.02	−208
$\beta_{i(T)}$	0.9	0.49	–	–
$\beta_{i(P_B)}$	1.7	2.93	0.31	144
$\beta_{i(p)}$	–	−1.25	−0.12	–
$\beta_{i(Q_{SF_6})(T)}$	−1.4	–	–	–
$\beta_{i(Q_{SF_6})(P_B)}$	−2.2	0.38	0.11	−166
$\beta_{Q_{SF_6}}{}^2$	7.6	−3.8	–	207
$\beta_{i(P_B)(p)}$	–	−0.77	0.08	–
$\beta_{i(P_{\text{ofortt}]\text{B}[\text{cfortt}])^2}$	–	−1.05	−0.13	–

[a] Intercept was negligible, but included in model.

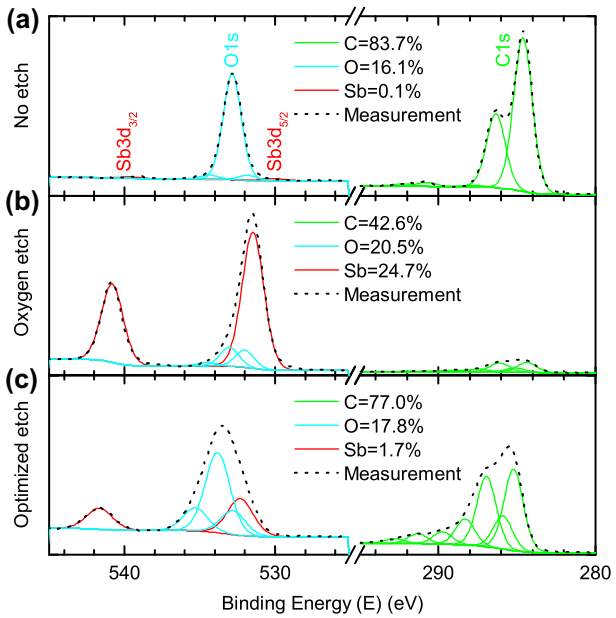

Fig. 1. XPS measurements on processed SU-8 surfaces. Surveys of all samples showed that C, O, Sb, and F were the only elements in the polymer surface. The spectrum analysis showed four different carbon bonds, shown as green curves. Oxygen and antimony were discerned by fixing the ratio of distance and size between the $Sb3d_{5/2}$ peak to the $Sb3d_{3/2}$ peak to fit the $Sb3d_{5/2}$ while O2s was fitted for the remaining area. The oxygen contribution was divided in two types of carbon bonds. Fluorine spectra are not shown, but two bonds for fluorine were used to find the total atomic concentration. Etching of both (b) and (c) were done at $P_C = 1000$ W, $P_B = 30$ W, and $Q_{O_2} = 99$ sccm. For (b) $p = 20$ mTorr, $T = 10$ °C, and $Q_{SF_6} = 0$ sccm was used, while for (c) $p = 40$ mTorr, $T = 30$ °C and $Q_{O_2} = 17$ sccm was used.

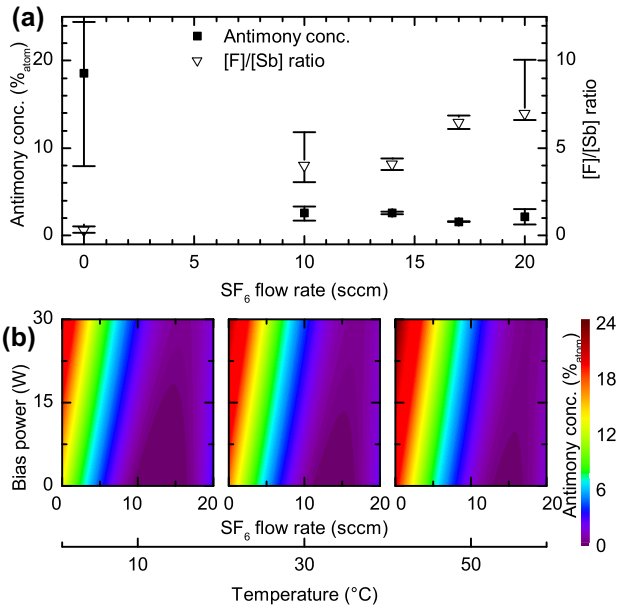

Fig. 2. Antimony surface concentration ([Sb]) as a function of relevant etch parameters. [Sb] and [F]/[Sb] ratio were highly dependent on Q_{SF_6}. (a) Low Q_{SF_6} caused high [Sb] while the [F]/[Sb] ratio became low. (b) [Sb] was primarily dependent on Q_{SF_6} but also T and P_B while p did not show any influence on [Sb].

plots shown in Fig. 2b, independent of the other parameters. Moreover the [F]/[Sb] ratio, also shown in Fig. 2a, increased from below one to three or more. This indicates that most fluorine from the photo initiator desorbed from the surface if fluorine was not added to the gas phase.

For samples etched at low SF_6 flow, the [F]/[Sb] ratio was much lower than the expected six that should be present considering the catalyst stoichiometry. The low ratio suggests that the SbF_6^+ ion reacts in the plasma to form other antimony compounds such as atomic antimony or antimony oxides. Atomic antimony and antimony oxide both have high boiling points of 1587 and 1425 °C [20]. Hence low vapor pressures of antimony and antimony oxides are expected at the processing temperatures used and antimony is expected to stay on the surface. For samples processed at high SF_6 flow rate, fluorinated compounds are expected on the surface. Antimony trifluoride and pentafluoride have boiling points of 376 and 141 °C [20], and in consequence much higher vapor pressures at the processing temperatures. Therefore, these compounds are more likely to evaporate from the surface, resulting in low antimony concentration and a [F]/[Sb] ratio close to the one of the photo-initiator.

Bias power as well as first order interaction with SF_6 flow rate also had an effect on the antimony surface concentration, with higher bias power resulting in higher antimony concentrations. This might be ascribed to ion-enhanced etching [21] with more active sites generated on the polymer backbone. Consequently the polymer etch rate may increase more than the antimony etch rate resulting in a faster antimony accumulation. However the increased antimony accumulation rate could be alleviated by adding more SF_6 to the plasma.

Antimony surface concentration only showed a small dependency on temperature. The antimony surface concentration increased at elevated temperatures. This may be explained by an increase in polymer etch rate for higher temperatures. In other words, the rate of antimony removal is slower than the polymer etch rate. The pressure was found to not influence the antimony concentration.

3.2. SU-8 etch rate

Specific etch depths are usually obtained by control of the etch duration and hence the etch rate must be known. Our experiments showed a dependency of the etch rate on all parameters, see Fig. 3.

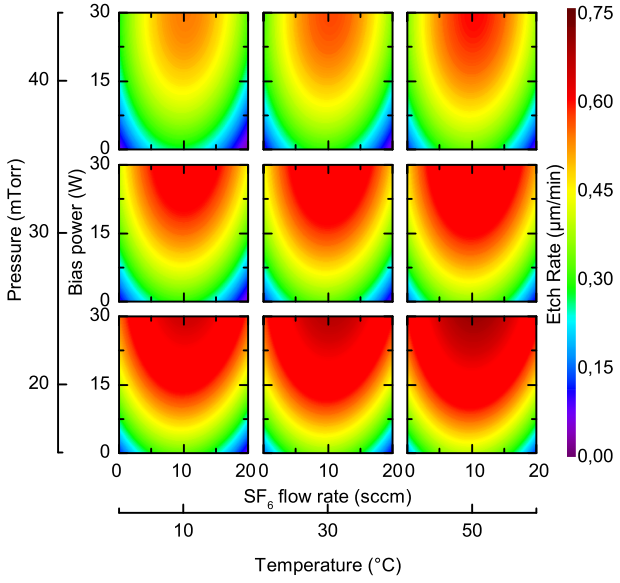

Fig. 3. Etch rate (r) as a function of etch parameters. Etch rate showed a dependency on all parameters. Q_{SF_6} and P_B both have a strong influence on etch rate. p also affected the etch rate significantly with higher p resulting in lower etch rates. T only slightly influences etch rate and does not interact with any of the other parameters.

The most notable dependency was on bias power which controls the ion energy during etch. Increased bias power led to faster etching, either due to sputtering or more likely ion-enhanced etching [21]. Supporting the hypothesis of ion-enhanced etching, the gain in etch rate was more significant for low bias powers.

The SF_6 flow rate to the second order, also significantly affected the etch rate. The response showed curvature with reduced etch rate for both high and low SF_6 flow rates. For low SF_6 flow rates antimony accumulates at the surface, resulting in partial masking of the surface which reduces the etch rate. The decrease in etch rate at higher SF_6 flow rates might be explained by reactions between SF_5 radicals and O, which will reduce the amount of reactive oxygen available for the polymer etch.

Higher pressure in general reduced the etch rate. Interaction between pressure and bias power slightly influenced this tendency. The change in etch rate due to the interaction was most pronounced at high bias powers, while for lower bias power the effect of pressure on etch rate decreased. The decreased etch rate at higher pressures may be due to dilution of plasma species, decreased ion sputtering due to lower mean free path and lower ion energy, or a combination.

Finally, the substrate temperature also influenced the etch rate. Higher temperature increased the etch rates due to thermal activation and higher vapor pressures. Temperature was the only parameter on which etch rate exhibited a linear dependency within the parameter space, while all other parameters interacted with bias power.

In Fig. 3 an overview of the influence of the four parameters on etch rate is shown. From the graphs it is obvious that high bias power and medium SF_6 flow rate give the highest etch rates.

3.3. Etch anisotropy

In addition to etch rate, control of etch anisotropy is important for optimal pattern transfer. The etch anisotropy was calculated as $A = 1 - r_L/r$ where r_L is the lateral etch rate. It was observed that bias power had the largest effect on the anisotropy of the etch, see Fig. 4. As expected increased bias power improved the etch anisotropy due to higher ion energy and thus improved directionality of the etch.

Pressure also influenced etch anisotropy, and a weak interaction between bias power and pressure was evident. At higher pressures the etch was more isotropic due to the reduction of the mean free path in the plasma and hence reduced ion energy and directionality.

The interaction between the SF_6 flow rate and the bias power was significant. However, as seen in Fig. 4, for both anisotropic and isotropic etching high SF_6 flow rate was optimal. SF_6 can introduce more directionality by adding more heavy, charged particles to the plasma body. However SF_6 does not only add charged particles, but also heavy non charged particles, which limits the directionality. Hence bias power determines the shift from one regime to the other. High bias power is necessary to maintain high anisotropy when the SF_6 flow rate is increased.

Etch anisotropy did not show any dependency on temperature.

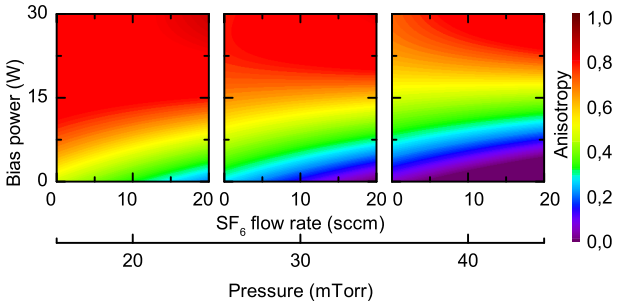

Fig. 4. Etch anisotropy (A) as a function of etch parameters. The anisotropy showed no dependency on the T, whereas the three other parameters all influenced the outcome. Of notice is the dependency on Q_{SF_6} as both for isotropic and anisotropic etches high Q_{SF_6} gives the best result.

3.4. Roughness

The surface roughness is primarily controlled by the SF_6 flow rate, with decreased roughness as a response to more fluorine in the plasma. The SF_6 flow rate affects the roughness response to both first and second order. The interaction between the SF_6 flow rate and bias power, and bias power to first order also influenced the roughness, with increased roughness at higher bias power. The nature of the dependencies on SF_6 flow rate and bias power, indicates that roughness and antimony surface concentration are closely linked. In Fig. 5a the roughness is plotted against the antimony concentration, and a clear tendency is detected such that if the antimony concentration is kept low, the roughness will also be low.

It is worth noticing that for low roughness the [F]/[Sb] ratio in the surface layer is high. Comparing the [F]/[Sb] ratio with the Sb concentration indicates a threshold at which the amount of fluorine in the surface layer is enough to generate volatile antimony compounds. From Fig. 5a it seems that a ratio of [F]/[Sb] of 3:1 enables the antimony to start leaving the surface. This correlates fine with the hypothesis that SbF_3 and SbF_5 may be the volatile compounds formed.

The contour plot in Fig. 5b of the influence of the different parameters on surface roughness shows the same tendencies as for antimony concentration. However, the interaction between bias power and SF_6 flow rate is more pronounced for roughness than antimony surface concentration. From the contour plot it is clear that the roughness can become quite high. The high surface roughness was visible with the naked eye as a dull surface, and in SEM pictures it is readily identified. Fig. 6b shows a sample

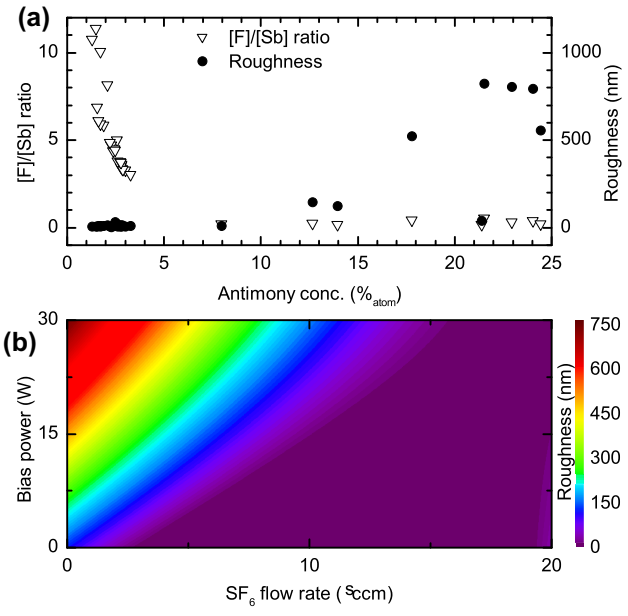

Fig. 5. Root mean square surface roughness (R_{rms}) as a function of relevant etch parameters and R_{rms} and [Sb] concentration correlations. (a) Low [Sb] ensure low R_{rms}, note, that to reach low [Sb] [F] has to be relatively high. (b) The roughness contour shows similar tendencies as the antimony response, however T did not have and effect on R_{rms} just as p also does not.

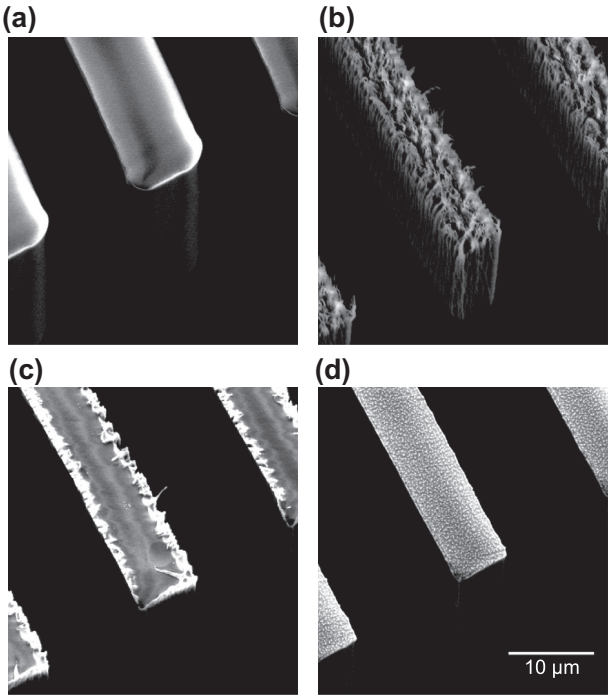

Fig. 6. Surface topology of etched samples. (a) A wafer just after development of the SU-8 layer. (b) The pure oxygen plasma (P_B=30 W, T = 10 °C, p = 20 mTorr, Q_{SF_6} = 0 sccm) causes a high roughness. (c) Optimized etch (P_B=30 W, T = 30 °C, p = 40 mTorr, Q_v = 17 sccm) with high anisotropy at reasonable etch rate and with a smooth surface. (d) Optimized etch (P_B = 0 W, T = 10 °C, p = 20 mTorr, Q_{SF_6} = 14 sccm) at low anisotropy with moderate etch rate and a smooth surface.

etched in a pure oxygen plasma; this sample has a high roughness compared to that of a non-etched sample as shown in Fig. 6a. In Fig. 6c and 6d two samples etched with optimized parameters for low roughness are shown. The two etch processes were optimized for different anisotropy; in Fig. 6c the anisotropy is 0.9 while in Fig. 6d the anisotropy is 0.3. This gives a good indication that relatively smooth surfaces can be obtained with both high and low anisotropy.

Sidewall and edge roughness as seen in Fig. 6c were linked directly to the bias power, with generation of edge roughness when a non zero bias power was applied. The dependency on bias power suggest that sidewall roughness is an effect of plasma directionality. For highly anisotropic etches antimony fluoride desorption on vertical surfaces is not assisted by ion bombardment. For samples etched with no bias power the absence of roughness can be explained by the lower etch rate for these samples. Samples with rough sidewalls always showed rough edges.

4. Conclusion

A DoE study of SU-8 plasma etching enabled improved control of surface properties of the polymer. For a pure oxygen plasma, high antimony concentration, high roughness, and low etch rate were observed. The amount of antimony accumulated at the surface could be reduced to a few percent by addition of SF_6 to the oxygen plasma, which directly lowered the surface roughness. Reasonable etch rates up to 0.8 μm min^{-1} could be obtained at high anisotropy, while optimizing for an isotropic etch will inevitable cause a reduction of the etch rate.

The high concentration of antimony accumulated at the surface must be considered when SU-8 devices are to be used for biological application. For short plasma treatments the antimony concentration will not increase much, but if samples are processed for longer times it will definitely be an issue. For complete removal of the SU-8 antimony surface accumulation results in a contaminated surface. However, adding SF_6 to the plasma chemistry can minimize the residue level and improve the usability of SU-8 as sacrificial mask.

Acknowledgment

CINF – Center for Individual Nanoparticle Functionality is supported by the Danish National Research Foundation.

References

[1] J.D. Gelorme, R.J. Cox, S.A.R. Gutierrez, Photoresist composition and printed circuit boards and packages made therewith, Patent, US 4882245 (11) 1989.
[2] Momentive Specialty Chemicals Inc., EPON™ resin SU-8 (a.k.a. EPIKOTE™157), Web. 8 January 2013 (September) 2001. http://www.momentive.com/Products/TechnicalDataSheet.aspx?id=3603
[3] K.Y. Lee, N. LaBianca, S.A. Rishton, S. Zolgharnain, J.D. Gelorme, J. Shaw, T.H.P. Chang, J. Vac. Sci. Technol. B 13 (6) (1995) 3012, http://dx.doi.org/10.1116/1.588297.
[4] L. Guerin, M. Bossel, M. Demierre, S. Calmes, P. Renaud, in: Transducers 97, vol. 2, IEEE, Chicago, 1997, pp. 1419–1422, http://dx.doi.org/10.1109/SENSOR.1997.635730.
[5] R.J. Jackman, T.M. Floyd, R. Ghodssi, M.A. Schmidt, K.F. Jensen, J. Micromech. Microeng. 11 (3) (2001) 263–269, http://dx.doi.org/10.1088/0960-1317/11/3/316.
[6] K.B. Mogensen, J. El-Ali, A. Wolff, J.P. Kutter, Appl. Opt. 42 (19) (2003) 4072, http://dx.doi.org/10.1364/AO.42.004072.
[7] S. Balslev, A.M. Jorgensen, B. Bilenberg, K.B. Mogensen, D. Snakenborg, O. Geschke, J.P. Kutter, A. Kristensen, Lab. Chip. 6 (2) (2006) 213, http://dx.doi.org/10.1039/b512546d.
[8] M. Nordström, S. Keller, M. Lillemose, A. Johansson, S. Dohn, D. Haefliger, G. Blagoi, M. Havsteen-Jakobsen, A. Boisen, Sensors 8 (3) (2008) 1595–1612, http://dx.doi.org/10.3390/s8031595.
[9] F. Walther, T. Drobek, A.M. Gigler, M. Hennemeyer, M. Kaiser, H. Herberg, T. Shimitsu, G.E. Morfill, R.W. Stark, Surf. Interface Anal. 42 (12-13) (2010) 1735–1744, http://dx.doi.org/10.1002/sia.3515.
[10] P.M. Dentinger, W.M. Clift, S.H. Goods, Microelectron. Eng. 61-62 (2002) 993–1000, http://dx.doi.org/10.1016/S0167-9317(02)00490-2.
[11] G. Hong, A. Holmes, M. Heaton, Microsys. Technol. 10 (5) (2004) 357–359, http://dx.doi.org/10.1007/s00542-004-0413-4.
[12] H. Mischke, G. Gruetzner, M. Shaw, Plasma etching of polymers like SU8 and BCB, in: J.A. Yasaitis, M.A. PerezMaher, J.M. Karam (Eds.), Micromachining and Microfabrication Process Technology VIII, Vol. 4979 of Proceedings of the Society of Photo-optical Instrumentation Engineers (SPIE), SPIE, 2003, pp. 372–381. doi: http://dx.doi.org/10.1117/12.472734.
[13] M.F.L. De Volder, R. Vansweevelt, P. Wagner, D. Reynaerts, C. Van Hoof, A.J. Hart, ACS Nano 5 (8) (2011) 6593–6600, http://dx.doi.org/10.1021/nn201976d.
[14] T. Gebel, Chem. Biol. Interact. 107 (3) (1997) 131–144, http://dx.doi.org/10.1016/S0009-2797(97)00087-2.
[15] K. Kuroda, G. Endo, A. Okamoto, Y.S. Yoo, S.-i. Horiguchi, Mutat. Res. Lett. 264 (4) (1991) 163–170, http://dx.doi.org/10.1016/0165-7992(91)90072-C.
[16] L. Bregoli, F. Chiarini, A. Gambarelli, G. Sighinolfi, A.M. Gatti, P. Santi, A.M. Martelli, L. Cocco, Toxicology 262 (2) (2009) 121–129, http://dx.doi.org/10.1016/j.tox.2009.05.017.
[17] L. Amato, S.S. Keller, A. Heiskanen, M. Dimaki, J. Emnéus, A. Boisen, M. Tenje, Microelectron. Eng. 98 (2012) 483–487, http://dx.doi.org/10.1016/j.mee.2012.07.092.
[18] T. Honma, R. Sato, Y. Benino, T. Komatsu, V. Dimitrov, J. Non-Cryst. Solids 272 (1) (2000) 1–13, http://dx.doi.org/10.1016/S0022-3093(00)00156-3.
[19] J.F. Moulder, J. Chastain, Handbook of X-ray Photoelectron Spectroscopy: A Reference Book of Standard Spectra for Identification and Interpretation of XPS Data, Physical Electronics Division, Perkin-Elmer Corp., Eden Prairie, MN, 1992.
[20] W.M. Haynes, CRC Handbook of Chemistry and Physics: A Ready-Reference Book of Chemical and Physical Data, 93rd ed., CRC Press/Taylor & Francis, Boca Raton, FL, 2012.
[21] J.D. Plummer, M. Deal, P.B. Griffin, Silicon VLSI Technology: Fundamentals, Practice and Modeling, Prentice Hall, Upper Saddle River, 2000.

Appendix C

MNE 2013

The work on TOPAS® was presented at the 39th International Conference on Micro and Nano Engineering. The conference was held in London, England, in September 2013. Below both abstract and poster as presented are shown.

Dry etching of TOPAS® in oxygen based plasma

Kristian Hagsted Rasmussen [a], Stephan Sylvest Keller [a], Flemming Jensen [b], Anders Michael Jorgensen [b], Ole Hansen [a]

[a] Department of Micro- and Nanotechnology, Technical University of Denmark, DTU Nanotech Building 345E, DK-2800 Kgs. Lyngby, Denmark
[b] DTU Danchip, Technical University of Denmark, Oersteds Plads 347, DK-2800 Kgs. Lyngby, Denmark.
e-mail: khara@nanotech.dtu.dk

Keywords: TOPAS®, ICP-RIE, etching, microfluidics

Cyclic Olefin Copolymer (COC) also known by its commercial name TOPAS©, is widely used for fabrication of microfluidic systems due to its high chemical and physical stability and biocompatibility. Furthermore, TOPAS© has also been used for optics [1] and for sensor applications [2]. TOPAS© is well suited for use in optical diagnostics as it is highly transparent to light with some TOPAS© grades transmitting light down to wavelengths of 220 nm. Combining the transparency of TOPAS© with microfluidics enables the fabrication of advanced microfluidic devices for diagnostics. The channel size and surface properties of microfluidic devices are important for the usability of the final devices. This puts some requirements on parameters such as depth control (etch rate), uniformity and roughness. These and other parameters were investigated for etching of TOPAS© in a plasma containing a mixture of oxygen and carbon dioxide.

The samples for etching were prepared by dissolving 8 g of TOPAS© 6013 in 32 g of o-xylene at 60 °C with magnetic stirring for 24 h, followed by spin coating of the dissolved polymer on silicon wafers at 2500 rpm followed by a bake out at 150 °C. The final film thickness was 2.5 μm. A 50 nm aluminum layer was deposited by E-beam evaporation and patterned by standard photolithography serving as mask for pattern transfer. During the photolithography, the developer removes the aluminum in the resist windows during pattern development, see fig. 1. The etching experiments were done in an Advanced Silicon Etcher system from SPTS refitted for polymer etching. The total gas flow was fixed to 100 sccm, with a composition of oxygen (O_2) and carbon dioxide (CO_2), where the content of O_2 and CO_2 was varied between 0 and 100 % as one parameter in a Design of Experiment (DoE) setup. The coil power used for plasma generation was varied between 800 W and 1000 W. The bias power which promotes the physical etching was varied between 0 W and 30 W. As a fourth and final parameter, the chamber pressure was varied between 20 mTorr and 40 mTorr. The pressure was controlled by automatic pressure control (APC), which adjusts a valve in the pumping line to keep a constant chamber pressure during etching.

The initial DoE showed a curvature in parameter responses and was augmented by eight face-centered points. The final set of experiments shows that it is possible to obtain high uniformity, see fig. 2, or high etch rate, see fig.3. However, it is not possible to obtain both simultaneously with one set of processing conditions in the parameter space used for the experiments. The roughness did not show any significant dependency on the etch parameters and was in general low for all samples. This is not equal to unchanged surface properties by etching, because an XPS analysis reveals an increase in surface attached oxygen between unetched and etched samples. For all etched samples the atomic concentration of oxygen in the surface layer was doubled at the expense of carbon, see fig. 4. The increase of surface bound oxygen can influence important properties for the device use, since it may increase the hydrophilicity of the surface and hence change the wetting properties of the final devices.

[1] C. Markos, A. Stefani, K. Nielsen, H. K. Rasmussen, W. Yuan, O. Bang. Optics Express 21 (4) (2013) 4758
[2] F. Bosco, DVD-ROM based high-throughput cantilever sensing platform. Ph.D. thesis, Department of Micro- and Nanotechnology, Technical University of Denmark, 2012.

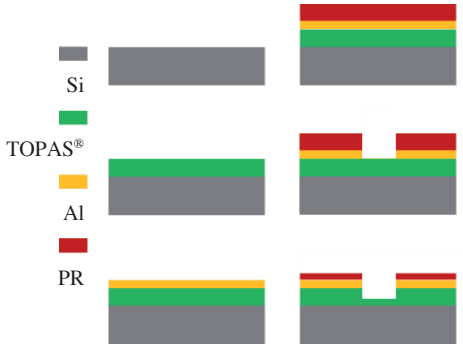

Figure 1. Process flow for DoE etching of TOPAS®.

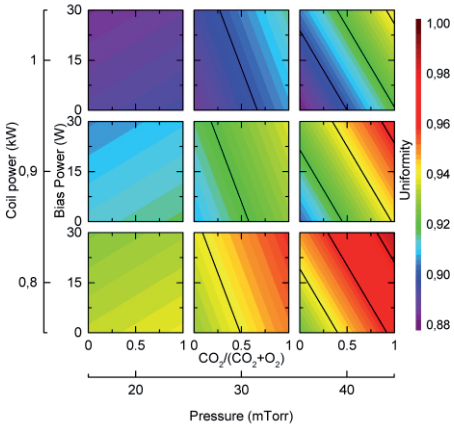

Figure 2. Uniformity of TOPAS® etching dependent on four parameters.

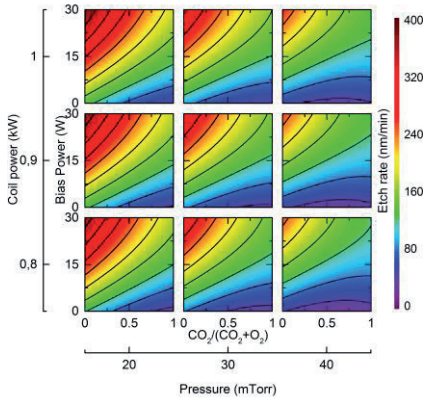

Figure 3. Etch rate of TOPAS® dependent on four parameters.

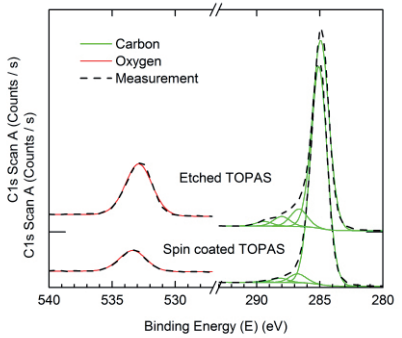

Figure 4. XPS surface measurement before (lower) and after (upper) etching of TOPAS® spun on silicon wafers, an obvious increase in oxygen level on the surface is seen for all etched wafers. The XPS shown is for a wafer etched in CO_2.

DTU Nanotech
Department of Micro- and Nanotechnology

Dry etching of TOPAS® in oxygen based plasma

Kristian Hagsted Rasmussen*†, Ole Hansen†, Flemming Jensen‡, Stephan S. Keller†, and Anders M. Jorgensen‡

ICP-RIE etching of TOPAS can be used in many fields of research, such as microfluidics and optics.

● Optimal etch

Experimental setup

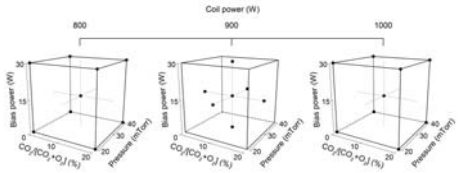

A total of 30 etching experiments were carried out as a full factorial in 4 parameters with face centered point. Chamber pressure, bias power, coil power, and the ratio of oxygen and carbon dioxide flow rate, were varied. Temperature and other parameters were kept constant.

Edge definition

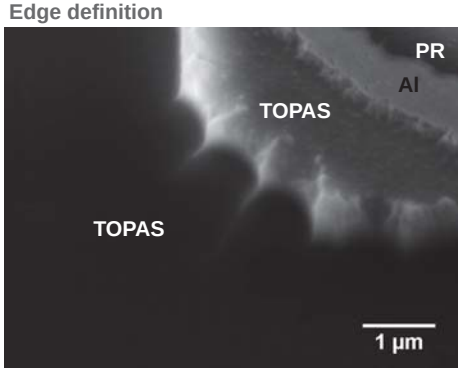

A hard mask serves two purposes; it ensures no mixing of TOPAS and photo resist and functions as etch stop if all resist is removed. The edge definition with an aluminum hard mask was poor. A silicon hard mask improved the edge definition, since silicon is not etched by photo resist developer. If all photo resist is removed before etch is completed, sputtering and redeposition of the hard mask material results in surface roughening.

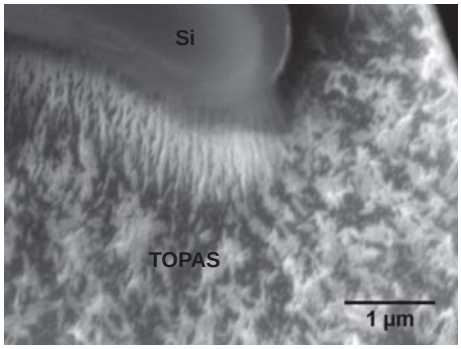

Process flow

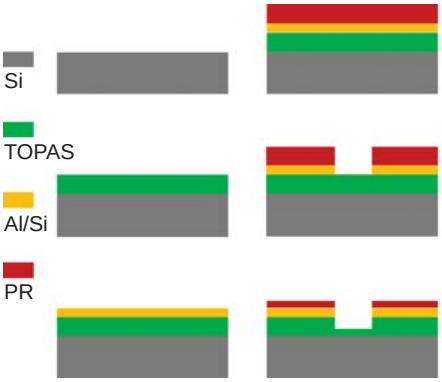

Etch selectivity to photo resist

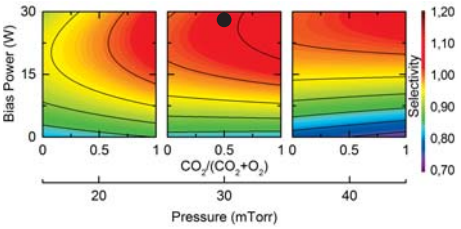

Selectivity to PR is important as a hard mask introduce surface roughness. Selectivities above 1 could be obtained with good center to edge uniformity, at the cost of lower etch rate.

Center to edge uniformity

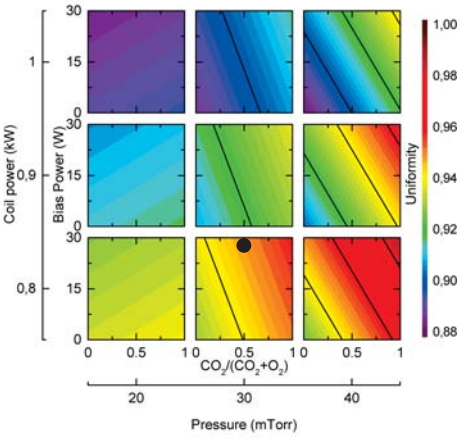

Center to edge uniformity is dependent on all varied parameters. Coil power has a large impact on the uniformity while pressure and carbon dioxide to oxygen ratio affect the center to edge uniformity significantly.

Etch rate

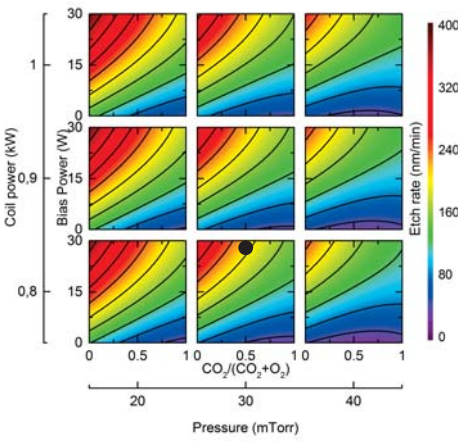

The etch rate depends on all parameters included in the design. Coil power only had a small influence on the rate. Bias power, pressure, and carbon dioxide to oxygen ratio contributions were much more significant and entwined with each other.

Surface composition

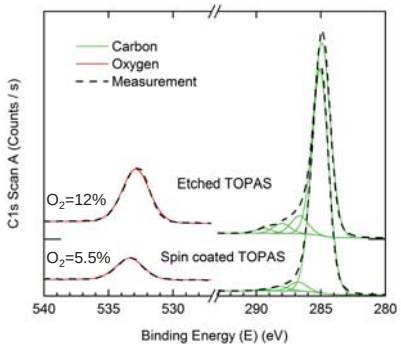

The surface composition of TOPAS® is changed after etching. The amount of oxygen in the surface layer is increased by plasma etching. No correlation between etch chemistry and oxygen surface content was seen.

TOPAS® can be etched with good surface and edge morphology. The choice of hard mask will influence the edge morphology. Some under etching will occur. After etching the surface oxygen concentration increases.

†DTU Nanotech, Technical University of Denmark
Oersteds Plads, building 345E
DK-2800 Kongens Lyngby, Denmark

‡DTU Danchip, Technical University of Denmark
Oersteds Plads, building 347
DK-2800 Kongens Lyngby, Denmark

*Presenting author: Kristian Hagsted Rasmussen
kristian.rasmussen@nanotech.dtu.dk